A comprehensive study of kinetics mechanism of Fischer-Tropsch synthesis over cobalt-based catalyst

Moazami, Nima; Wyszynski, Miroslaw; Rahbar, Kiyarash; Tsolakis, Athanasios; Mahmoudi, Hamid

DOI:
10.1016/j.ces.2017.05.022

Document Version
Peer reviewed version

Citation for published version (Harvard):
Moazami, N, Wyszynski, M, Rahbar, K, Tsolakis, A & Mahmoudi, H 2017, 'A comprehensive study of kinetics mechanism of Fischer-Tropsch synthesis over cobalt-based catalyst', Chemical Engineering Science, vol. 171, pp. 32-60. https://doi.org/10.1016/j.ces.2017.05.022

A comprehensive study of kinetics mechanism of Fischer-Tropsch synthesis over cobalt-based catalyst

Nima Moazami, Miroslaw Lech Wyszynski, Kiyarash Rahbar, Athanasios Tsolakis, Hamid Mahmoudi

Department of Mechanical Engineering, College of Engineering and Physical Sciences, The University of Birmingham, Edgbaston, Birmingham, B15 2TT, UK

Abstract:

A comprehensive kinetics study of Fischer-Tropsch (FT) synthesis mechanism was investigated over an in-house 37% Co-based catalyst on a SiO_2 support. A series of combined FT and water gas shift (WGS) reaction mechanisms were developed in order to calibrate the model at twelve different operating conditions. Two different approaches were used to develop a model for the FT synthesis reaction network. The first was based on an empirical approach; whereas the second approach explained the novel mechanistic details of FT kinetics. In the former, the rate equations were derived by power-law rate expressions, while in the latter the rate equations were derived by the Langmuir–Hinshelwood-Hougen-Watson (LHHW) rate theory. The limitations of power-law rate model were highlighted for the applications that wider range of operating conditions has to be selected. In contrast the advantages of LHHW for predicting a wider range of operating conditions were underlined. A comprehensive plausible mechanism-derived FT kinetics models with eight elementary reaction pathways along with seven WGS kinetics models were developed. Such reaction networks were investigated to fit and validate against the newly obtained experimental results which can be used as a key tool to emphasise the most significant facts of FT synthesis catalysis and chemistry. Model validation was carried out subsequent to completion of the model calibration and the estimation of proper kinetic parameters. The overall purpose of the validation study was to ensure that the model provides a robust and realistic assessment of all the parameters. In order to ensure model is precise to an appropriate level, the model was assessed against experimental data at four different operating conditions. The results obtained from kinetic study were compared to the most recent findings that have been reported in literature. It was shown that the novel developed kinetic model based on a combination of alkyl/alkenyl mechanism for FT reactions (for production of n-paraffins and α-olefins) along with formate mechanism for WGS reaction can provide the most accurate predictions.

1. Introduction

Nowadays there is a worldwide demand to develop energy-efficient and economical processes for sustainable production of alternative chemical compounds and fuels as a substitute for those emerging from petroleum. The excessive dependency of the world on conventional fossil fuels risks the future of the globe. The consistent existence of the present condition will result in an increase of the average temperature of ocean surfaces and global land by 5℃ in 2100; this will cause rising sea levels, which will be the next global crisis [1]. Climate change and global warming, due to the increase of carbon dioxide (CO_2) concentration in the atmosphere formed from the combustion of fossil fuel, and also air pollution, are major environmental concerns as a consequence of their direct influence on human breath and life. As a result, environmental agencies everywhere in the world have delivered more severe regulations to meet the current and forthcoming threats caused by emissions to the

atmosphere e.g. the control of emission standards for particulates from diesel vehicles and residual sulphur in diesel fuel. All these facts have lately increased a renewed interest in Fischer–Tropsch (FT) synthesis. FT synthesis can be defined as the means of indirect liquefaction, in which synthesis gas (a mixture of predominantly CO and H_2) obtained from either coal, peat, biomass or natural gas is catalytically converted to a multicomponent mixture of gaseous, liquid and solid hydrocarbons [2]. The increased interest in FT synthesis is due to its ability to produce ultra-clean diesel oil fraction with a high cetane number (typically above 70) without any aromatic, sulphur and nitrogen compounds; with a very low particulate formation; and CO emissions [3-6].

Currently, there are three main aspects for consideration regarding the FT synthesis processes. Firstly, there exists the FT synthesis reaction mechanism, the details of which are still not fully understood. Furthermore, from the outlook of chemical engineering, there is the design and scale-up of the commercial FT synthesis plant in which studies of the kinetics mechanisms as well as optimization study play significant roles. An optimal design of a commercial-scale reactor requires detailed information of the hydrodynamics and the reaction kinetics, as well as the mathematical model of the catalytic reactor. In fact, to reach the ideal performance of the FT process, a precise comprehensive kinetics model that can describe the product distribution of FT synthesis is essential which this is the main goal of the present study.

The kinetics studies of FT synthesis are distinguished into two categories. In the first category the aim is to focus on the rate of syngas (mixture of CO and H_2) disappearance only. In this category, no information is given related to product distribution, because FT synthesis products are very widespread and the description of the FT kinetics is quite challenging. In the second category however, information about the formation of product compositions are also considered. In both categories, the rate expressions can be derived either empirically (e.g. power-law rate expression), semi-empirically, or mechanistically. In the latter case, the detailed mechanistic of FT kinetics can be accomplished by considering appropriate sequential reaction pathways together with the assumptions about rate-determining steps. Many equations describing the intrinsic rate of FT synthesis have been proposed in the literature. A number of kinetics studies have been reported based on an empirical power-law rate expression for Co- and Fe-based catalysts to fit the experimental data. A summary of these studies; the type of rector and catalyst used; operating conditions i.e. temperature, pressure and H_2/CO molar ratio; as well as the proposed rate equation; are given in Table 1 in the order of publication date [7-19]. In other studies the rate of FT synthesis reactions was expressed based on a proposed mechanism with a postulated rate deterring step (RDS). A summary of these studies are tabulated in Table 2. Overall each model presented in Table 2 had some limitations which are summarized and given in Table 3.

Majority of the conducted studies employed an iron-based catalyst for the kinetic analysis; however, the kinetic study on a cobalt-based catalyst was less abundant. Among the reported studies that utilized the cobalt-based catalyst, most of them investigated the kinetics at either constant reaction temperature, total pressure or space velocity. Furthermore, majority of the reported studies only investigated either the kinetics mechanism of the FT reactions or the WGS reaction model; however, there is lack of published work considering the combined FT and WGS reaction mechanism due to the complex FT synthesis reaction network. In addition, the reported studies only estimated the kinetics parameters to calibrate their models with the experimental data; however, the model validation was not taken into account.

Table 1 FT synthesis overall reaction rate and/or consumption rate (in terms of either CO species or total syngas conversion) based on empirical power-law rate expression

Reactor Type	Catalyst	T (*K*)	P (*bar*)	H_2/CO molar ratio	Rate equation	Equation	Reference
Fixed bed	Co-MgO/ThO_2-Kieselguhr	458-473	1	2.0	$r_{C,org} = kP_{CO}P_{H_2}^2$	Equation 1	Brotz [7]
Fixed bed	Fe	523-593	20.2-40.2	2.0	$-r_{CO+H_2} = kP_{total}$	Equation 2	Hall *et al.* [8]
Fixed bed	Reduced and nitride Fe	498-528	20.2	0.25-2.0	$r_{FT} = \frac{kP_{CO}P_{H_2}}{P_{CO} + aP_{H_2O}}$	Equation 3	Anderson *et al.* [9]
Fixed bed	Promoted Fe	513	10-20	1.2-7.2	$-r_{CO+H_2} = kP_{H_2}$	Equation 4	Dry *et al.* [10]
Fixed bed	Co/CuO/Al_2O_3	458-473	17-55	1.0-3.0	$-r_{CO+H_2} = kP_{CO}^{-0.5}P_{H_2}$	Equation 5	Yang *et al.* [11]
Gradientless	100 Fe/5 Cu/4.2 K/25 SiO_2	522-562	3-20	N/A	$r_j = k_j P_{CO}^{m_j} P_{H_2}^{n_j}$	Equation 6	Bub and Baerns [12]
Berty	Co/La_2O_3/Al_2O_3	488	5.2-8.4	2.0	$-r_{CO+H_2} = kP_{CO}^{-0.33}P_{H_2}^{0.55}$	Equation 7	Pannell *et al.* [13]
Berty	Co/B/Al_2O_3	443-468	10-20	0.25-4.0	$-r_{CO} = kP_{CO}^{-0.5}P_{H_2}^{0.68}$	Equation 8	Wang [14]
Fixed bed	Fe	523	25	N/A	$-r_{CO} = kP_{H_2}$	Equation 9	Jess *et al.* [15]
Fixed bed	Co/TiO_2	453-513	8-16	1-4	$-r_{CO} = kP_{CO}^{-0.24}P_{H_2}^{0.74}$	Equation 10	Zennaro *et al.* [16]
CSTR	Co/ Al_2O_3	483-503	20-30	2.1	$-r_{CO} = kP_{CO}^{m}$	Equation 11	Zhan *et al.* [17]
Fixed bed	Biofunctional Fe-HZSM5	573	17	0.96	$r_j = k_j P_{CO}^{m_j} P_{H_2}^{n_j}$	Equation 12	Marvast *et al.* [18]
CSTR	Co/SiO_2	483	22	1.0-2.4	$r_j = \frac{0.883\ P_{CO}^{-0.25}\ P_{H2}^{0.5}}{1 - 0.155(P_{H2O}/P_{H2})}$	Equation 13	Das *et al.*[19]

Table 2 FT kinetics rate models based on semi-empirical or mechanistic approach

Model	Name and Reference	Reactor Type	Catalyst	T (*K*)	P (*bar*)	H_2/CO Ratio	Intrinsic Kinetics Expression	Equation
L-FT–I	Rautavuoma and van der Baan [20]	Plug flow Fixed bed reactor (low conversion)	Co/Al_2O_3	523	1.0	0.2-4.0	$-r_{CO+H2} = \frac{k\ P_{CO}^{0.5}\ P_{H_2}}{(1\ +\ K_1 P_{CO}^{0.5}\ )^3}$	Equation 14
L-FT–II	Wojciechowski [21]	Berty	Co/Kieselguhr	463	2.0-15.0	0.5-8.3	$-r_{CO} = \frac{kP_{CO}P_{H_2}^{0.5}}{(1\ +\ K_1 P_{CO}\ + K_2 P_{H_2}^{0.5}\ )^2}$	Equation 15
L-FT–III	Sarup and Wojciechowski [22]	Internal recycle reactor (Berty)	Co/Kieselguhr	463	2.0-15.0	0.5-8.3	$-r_{CO} = \frac{kP_{CO}^{0.5}P_{H_2}^{0.5}}{(1\ +\ K_1 P_{CO}^{0.5}\ + K_2 P_{H_2}^{0.5}\ )^2}$	Equation 16
L-FT–IV	Yates and Satterfield [23]	Slurry	$Co/MgO/SiO_2$	493-513	5.0-15.0	1.5-3.5	$-r_{CO} = \frac{kP_{CO}P_{H_2}}{(1+KP_{CO})^2}$	Equation 17
L-FT–V	Iglesia *et al.* [24]	Fixed bed reactor	Co	473-483	1.0-21.0	1.0-10.0	$-r_{CO} = \frac{kP_{CO}^{0.65}P_{H_2}^{0.6}}{1+aP_{CO}}$	Equation 18
L-FT–VI	Zennaro *et al.* [16]	Fixed bed reactor	Co/TiO_2	473-513	20	1.0-4.0	$-r_{CO} = \frac{kP_{CO}P_{H_2}^{0.74}}{(1+KP_{CO})^2}$	Equation 19
L-FT–VII	Elbashir [25]	Fixed bed reactor	15% Co/Al_2O_3	523	60.0	0.5-2.0	$-r_{CO} = \frac{kP_{CO}^{0.5}P_{H_2}^{0.5}}{(1\ +\ aP_{H_2}^{0.5}\ + bP_{CO}^{0.5}\ + cP_{CO}\ )^2}$	Equation 20
L-FT–VIII	Botes *et al.* [26]	Slurry	$Co/Pt/Al_2O_3$	503	5.0-40.0	1.6-3.2	$\frac{-r_{CO}}{kP_{CO}^{0.5}P_{H_2}^{0.75}} = \frac{}{(1\ +\ a\ P_{CO}^{0.5}P_{H_2}^{0.25}\ + bP_{CO}^{0.5}P_{H_2}^{-0.25})^2}$	Equation 21
L-FT–IX	Atashi *et al.* [27]	Fixed bed micro reactor	$15\%Co/10\%K/Al_2O_3$	483-513	8.0	1.0-3.0	$-r_{CO} = \frac{kP_{CO}\ P_{H_2}}{1+aP_{CO}}$	Equation 22

Table 3 Limitation of different kinetic studies reported in the literature for FT synthesis over a Co-based catalyst

Model	Limitation
Rautavuoma and van der Baan [20]	Only investigated at constant temperature and total pressure (523 *K* and 1 *bar*). It may not be applicable at other temperatures and/or pressure conditions.
Wojciechowski [21]	Only investigated at constant temperature (463 *K*). It may not be applicable at other temperature conditions.
Sarup and Wojciechowski [22]	Only the CO consumption rate was investigated and no information related to the product distribution was reported. Large discrepancy between the models and experimental data was reported, which was about 40% for two out of six models. The best model was also rejected due to the physically unrealistic and meaningless value calculated for the adsorption coefficient.
Yates and Satterfield [23]	Simplification towards the adsorbed intermediate and chemical species occupied the total active site, such that CO is the predominant adsorbed species and other surface intermediates were ignored.
Iglesia *et al.* [24]	Narrow temperature range was investigated Water gas shift reaction mechanism was not considered in the developed model
Zennaro *et al.* [16]	Only investigated at constant pressure and space velocity (20 *bar* 5000 h^{-1}). It may not be applicable at other temperature conditions.
Elbashir [25]	Only investigated at constant temperature and total pressure (503 *K* and 60 *bar*). It may not be applicable at other temperature and/or pressure conditions.
Botes *et al.* [26]	The results were in good agreement with the measured data; however, the models were developed semi-empirically based on two and three rate parameters. Only investigated at constant temperature (523 *K*). It may not be applicable at other temperature conditions.
Atashi *et al.* [27]	Only the CO consumption rate was investigated and no information related to the product distribution was reported. Only investigated at constant pressure (8 *bar*). It may not be applicable at other temperature conditions. Simplification towards the adsorbed intermediate and chemical species occupied the total active site, such that CO is the predominant adsorbed species and other surface intermediates were ignored.

2. Experimental setup

The experimental apparatus was designed by a co-worker [1] in the School of Mechanical Engineering. A mini-scale FT plant with fixed bed reactor was designed and built to study the production of liquid hydrocarbons over Co-based FT catalysts. According to this study, a series of eggshell Co catalysts on powder SiO_2 support with dissimilar structure were investigated in the FT synthesis process. The detailed experimental set-up, catalyst preparation procedures and different characterization experiments including methods and tools can be found in the literature [1]. The overall information about the experimental study is highlighted to facilitate the development of kinetics model. The experimental work aimed at the development of a miniaturised version of the FT plant that could accomplish a preliminary investigation of the synthesis process before being scaled-up to a pilot plant. The FT synthesis was conducted in a fixed bed reactor packed with a cobalt catalyst supported with silica powder. Figure 1 shows the schematic illustration of the apparatus as well as the Process Path Flow (PPF) that implements the path of the syngas conversion into the liquid hydrocarbon products. In this process, a

simulated N_2-rich syngas bottle (containing: 33% H_2, 17% CO and 50% N_2) was used to feed into the reactor inlet for the production of synthetic fuels. The catalytic reactor bed was purged by the N_2 bottle and the bed was activated by employing the H_2 gas bottle. Both bottles comprised of a highly precise compressed gas pressure regulator to decrease the gaseous pressure in the cylinders to a value necessitated for the next steps. The syngas conversion was carried out in the FT unit with a seamless stainless steel single mini-structured downdraft fixed bed reactor with a tube length of 52.83 cm, outer diameter of 19.05 mm and wall thickness of 1.651 mm. The reactor was mounted in a tube furnace (with the temperature ranging from 50 to 1100 °C). The tube furnace was used to provide the heat zone and it was controlled by a thermocouple that was placed along the centreline of the reactor located roughly 60-80 mm inside the catalytic bed. Additionally, a metal jacket was installed between the furnace and the reactor and it surrounded the reactor to deliver a uniform wall temperature along the reactor bed length. The Co catalyst in the form of powder was diluted by inert diluent i.e. silicon carbide (SiC) to have better heat removal as well as an effective use of the catalytic bed. In fact, the reactant conversions are highly impacted by the nature of the diluters in exothermic heterogeneous catalytic reactions; so that the diluent will aid the heat transfer, minimize the formation of the heat spot, and improve the temperature distribution along the reactor bed. This is a common practice in laboratory-scale FT synthesis processes, which is also reported by the literature [28]. The catalyst's particles were stabilized by employing a commercial sphere silica support (provided by Fuji Silysia^{TM} Chemical Ltd) because it has significant characteristics such as: stability under reaction condition, high mechanical strength (due to its high purity), inertness, its remarkable high porosity degree and surface roughness and having low manufacturing costs [29]. The supports were stable chemically and mechanically due to their high purity.

After the catalytic bed was purged by the N_2 bottle and the bed was activated by employing the H_2 gas bottle, the synthesis gas then entered into the reactor from the inlet and the system was pressurized to the desired pressure for the FT process to begin. After the inlet flow rate was regulated to the desired reaction space velocity the FT activity was started. The catalytic performances were considered as a function of time on stream for 12 h. The changes in the CO_2 and CO concentration were monitored on-line by using a modified CO analyser (AVL Digas^{TM} 440). An HP$^{®}$ 5890 gas chromatograph, equipped with a Flame Ionisation Detector (FID) and Pora-Plot Q column, was utilized to analyse the effluent gas products. The concentration of different compounds in a sample gas was measured quantitatively. The liquid hydrocarbon products were analysed off-line using a DB1 column combined with a gas chromatography-mass spectrometry (GC-MS) PerkinElmer^{TM}. For liquid samples, the qualitative analysis was performed to identify the components. The experiments were carried out at sixteen different operating conditions (i.e. reaction temperature range of 503-543 *K*, pressure range of 10-25 *bar* and gas hourly space velocity per mass of catalyst range of 1800-3600 $Nm\ell\ (STP)\ g_{cat}^{-1}\ h^{-1}$). The values of the operating conditions, measured CO conversion, CO_2, CH_4, and C_{5+} selectivity are listed in Table 4. Also. Table 5 shows selectivity of available olefins and paraffins' components with carbon number C_2-C_7 at sixteen different operating conditions.

In this research, A series of eggshell cobalt catalysts supported with silica powder were used. The utilization of the eggshell catalyst in a mini-scale fixed bed reactor is an advanced technique, which can overcome the mass transfer limitation due to diffusion limitations in catalyst pellets in the fixed bed reactor system [1, 30]. In the present work, the catalyst was loaded in the reactor in powder form (2 g catalyst with particle size of 75-150 µm)

in order to prevent internal mass transfer limitations. The above assumption was also taken into account by other investigators utilizing a catalyst in the form of powder to prevent the internal mass transfer limitations [31]. Based on the above justifications, the effects of the internal and external mass transfer resistances (interphase and intraparticle mass transport) were neglected; hence only the rate of surface reaction in the reactor was the controller.

In order to improve the temperature distribution along the catalytic beds, minimize the formation of heat spots and prevent the temperature gradients caused by the strongly exothermic FT synthesis reaction, 2 g of the pre-calcined catalyst was weighted for each experiment and then diluted with 12 g of inert silicon carbide (mesh particle size 200-450). The dilution of the catalyst avoids local hot-spots [1]. Dilution of a solid catalyst (in powder form) with inert diluent (i.e. silicon carbide) is a common practice in the laboratory scale FT synthesis process to have better heat removal as well as an effective use of a catalyst bed [32]. In addition, to provide a uniform wall temperature along the reactor bed length, a metal jacket was installed between the furnace and the fixed bed reactor and it surrounded the reactor.

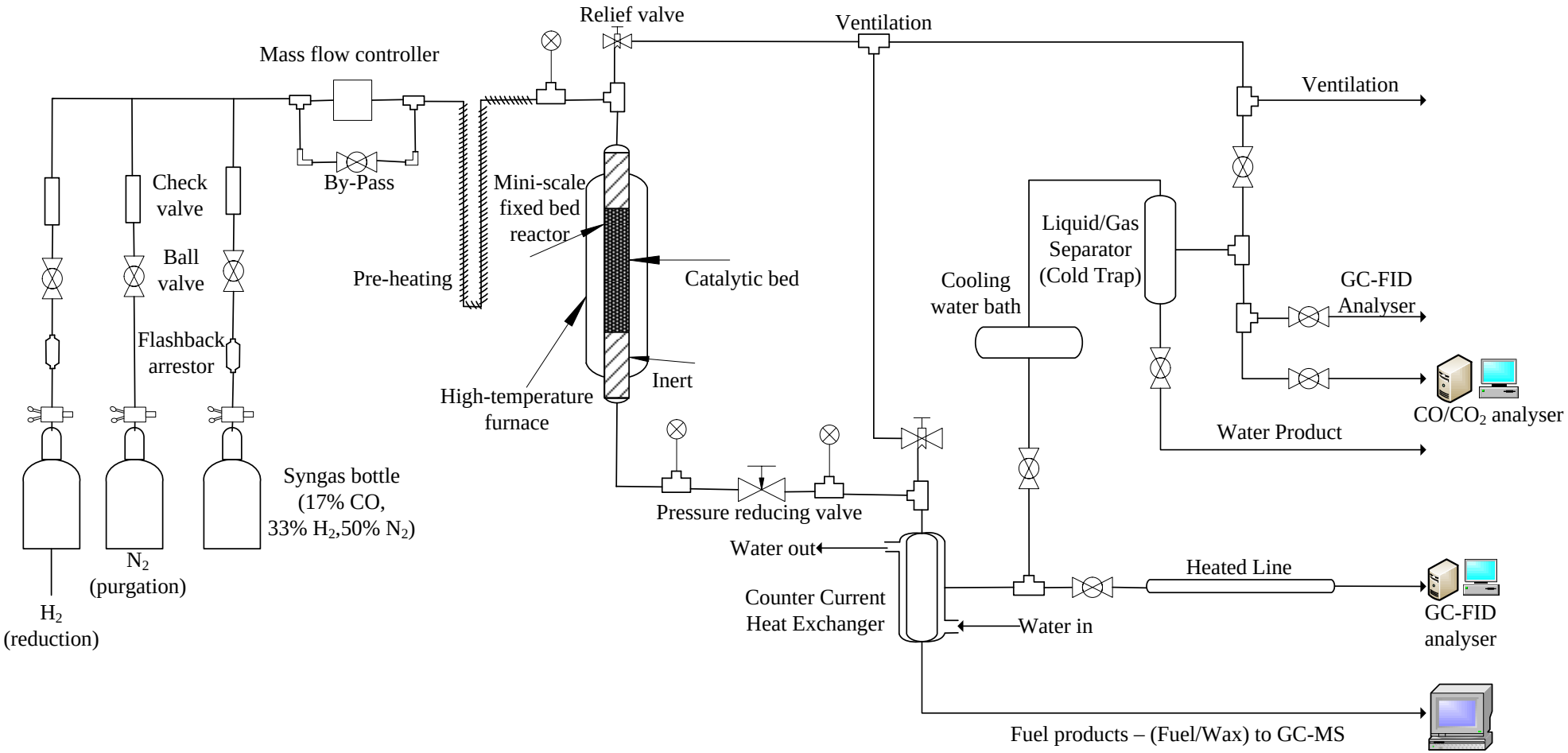

Figure 1 Schematic diagram of experimental setup designed for FT synthesis process.

Table 4 Experimental results at sixteen different operating conditions with respect to reaction temperature, total inlet pressure and GHSV.

No.	T (K)	P_{tot} (bar)	GHSV ($Nm\ell$ (STP) g_{cat}^{-1} h^{-1})	P_{H_2} (bar)	P_{CO} (bar)	X_{CO} (%)	S_{CO_2} (%)	S_{CH_4} (%)	$S_{C_{5+}}$ (%)
1	503	10	1800	3.30	1.70	78.04	4.52	7.06	90.45
2	503	15	2400	4.95	2.55	79.34	4.46	16.59	76.23
3	503	20	3000	6.60	3.4	66.55	2.63	11.17	81.88
4	503	25	3600	8.25	4.25	54.34	1.72	12.60	81.43
5	518	10	2400	3.30	1.70	93.03	14.10	23.27	68.57
6	518	15	1800	4.95	2.55	99.15	14.68	10.96	85.29
7	518	20	3600	6.60	3.40	92.52	10.25	24.38	66.52
8	518	25	3000	8.25	4.25	98.22	11.45	16.25	77.79
9	528	10	3000	3.30	1.70	90.78	16.38	28.72	57.46
10	528	15	3600	4.95	2.55	96.81	17.05	38.25	48.93
11	528	20	1800	6.60	3.40	99.96	20.70	21.55	71.72
12	528	25	2400	8.25	4.25	99.74	18.34	28.25	62.41
13	543	10	3600	3.30	1.70	93.95	21.01	39.66	48.38
14	543	15	3000	4.95	2.55	99.74	24.75	35.89	54.03
15	543	20	2400	6.60	3.40	99.59	25.36	55.82	23.61
16	543	25	1800	8.25	4.25	99.88	24.93	49.72	37.98

Table 5 Experimental results at different operating conditions, selectivity of available olefins and paraffins' components with carbon number less than seven (C_2-C_7)

No.	$S_{C_2H_4}$ (%)	$S_{C_2H_6}$ (%)	$S_{C_3H_6}$ (%)	$S_{C_3H_8}$ (%)	$S_{C_4H_{10}}$ (%)	$S_{C_5H_{12}}$ (%)	$S_{C_6H_{14}}$ (%)	$S_{C_7H_{16}}$ (%)
1	0.03	0.55	0.65	0.35	0.17	0.10	0.09	0.05
2	0.07	1.39	1.89	0.89	0.34	0.26	0.15	0.13
3	0.10	1.42	2.09	0.82	1.58	0.12	0.08	0.01
4	0.08	0.97	1.56	0.56	1.22	0.76	0.48	0.23
5	0.04	2.24	1.28	1.86	0.87	0.44	0.19	0.08
6	0.01	1.04	0.55	0.93	0.33	0.15	0.07	0.02
7	0.06	2.32	1.58	1.90	1.17	0.41	0.27	0.12
8	0.04	1.54	1.28	1.13	0.78	0.47	0.13	0.06
9	0.10	3.76	2.52	2.85	1.65	1.65	1.03	0.64
10	0.08	3.81	1.39	3.27	1.17	0.47	0.35	0.17
11	0.01	2.04	0.48	2.05	0.38	0.08	0.07	0.04
12	0.01	2.77	0.86	2.66	0.65	0.28	0.18	0.10
13	0.08	3.66	1.75	2.85	1.03	0.35	0.22	0.15
14	0.02	3.43	0.45	3.19	0.55	0.32	0.13	0.03
15	5.28	5.40	0.45	5.07	0.70	0.43	0.07	0.02
16	0.01	4.54	0.08	4.24	0.41	0.19	0.07	0.02

3. The comprehensive developed kinetic model

Two different approaches were considered to develop a model for the FT synthesis reaction network in the present study. The first was based on an empirical approach; whereas the second approach explained the mechanistic details of FT kinetics in more depth. In the former, the rate equations were derived by power-law rate expressions, while in the latter the rate equations were derived by the Langmuir–Hinshelwood-Hougen-Watson (LHHW) rate theory. It is worth mentioning that the power-law rate model has limited applications to catalytic reactions to some extent; that is to say, they usually predict rates well over a narrow range of experimental conditions; whereas the LHHW rate theory, due to its fundamental origin, predicts rates over a wider range of conditions. However, it is unclear which combination of a number of rate expressions and kinetics models of syngas conversion and product selectivity can provide the best representation of available data; this will be the main objective of this study. The goal was to employ the newly obtained experimental results to fit several plausible mechanism-derived FT kinetics models, which were likely to reflect the most significant facts of FT synthesis catalysis and chemistry.

3.1. Empirical study of FT synthesis kinetics (first approach)

Kinetics models of reduced complexity are attractive for reactor analysis and design purposes. These models are capable of capturing the essential features of the FT synthesis products' distribution without the need for a parameter such as chain growth probability (α). The reaction network can be classified as a number of lumped reactions by means of the kinetics characteristics of reaction molecules. For the first approach, the rate of reaction was derived based on a power-law rate expression. In this model, the rates of disappearance of reactants, as well as the formation of products' species, were taken into account. Equation 23 below is the general form of the rate expression for a proposed j^{th} reaction. In this equation, P_{CO} and P_{H_2} stand for carbon monoxide and hydrogen partial pressures, respectively; A_j denotes the pre-exponential factor of rate constant and E_j denotes the activation energy of reaction 'j'; n_j and m_j indicate the order of reaction with respect to CO and H_2 partial pressures, respectively. The reaction network consisted of 11 reacting components (i.e. CO, H_2, CO_2, H_2O, CH_4, C_2H_4, C_2H_6, C_3H_8, i-C_4H_{10}, n-C_4H_{10}, and C_{5+}). From R. 1 to R. 8 the proposed reaction scheme in this work is shown. The representative single reaction equation is R. 7; it corresponds to the lumped rate of C_{5+} formation (which is the rate of formation of liquid hydrocarbon compositions) by setting $C_{6.05}H_{12.36}$ as the average molecular value of higher hydrocarbon compounds [33-36].

$$R_j = A_j exp\left(-\frac{E_j}{R_g T}\right) P_{CO}^{n_j} P_{H_2}^{m_j} \qquad \text{Equation 23}$$

Table 6 Proposed lumped FT synthesis kinetics approach (i) over Co/SiO_2 catalyst

Postulated reactions pathway	No.
$CO + 3H_2 \overset{R_1}{\rightarrow} CH_4 + H_2O$	R. 1
$2CO + 4H_2 \overset{R_2}{\rightarrow} C_2H_4 + 2H_2O$	R. 2
$2CO + 5H_2 \overset{R_3}{\rightarrow} C_2H_6 + 2H_2O$	R. 3
$3CO + 7H_2 \overset{R_4}{\rightarrow} C_3H_8 + 3H_2O$	R. 4

$4CO + 9H_2 \xrightarrow{R_5} i - C_4H_{10} + 4H_2O$	R. 5
$4CO + 9H_2 \xrightarrow{R_6} n - C_4H_{10} + 4H_2O$	R. 6
$6.05CO + 12.23H_2 \xrightarrow{R_7} C_{6.05}H_{12.36}(C_{5+}) + 6.05H_2O$	R. 7
$CO + H_2O \overset{R_8}{\leftrightarrow} CO_2 + H_2$	R. 8

The rate of formation and disappearance of the species can be calculated by the sum of the products of the species' stoichiometric coefficient and the reaction rate of the corresponding reaction. Hence, the rates of the consumption of reactants as well as the formation of products' species mentioned above are as follows:

$$r_{CO} = \sum_{j=1}^{NR} v_j^{CO} R_j = -R_1 - 2R_2 - 2R_3 - 3R_4 - 4R_5 - 4R_6 - 6.05R_7 - R_8 \quad \text{Equation 24}$$

$$r_{H_2} = \sum_{j=1}^{NR} v_j^{H_2} R_j = -3R_1 - 4\,R_2 - 5R_3 - 7R_4 - 9R_5 - 9R_6 - 12.23R_7 + R_8 \quad \text{Equation 25}$$

$$r_{H_2O} = \sum_{j=1}^{NR} v_j^{H_2O} R_j = +R_1 + 2R_2 + 2R_3 + 3R_4 + 4R_5 + 4R_6 + 6.05R_7 - R_8 \quad \text{Equation 26}$$

$$r_{CO_2} = \sum_{j=1}^{NR} v_j^{CO_2} R_j = +R_8 \quad \text{Equation 27}$$

$$r_{CH_4} = \sum_{j=1}^{NR} v_j^{CH_4} R_j = +R_1 \quad \text{Equation 28}$$

$$r_{C_2H_4} = \sum_{j=1}^{NR} v_j^{C_2H_4} R_j = +R_2 \quad \text{Equation 29}$$

$$r_{C_2H_6} = \sum_{j=1}^{NR} v_j^{C_2H_6} R_j = +R_3 \quad \text{Equation 30}$$

$$r_{C_3H_8} = \sum_{j=1}^{NR} v_j^{C_3H_8} R_j = +R_4 \quad \text{Equation 31}$$

$$r_{i-C_4} = \sum_{j=1}^{NR} v_j^{i-C_4} R_j = +R_5 \quad \text{Equation 32}$$

$$r_{n-C_4} = \sum_{j=1}^{NR} v_j^{n-C_4} R_j = +R_6 \quad \text{Equation 33}$$

$$r_{C_{5+}} = \sum_{j=1}^{NR} v_j^{C_{5+}} R_j = +R_7 \quad \text{Equation 34}$$

3.2. Mechanistic study of FT synthesis kinetics (second approach)

Unlike most of the kinetics studies in the literature, the combined kinetics of FT synthesis reactions and the WGS reaction were studied mechanistically and different mechanisms with postulated reaction pathways were proposed for both rate models (i.e. FT and WGS reactions). All rate equations were derived on the basis of various elementary step reaction routes and carbon chain distribution pathways (i.e. adsorption, initiation, propagation, and termination steps). The elementary step reactions proposed for each kinetic model are given in Table 7 and Table 8 respectively for FT reactions and WGS reaction. The proposed rate equations were used successfully to describe the kinetics of the reactants' consumption (i.e. carbon monoxide and hydrogen) for the formation of n-paraffins and α-olefins, as well as CO_2 and H_2O by-products, under the FT synthesis condition over a Co-based catalyst. The formation of oxygenates compounds were not taken into account due to the very small amount produced in the present study.

In order to derive the rate equation for each kinetic model, firstly a few elementary reactions were assumed to be rate-determining steps and the other remaining steps were considered at equilibrium state. The combined FT and WGS reaction models were then assessed separately against the experimental data to find the best kinetics model and rate expression for FT synthesis over a Co-based catalyst.

3.2.1. **FT Reaction Rate Mechanism**

In the present study, the proposed kinetics models for FT reactions consisted of surface elementary reaction steps in four categories as follows:

i. Adsorption of the reactants (molecular CO and H_2 species) on the catalyst surface.

ii. Chain initiation step.

iii. Chain growth (propagation) step.

iv. Chain termination and desorption of the products step.

Herein, eight different sets of elementary reaction pathways were proposed for the FT synthesis reactions and they are listed in Table 7. In this table, for instance, '$C-\psi$' is the adsorbed carbon atom on the vacant active site and 'ψ' stands for the total vacant surface coverage fraction of the active site of the solid catalyst in the FT rate model. At the beginning, the molecular adsorption of CO and H_2 with their subsequent dissociation takes place on the free active sites (ψ) of the surface of the cobalt catalyst. Previously, the dissociative adsorption of CO was demonstrated by X-ray photoelectron spectroscopy (XPS) and pulse techniques on Ni, Co, Ru, and Fe [37]. As a consequence, CO first chemisorbed reversibly in the molecular state (step 1); H_2 chemisorbed reversibly on two adjacent free catalytic sites (2ψ) in the dissociated state (step 2). The above assumptions were taken into account in all developed models from FT–I to FT–VIII listed in Table 7. These eight reaction paths were distinguished on the basis of different assumptions considered for adsorption of reactants and the remaining three polymerizations steps mentioned above. In all kinetics models, the combined alkyl and alkenyl mechanisms were adapted to describe the chain initiation, propagation and termination steps. The last seven steps of all developed FT models were written with the same assumptions so that the initiation, propagation and termination steps were proposed separately for olefins and paraffins' formation. In fact, the alkenyl mechanism represents the above three main steps exclusively for the formation of α-olefins; whereas the alkyl mechanism characterises these steps solely for n-paraffins. However, different hypotheses were made in proposing reaction steps of model FT–IV. Unlike the previous theory related to building blocks (i.e. methylene ($CH_2-\psi$) species), instead in these models methylidyne ($CH-\psi$) intermediate together with the addition of hydrogen atoms were assumed to be responsible for the growth mechanisms (see Table 7). In the present study, using a cobalt-based catalyst showed a higher tendency for the formation of paraffinic compounds compared to olefin products. The research studies also indicated that generally using Co and Ru transition metals as a catalyst present a higher tendency for the formation of paraffin compositions, in comparison with olefin formation [38]. Indeed, the alkyl mechanism favoured the formation of paraffins rather than olefins; hence it is a better choice for this case compared to other mechanisms e.g. alkenyl, CO insertion and/or enol mechanisms. However, using alkyl mechanism only, the olefins' selectivities were underestimated. To alleviate the prediction, the alkenyl mechanism which failed to explain the primary yielding of n-paraffins, can be incorporated for prediction of the formation of α–olefins

without increasing the formation of n-paraffins. In addition, in these eight models, three main routes from reactants' adsorption towards building blocks and chain initiation were considered i.e. unassisted CO dissociation (FT–I), H-assisted CO dissociation (FT–II to FT–V) and finally molecular H_2-assisted CO dissociation (FT–VI to FT–VIII). Models FT–I, FT–II and FT–VI were based on the assumption that the FT synthesis mechanism involved the hydrogenation of surface carbon formed by dissociation of chemisorbed CO, either directly (FT–I, step 3), leading to the oxygen atom formation, or by dissociation of $\mathrm{COH}-\psi$ isomers (FT–II, reaction step 4) leading to the hydroxyl species formation, or by interaction with molecular hydrogen (FT–VI, reaction step 3) which leads to the water formation. Very recently density functional theory (DFT) calculations seem to support the key role of H-assisted CO dissociation on both Fe and Co catalysts. A literature study provides both experimental (kinetics) and theoretical (DFT) evidence for the role of H-assisted CO activation as the exclusive kinetically relevant pathway on Co catalysts at conditions typical of FT synthesis practice [39]. Due to the above-mentioned facts, four different pathways, i.e. from FT–II to FT–V, were proposed on the basis of H-assisted chemisorbed CO dissociation to develop the FT reaction rates. Due to a higher formation of methane compared to other paraffinic values, the formation rate mechanism could not be the same as other n-paraffins. Hence, termination to methane was postulated by a different reaction step in which the methane was formed by H-addition of surface methyl intermediate. In addition, the selectivity of ethene was much lower than of other olefin species as indicated from the measured data. Hence, a different reaction step was proposed for the ethene formation so that two adjacent methylene intermediates were reacted at the surface of the catalyst to desorb the ethene molecule. From the outlook of the kinetic descriptions indicated above, eight different elementary reaction steps were proposed as follows:

Model FT–I: Model FT–I was based on unassisted CO dissociation. Considering the steps 1 and 2 explained above, this is followed by direct dissociation of adsorbed surface CO intermediate to form surface carbon and surface oxygen (step 3). Then, the reaction of surface oxygen with adsorbed hydrogen yielded the formation of hydroxyl (step 4); that in turn reacted with adsorbed hydrogen yielding the most abundant product, water molecule (step 5). The sequential hydrogenation of surface carbon led to formation of surface methylidyne (step 6), surface methylene (step 7) and surface methyl (step 8) species. The surface methylene intermediate is regarded as the monomer (building block) in this reaction scheme. The surface methyl species ($-\mathrm{CH_3}$) was assumed to be the chain initiator. The chain initiation step in the 'alkyl' mechanism takes place via this reaction pathway. Van Barneveld and Ponec [40] stated that the formation of CH_3 intermediate is essentially irreversible. This assumption was taken into account herein when the rate expressions were developed for each kinetic model.

Model FT–II: This model is described by dissociation of chemisorbed CO via the H-assisted mechanism. The first hydrogenation (H-assisted) of adsorbed CO led to the formation of surface $\mathrm{COH}-\psi$ isomers (step 3) followed by the formation of surface carbon atoms and hydroxyl intermediates from its dissociation (i.e. $\mathrm{COH}-\psi$ isomers) (step 4). Similar to FT–I, water formed by the addition of hydrogen atoms to hydroxyl (step 5) and the sequential hydrogenation of surface carbon led to the formation of surface methylidyne, methylene and methyl intermediates (steps 6-8).

Model FT–III: Similar to Model FT–II, this model is described by H-assisted chemisorbed CO, except that chemisorbed CO is hydrogenated two times giving the formyl intermediate $\mathrm{HCO}-\psi$ after the first H-addition

(step 3, $H-\psi$ addition to the C-atom in $CO-\psi$) and the hydroxymethylene species $HCOH-\psi$ after the second hydrogenation (step 4, $H-\psi$ addition to the O-atom in $HCO-\psi$). Hydroxymethylene dissociation then led to the formation of methylidyne and hydroxyl intermediates (step 5); that in turn reacted with adsorbed hydrogen atoms forming the polymerization monomer CH_2 (step 7), the initiator required for the chain growth (methyl species, CH_3, step 8) and products H_2O (step 6).

Model FT–IV: This model was similar to model FT–III but the first H-addition of adsorbed CO (step 3) was then followed by dissociation of formed formyl species into methylidyne and surface oxygen atoms (step 4). This model was also different from other H-assisted models in order that the adsorbed reactive surface methylidyne could react with two adjacent hydrogen atoms producing surface methyl (step 7) i.e. the chain initiation for production of paraffinic compounds. Unlike the other FT models, the chain initiator ($C_2H_3-\psi$) for the olefins' production was suggested to be formed by two-adjacent methylidyne species and successive interaction of two hydrogen atoms.

Model FT–V: The addition of $H-\psi$ to the C−atom in $HCO-\psi$ formed $CH_2O-\psi$ intermediates which was followed by dissociation to $CH_2-\psi$ and $O-\psi$ in which the oxygen atom was rejected through this step; possessing high activation barriers (see section 4.2.1). Water formed by the addition of hydrogen atoms to the hydroxyl (step 8) formed by hydrogenation of surface oxygen atoms and the hydrogenation of surface methylene led to the formation of methyl intermediates (step 6). The chain growth mechanism was similar to that reported for FT–III.

Model FT–VI: It is evident that an adsorbed reactive CO could also react with dihydrogen, which leads to the formation of dissociated carbon atoms and water molecules (step 3). This mechanism was regarded as molecular H_2-assisted CO dissociation. The dissociated carbon atoms hydrogenated sequentially (steps 4-6) to finally form the initiator required for the chain growth.

Model FT–VII: Similar to model FT–VI, this model is described by an H_2-assisted mechanism, but instead the reaction between adsorbed CO with dihydrogen formed hydroxymethylene species (step 3) which is then hydrogenated by H-addition forming surface methylidyne and surface water (step 4). Similar to model FT–VI, the adsorbed methylidyne hydrogenated in two successive steps (steps 6-7) to finally form the initiator required for the chain growth.

Model FT–VIII: Same as model FT–VII, the building block and chain initiator in model FT–VIII were respectively adsorbed methylene and methyl, but formation of the building block differs from the former when the hydroxymethylene species reacted with the hydrogen molecule at the surface instead forming the methylene intermediate and water molecule (step 4).

From the above eight kinetics mechanisms and elementary reaction paths tabulated in Table 7, twenty-four possible rate expressions were derived for overall conversion and FT reaction rates by considering different assumptions and various RDSs. The derivation of the rate equations for the FT reaction was explained in section 3.2.2.

Table 7 Sequence of elementary reaction steps of FT synthesis reaction in the present study

Model	No.	Elementary reaction steps	Model	No.	Elementary reaction steps
FT–I	1	$CO + \psi \rightleftarrows CO - \psi$	FT–III	1	$CO + \psi \rightleftarrows CO - \psi$
	2	$H_2 + 2\psi \rightleftarrows 2H - \psi$		2	$H_2 + 2\psi \rightleftarrows 2H - \psi$
	3	$CO - \psi + \psi \rightleftarrows C - \psi + O - \psi$		3	$CO - \psi + H - \psi \rightleftarrows HCO - \psi + \psi$
	4	$O - \psi + H - \psi \rightleftarrows OH - \psi + \psi$		4	$HCO - \psi + H - \psi \rightleftarrows HCOH - \psi + \psi$
	5	$OH - \psi + H - \psi \rightleftarrows H_2O + 2\psi$		5	$HCOH - \psi + \psi \rightleftarrows CH - \psi + OH - \psi$
	6	$C - \psi + H - \psi \rightleftarrows CH - \psi + \psi$		6	$OH - \psi + H - \psi \rightleftarrows H_2O + 2\psi$
	7	$CH - \psi + H - \psi \rightleftarrows CH_2 - \psi + \psi$		7	$CH - \psi + H - \psi \rightleftarrows CH_2 - \psi + \psi$
	8	$CH_2 - \psi + H - \psi \rightarrow CH_3 - \psi + \psi$		8	$CH_2 - \psi + H - \psi \rightarrow CH_3 - \psi + \psi$
	9	$CH_3 - \psi + H - \psi \rightarrow CH_4 + 2\psi$		9	$CH_3 - \psi + H - \psi \rightarrow CH_4 + 2\psi$
	10	$CH_2 - \psi + CH_2 - \psi \rightarrow C_2H_4 + 2\psi$		10	$CH_2 - \psi + CH_2 - \psi \rightarrow C_2H_4 + 2\psi$
	11	$CH_2 - \psi + CH - \psi \rightarrow C_2H_3 - \psi + \psi$		11	$CH_2 - \psi + CH - \psi \rightarrow C_2H_3 - \psi + \psi$
	12	$C_{n-1}H_{2n-1} - \psi + CH_2 - \psi \rightarrow C_nH_{2n+1} - \psi + \psi\ ;\ n \geq 2$		12	$C_{n-1}H_{2n-1} - \psi + CH_2 - \psi \rightarrow C_nH_{2n+1} - \psi + \psi\ ;\ n \geq 2$
	13	$C_nH_{2n+1} - \psi + H - \psi \rightarrow C_nH_{2n+2} + 2\psi$		13	$C_nH_{2n+1} - \psi + H - \psi \rightarrow C_nH_{2n+2} + 2\psi$
	14	$CH_2 - \psi + C_{n-1}H_{2n-3} - \psi \rightarrow C_nH_{2n-1} - \psi + \psi$		14	$CH_2 - \psi + C_{n-1}H_{2n-3} - \psi \rightarrow C_nH_{2n-1} - \psi + \psi$
	15	$C_nH_{2n-1} - \psi + H - \psi \rightarrow C_nH_{2n} + 2\psi$		15	$C_nH_{2n-1} - \psi + H - \psi \rightarrow C_nH_{2n} + 2\psi$
FT–II	1	$CO + \psi \rightleftarrows CO - \psi$	FT–IV	1	$CO + \psi \rightleftarrows CO - \psi$
	2	$H_2 + 2\psi \rightleftarrows 2H - \psi$		2	$H_2 + 2\psi \rightleftarrows 2H - \psi$
	3	$CO - \psi + H - \psi \rightleftarrows COH - \psi + \psi$		3	$CO - \psi + H - \psi \rightleftarrows HCO - \psi + \psi$
	4	$COH - \psi + \psi \rightleftarrows C - \psi + OH - \psi$		4	$HCO - \psi + \psi \rightleftarrows CH - \psi + O - \psi$
	5	$OH - \psi + H - \psi \rightleftarrows H_2O + 2\psi$		5	$O - \psi + H - \psi \rightleftarrows OH - \psi + \psi$
	6	$C - \psi + H - \psi \rightleftarrows CH - \psi + \psi$		6	$OH - \psi + H - \psi \rightleftarrows H_2O + 2\psi$
	7	$CH - \psi + H - \psi \rightleftarrows CH_2 - \psi + \psi$		7	$CH - \psi + H_2 \rightarrow CH_3 - \psi$
	8	$CH_2 - \psi + H - \psi \rightarrow CH_3 - \psi + \psi$		8	$CH_3 - \psi + H - \psi \rightarrow CH_4 + 2\psi$
	9	$CH_3 - \psi + H - \psi \rightarrow CH_4 + 2\psi$		9	$CH - \psi + CH - \psi + 2H - \psi \rightarrow C_2H_4 + 4\psi$
	10	$CH_2 - \psi + CH_2 - \psi \rightarrow C_2H_4 + 2\psi$		10	$CH - \psi + CH - \psi + H - \psi \rightarrow C_2H_3 - \psi + 2\psi$
	11	$CH_2 - \psi + CH - \psi \rightarrow C_2H_3 - \psi + \psi$		11	$C_{n-1}H_{2n-1} - \psi + CH - \psi + H - \psi \rightarrow C_nH_{2n+1} - \psi + 2\psi\ ;\ n \geq 2$
	12	$C_{n-1}H_{2n-1} - \psi + CH_2 - \psi \rightarrow C_nH_{2n+1} - \psi + \psi\ ;\ n \geq 2$		12	$C_nH_{2n+1} - \psi + H - \psi \rightarrow C_nH_{2n+2} + 2\psi$
	13	$C_nH_{2n+1} - \psi + H - \psi \rightarrow C_nH_{2n+2} + 2\psi$		13	$CH - \psi + C_{n-1}H_{2n-3} - \psi + H - \psi \rightarrow C_nH_{2n-1} - \psi + 2\psi$
	14	$CH_2 - \psi + C_{n-1}H_{2n-3} - \psi \rightarrow C_nH_{2n-1} - \psi + \psi$		14	$C_nH_{2n-1} - \psi + H - \psi \rightarrow C_nH_{2n} + 2\psi$
	15	$C_nH_{2n-1} - \psi + H - \psi \rightarrow C_nH_{2n} + 2\psi$			

Model	No.	Elementary reaction steps
FT–V	1	$CO + \psi \rightleftarrows CO - \psi$
	2	$H_2 + 2\psi \rightleftarrows 2H - \psi$
	3	$CO - \psi + H - \psi \rightleftarrows HCO - \psi + \psi$
	4	$HCO - \psi + H - \psi \rightleftarrows CH_2O - \psi + \psi$
	5	$CH_2O - \psi + \psi \rightleftarrows CH_2 - \psi + O - \psi$
	6	$CH_2 - \psi + H - \psi \rightleftarrows CH_3 - \psi$
	7	$O - \psi + H - \psi \rightleftarrows OH - \psi + \psi$
	8	$OH - \psi + H - \psi \rightleftarrows H_2O + 2\psi$
	9	$CH_3 - \psi + H - \psi \rightarrow CH_4 + 2\psi$
	10	$CH_2 - \psi + CH_2 - \psi \rightarrow C_2H_4 + 2\psi$
	11	$CH_2 - \psi + CH - \psi \rightarrow C_2H_3 - \psi + \psi$
	12	$C_{n-1}H_{2n-1} - \psi + CH_2 - \psi \rightarrow C_nH_{2n+1} - \psi + \psi\ ;\ n \geq 2$
	13	$C_nH_{2n+1} - \psi + H - \psi \rightarrow C_nH_{2n+2} + 2\psi$
	14	$CH_2 - \psi + C_{n-1}H_{2n-3} - \psi \rightarrow C_nH_{2n-1} - \psi + \psi$
	15	$C_nH_{2n-1} + H - \psi \rightarrow C_nH_{2n} + 2\psi$
FT–VI	1	$CO + \psi \rightleftarrows CO - \psi$
	2	$H_2 + 2\psi \rightleftarrows 2H - \psi$
	3	$CO - \psi + H_2 \rightleftarrows C - \psi + H_2O$
	4	$C - \psi + H - \psi \rightleftarrows CH - \psi + \psi$
	5	$CH - \psi + H - \psi \rightleftarrows CH_2 - \psi + \psi$
	6	$CH_2 - \psi + H - \psi \rightarrow CH_3 - \psi + \psi$
	7	$CH_3 - \psi + H - \psi \rightarrow CH_4 + 2\psi$
	8	$CH_2 - \psi + CH_2 - \psi \rightarrow C_2H_4 + 2\psi$
	9	$CH_2 - \psi + CH - \psi \rightarrow C_2H_3 - \psi + \psi$
	10	$C_{n-1}H_{2n-1} - \psi + CH_2 - \psi \rightarrow C_nH_{2n+1} - \psi + \psi\ ;\ n \geq 2$
	11	$C_nH_{2n+1} - \psi + H - \psi \rightarrow C_nH_{2n+2} + 2\psi$
	12	$CH_2 - \psi + C_{n-1}H_{2n-3} - \psi \rightarrow C_nH_{2n-1} - \psi + \psi$
	13	$C_nH_{2n-1} + H - \psi \rightarrow C_nH_{2n} + 2\psi$
FT–VII	1	$CO + \psi \rightleftarrows CO - \psi$
	2	$H_2 + 2\psi \rightleftarrows 2H - \psi$
	3	$CO - \psi + H_2 \rightleftarrows HCOH - \psi$
	4	$HCOH - \psi + H - \psi \rightleftarrows CH - \psi + H_2O - \psi$
	5	$H_2O - \psi \rightleftarrows H_2O + \psi$
	6	$CH - \psi + H - \psi \rightleftarrows CH_2 - \psi + \psi$
	7	$CH_2 - \psi + H - \psi \rightarrow CH_3 - \psi + \psi$
	8	$CH_3 - \psi + H - \psi \rightarrow CH_4 + 2\psi$
	9	$CH_2 - \psi + CH_2 - \psi \rightarrow C_2H_4 + 2\psi$
	10	$CH_2 - \psi + CH - \psi \rightarrow C_2H_3 - \psi + \psi$
	11	$C_{n-1}H_{2n-1} - \psi + CH_2 - \psi \rightarrow C_nH_{2n+1} - \psi + \psi\ ;\ n \geq 2$
	12	$C_nH_{2n+1} - \psi + H - \psi \rightarrow C_nH_{2n+2} + 2\psi$
	13	$CH_2 - \psi + C_{n-1}H_{2n-3} - \psi \rightarrow C_nH_{2n-1} - \psi + \psi$
	14	$C_nH_{2n-1} + H - \psi \rightarrow C_nH_{2n} + 2\psi$
FT–VIII	1	$CO + \psi \rightleftarrows CO - \psi$
	2	$H_2 + 2\psi \rightleftarrows 2H - \psi$
	3	$CO - \psi + H_2 \rightleftarrows HCOH - \psi$
	4	$HCOH - \psi + H_2 \rightleftarrows CH_2 - \psi + H_2O$
	5	$CH_2 - \psi + H - \psi \rightarrow CH_3 - \psi + \psi$
	6	$CH_3 - \psi + H - \psi \rightarrow CH_4 + 2\psi$
	7	$CH_2 - \psi + CH_2 - \psi \rightarrow C_2H_4 + 2\psi$
	8	$CH_2 - \psi + CH_2 - \psi \rightarrow C_2H_3 - \psi + H - \psi$
	9	$C_{n-1}H_{2n-1} - \psi + CH_2 - \psi \rightarrow C_nH_{2n+1} - \psi + \psi\ ;\ n \geq 2$
	10	$C_nH_{2n+1} - \psi + H - \psi \rightarrow C_nH_{2n+2} + 2\psi$
	11	$CH_2 - \psi + C_{n-1}H_{2n-3} - \psi \rightarrow C_nH_{2n-1} - \psi + \psi\ ;\ n \geq 3$
	12	$C_nH_{2n-1} + H - \psi \rightarrow C_nH_{2n} + 2\psi$

3.2.2. **Derivation of FT rate equation**

In order to derive the rate equations from the detailed mechanistic kinetics models developed in section 3.2.1, the LHHW rate theory was used and the possible RDSs were identified; while all other steps were assumed to be at quasi-equilibrium. In order to derive the rate expressions, the FT synthesis (hydrocarbon formation) and WGS reaction were assumed to proceed on different active sites. Hence, there were two types of uniformly distributed active sites for FT synthesis and WGS reactions on the catalyst's surface. On the basis of the detailed sequence of elementary reaction steps for FT synthesis tabulated in Table 7, the rates of the n-paraffins and α-olefins' formation were derived for each kinetic model. Initially, it was assumed that the steady-state conditions were reached for both the surface composition of the catalyst and the concentration of all the intermediate species involved. Then, it was assumed that the rate constant parameter of the reaction steps for the hydrocarbon formation is independent of the carbon number of the intermediate species involved in the elementary steps. However, different rate constants were considered for methane and ethene in order to avoid the plausible deviation of the results; as from the experimental results (see section 2), it is clear that the amount of methane produced is much higher than other paraffins and this can cause the deviation. For the same reason, the rate constant of ethene was defined solely due to its low production rate value. The estimated values for rate constants are given in Table 14.

In order to derive the rate expressions, the kinetics model FT–III with RDS-1 in Table 7 was selected to be demonstrated as an example of the derivation of the rate equations. In fact not all of the kinetics parameters are kinetically significant; that is to say not all of them are controlling the overall rate. The rate determining step in a series of elementary steps is that step which has the maximum effect on the overall rate of reaction. Herein, steps 6 and 8 to 15 (model FT–III with RDS-1) were assumed to be RDSs. The remaining steps were assumed to be rapid and at an equilibrium condition. According to the literature [21, 41], the CH_3 intermediate has a high potential to be hydrogenated to form methane. This leads to the correspondingly low opportunity for the methanol and formic acid formation. From the elementary steps 9, 10, 13 and 15, respectively the rate of formation of methane, ethene, n-paraffins and α-olefins were written as follows:

$$R_{CH_4} = k_{meth}\psi_{CH_3}\psi_H \quad \text{Equation 35}$$

$$R_{C_2H_4} = k_{eth}{\psi_{CH_2}}^2 \quad \text{Equation 36}$$

$$R_{olefins} = k_{t,olef}\psi_{C_nH_{2n-1}}\psi_H \quad \text{Equation 37}$$

$$R_{parffins} = k_{t,par}\psi_{C_nH_{2n+1}}\psi_H \quad \text{Equation 38}$$

The elementary steps 1-5 and 7 were assumed to proceed at quasi-equilibrium so the net rate of these steps would be zero. From the kinetics model FT–III, the area coverage fraction of species (concentration of surface intermediate) i.e. $\psi_{CO}, \psi_H, \psi_{HCO}, \psi_{HCOH}, \psi_{CH}, \psi_{CH_2}, \psi_{OH}$ were expressed as a function of the partial pressure of CO, H_2, and H_2O. From the LHHW rate theory [42], the equilibrium mechanism of adsorption and desorption of reactants and products at the catalyst surface, was used to develop the rate expressions. Therefore, the following equations were written for the adsorption and desorption at the catalyst surface of the absorbent as:

$$\left(\frac{dn_i}{dt}\right)_{ads.} = R_{i,ads.} = k_{i,ads.}(1-\psi_i)P_i \quad \text{Equation 39}$$

$$\left(\frac{dn_i}{dt}\right)_{des.} = R_{i,des.} = k_{i,des.}\psi_i \quad \text{Equation 40}$$

Where P_i is the partial pressure of species 'i' and ψ stands for the total vacant surface coverage fraction of active site in the FT rate model. By applying the pseudo-equilibrium assumption for any elementary reaction step, the rate of adsorption equals to the rate of desorption, which can be expressed as Equation 41 and the equilibrium constant can be described by Equation 42. Hence, by extending these relations one can obtain the Langmuir isotherm as the adsorption by Equation 43.

$$R_{i,ads.} = k_{i,ads.}(1-\psi_i)P_i = R_{i,des.} = k_{i,des.}\psi_i \quad \text{Equation 41}$$

$$K_1 = \frac{k_{i,ads.}}{k_{i,des.}} = \frac{\psi_i}{P_i(1-S_i)} \quad \text{Equation 42}$$

$$\psi_i = \frac{k_{i,ads.}(1-\psi_i)P_i}{k_{i,des.}} \quad \text{Equation 43}$$

$R_{i,ads.}$ and $R_{i,des.}$ are respectively the rates of adsorption and desorption of adsorbent on the catalyst surface. The other adsorbed intermediates' surface coverages were found by the same way in the following forms:

$$\psi_{CO} = K_1 P_{CO}\psi \quad \text{Equation 44}$$

$$\psi_H = \sqrt{K_2}P_{H2}^{0.5}\psi \quad \text{Equation 45}$$

$$\psi_{HCO} = \frac{K_3\psi_{CO}\psi_H}{\psi} = K_1\sqrt{K_2}K_3P_{CO}P_{H2}^{0.5}\psi \quad \text{Equation 46}$$

$$\psi_{HCOH} = \frac{K_4\psi_{HCO}\psi_H}{\psi} = K_1K_2K_3K_4P_{CO}P_{H2}\psi \quad \text{Equation 47}$$

$$\psi_{CH} = \frac{K_5\psi_{HCOH}\psi}{\psi_{OH}} = K_1K_2^{1.5}K_3K_4K_5k_6\frac{P_{CO}P_{H2}^{1.5}}{R_{FT}}\psi^3 \quad \text{Equation 48}$$

$$\psi_{CH_2} = \frac{K_7\psi_{CH}\psi_H}{\psi} = K_1K_2^2K_3K_4K_5k_6K_7\frac{P_{CO}P_{H2}^2}{R_{FT}}\psi^3 \quad \text{Equation 49}$$

Since the rate of hydrogenation of the surface hydroxyl was the RDS, therefore the rate of FT synthesis was expressed by Equation 50. The rate of the initiation step (formation of methyl from hydrogenation of methylene) in model FT–III was also assumed to be an RDS as well, hence one can be written as Equation 51. Therefore, one can obtain the second expression for the rate of FT synthesis as Equation 52. So by substituting Equation 52 into the Equation 48 and Equation 49, the area coverage fraction of CH and CH_2 intermediates can be expressed in terms of partial pressures as Equation 53 and Equation 54.

$$R_{FT} = k_6\psi_{OH}\psi_H \quad \text{Equation 50}$$

$$R_{FT} = k_8\psi_{CH_2}\psi_H = K_1K_2^{2.5}K_3K_4K_5k_6K_7k_8\frac{P_{CO}P_{H2}^{2.5}}{R_{FT}}\psi^4 \quad \text{Equation 51}$$

$$R_{FT} = \sqrt{K_1K_2^{2.5}K_3K_4K_5k_6K_7k_8}P_{CO}^{0.5}P_{H2}^{1.25}\psi^2 \quad \text{Equation 52}$$

$$\psi_{CH} = \frac{K_1 K_2^{1.5} K_3 K_4 K_5 k_6}{\sqrt{K_1 K_2^{2.5} K_3 K_4 K_5 k_6 K_7 k_8}} P_{CO}^{0.5} P_{H2}^{0.25} \psi \quad \text{Equation 53}$$

$$\psi_{CH_2} = \frac{K_1 K_2^2 K_3 K_4 K_5 k_6 K_7 \frac{P_{CO} P_{H2}^2}{R_{FT}} \psi^3}{\sqrt{K_1 K_2^{2.5} K_3 K_4 K_5 k_6 K_7 k_8} P_{CO}^{0.5} P_{H2}^{1.25} \psi^2} = \sqrt{\frac{K_1 K_2^{1.5} K_3 K_4 K_5 k_6 K_7}{k_8}} P_{CO}^{0.5} P_{H2}^{0.75} \psi \quad \text{Equation 54}$$

From the Langmuir adsorption theory in a multicomponent system with a single site type, the area coverage fraction of species was written as stoichiometric balance concentrations. Normalization of the concentration of all intermediates on the catalyst surface leads to the following form of the total area coverage fractions:

$$\psi + \psi_{CO} + \psi_H + \psi_{HCO} + \psi_{HCOH} + \psi_{CH} + \psi_{CH_2} = 1 \quad \text{Equation 55}$$

Combining all the above equations and substitution of Equation 44-Equation 47 into Equation 55, the concentration of the total vacant active site ψ can be expressed in terms of partial pressure of different species and the equilibrium constant parameters as Equation 56. Substituting the above formula for the total free active site into the rate expression obtained from hydrogenation of methylene (Equation 51) gave the Equation 57 with respect to the partial pressure of species and kinetic parameters:

$$\psi = \frac{1}{\left(\begin{array}{l} 1 + K_1 P_{CO} + \sqrt{K_2} P_{H2}^{0.5} + K_1 \sqrt{K_2} K_3 P_{CO} P_{H2}^{0.5} + K_1 K_2 K_3 K_4 P_{CO} P_{H2} + \cdots \\ \frac{K_1 K_2^{1.5} K_3 K_4 K_5 k_6}{\sqrt{K_1 K_2^{2.5} K_3 K_4 K_5 k_6 K_7 k_8}} P_{CO}^{0.5} P_{H2}^{0.25} + \sqrt{\frac{K_1 K_2^{1.5} K_3 K_4 K_5 k_6 K_7}{k_8}} P_{CO}^{0.5} P_{H2}^{0.75} \end{array}\right)^2} \quad \text{Equation 56}$$

$$R_{FT} = \frac{\sqrt{k_8 K_7 k_6 K_5 K_1 K_2^{2.5} K_3 K_4} P_{CO}^{0.5} P_{H2}^{1.25}}{\left(\begin{array}{l} 1 + K_1 P_{CO} + \sqrt{K_2} P_{H2}^{0.5} + K_1 \sqrt{K_2} K_3 P_{CO} P_{H2}^{0.5} + K_1 K_2 K_3 K_4 P_{CO} P_{H2} + \cdots \\ \frac{K_1 K_2^{1.5} K_3 K_4 K_5 k_6}{\sqrt{K_1 K_2^{2.5} K_3 K_4 K_5 k_6 K_7 k_8}} P_{CO}^{0.5} P_{H2}^{0.25} + \sqrt{\frac{K_1 K_2^{1.5} K_3 K_4 K_5 k_6 K_7}{k_8}} P_{CO}^{0.5} P_{H2}^{0.75} \end{array}\right)^2} \quad \text{Equation 57}$$

The surface coverages of methyl and vinyl radical were obtained by considering the quasi-steady state assumption for the surface intermediate. From the model FT–III, the balance equations were obtained from reaction steps 8, 9 and 12 for methyl and steps 11 and 14 for vinyl. Rearranging Equation 58 and Equation 59 gave the expression of the intermediate ψ_{CH3} and ψ_{C2H3} (Equation 60 and Equation 61), respectively. Similarly, applying the quasi-steady state assumption for the surface intermediates $\psi_{C_nH_{2n-1}}$ and $\psi_{C_nH_{2n+1}}$ were as Equation 62 and Equation 63. Rearranging the above equations leads to the final expression for $\psi_{C_nH_{2n-1}}$ and $\psi_{C_nH_{2n+1}}$intermdiates (Equation 64 and Equation 65).

$$\frac{dS_{CH_3}}{dt} = 0 \Longrightarrow +R_8 - R_9 - R_{12} = 0 \Longrightarrow + k_{i,par} \psi_{CH_2} \psi_H - k_{meth} \psi_{CH_3} \psi_H - k_{p,par} \psi_{CH_3} \psi_{CH_2} = 0 \quad \text{Equation 58}$$

$$\frac{dS_{C_2H_3}}{dt} = 0 \Longrightarrow +R_{11} - R_{14} = 0 \Longrightarrow + k_{i,olef} \psi_{CH_2} \psi_{CH} - k_{p,olef} \psi_{CH_2} \psi_{C_2H_3} = 0 \quad \text{Equation 59}$$

$$\psi_{CH_3} = \frac{k_{i,par} \psi_{CH_2} \psi_H}{k_{p,par} \psi_{CH_2} + k_{meth} \psi_H} \quad \text{Equation 60}$$

$$\psi_{C_2H_3} = \frac{k_{i,olef}\psi_{CH}}{k_{p,olef}} \quad \text{Equation 61}$$

$$\frac{d\psi_{C_nH_{2n-1}}}{dt} = 0 \Longrightarrow +R_{12} - R'_{12} - R_{13} = 0$$
$$\Longrightarrow + k_{p,olef}\psi_{C_{n-1}H_{2n-3}}\psi_{CH_2} - k_{p,olef}\psi_{C_nH_{2n-1}}\psi_{CH_2} - k_{t,olef}\psi_{C_nH_{2n-1}}\psi_H = 0 \quad \text{Equation 62}$$

$$\frac{d\psi_{C_nH_{2n+1}}}{dt} = 0 \Longrightarrow +R_{12} - R'_{12} - R_{13} = 0$$
$$\Longrightarrow + k_{p,par}\psi_{C_{n-1}H_{2n-1}}\psi_{CH_2} - k_{p,par}\psi_{C_nH_{2n+1}}\psi_{CH_2} - k_{t,par}\psi_{C_nH_{2n+1}}\psi_H = 0 \quad \text{Equation 63}$$

$$\psi_{C_nH_{2n-1}} = \frac{k_{p,olef}\psi_{C_{n-1}H_{2n-3}}\psi_{CH2}}{k_{p,olef}\psi_{CH2} + k_{t,olef}\psi_H} \quad \text{Equation 64}$$

$$\psi_{C_nH_{2n+1}} = \frac{k_{p,par}\psi_{C_{n-1}H_{2n-1}}\psi_{CH_2}}{k_{p,par}\psi_{CH_2} + k_{t,par}\psi_H} \quad \text{Equation 65}$$

The dependence of the reaction rate and adsorption constants on temperature were expressed by the Arrhenius equation as follows:

$$k_j = k_{j,0}exp\left(-\frac{E_j}{RT}\right) \quad \text{Equation 66}$$

$$K_i = K_{i,0}exp\left(-\frac{\Delta H_{ads,i}}{RT}\right) \quad \text{Equation 67}$$

Where k_j is the rate constant of reaction 'j' and K_i is adsorption constant of component 'i'. It was shown that a different kinetics approach, which accounted for the polymerisation character of the FT synthesis, led to a rate formula which was identical to those derived previously in many aspects. As a consequence, repeating and reporting similar rate expressions developed by a different FT kinetics model is avoided. Hence, the mechanistically developed FT rate equations with three plausible RDS assumptions for each FT model are summarized in Table A. 1 to Table A. 8. For each derived rate equation, there is different kinetically relevant RDSs. Three different rate equations were derived for each FT kinetic model. In all models, the elementary steps for chain initiation, growth and termination reactions including formation of methane, ethene, as well as higher paraffins and olefins, were assumed as the RDSs.

3.3. WGS reaction rate mechanism

The WGS reaction models were discriminated on the basis of seven sets of elementary reaction steps (WGS-I to WGS-VII) under FT synthesis conditions. The sequence of elementary reaction pathways are tabulated in Table 8. These kinetics models were proposed based on two different mechanisms. The kinetics models from WGS-I to WGS-V were written based on a direct oxidation mechanism (redox mechanism). According to a literature study [43], the CO_2 can be formed either in an adsorbed or desorbed state via direct oxidation of surface CO intermediate. Both paths were considered for the kinetics analysis in the present study. As a consequence, models WGS-II and WGS-III and WGS-V were considered for direct oxidation via the formation of adsorbed CO_2; while another two kinetics models, i.e. WGS-I, WGS-IV, were considered to proceed via CO_2 desorbed state. The oxide ion $(O - \sigma)$ is formed either through the direct hydroxyl intermediate dissociation, viz. R. 9 or the direct dissociation of the water molecule in the vicinity of either one or two active sites (R. 10 and R. 11,

respectively). Apart from direct oxidation, the formate mechanism was also investigated in the development of the WGS reaction under FT synthesis conditions in the present study. Models WGS-VI and WGS-VII are both based on the formate mechanism in which the formate species is formed through the reaction between adsorbed CO intermediate and a hydroxyl surface species ($-$OH) viz. R. 12; that surface hydroxyl intermediate is formed via the decomposition of water by R. 13.

$$OH - \sigma + \sigma \rightleftarrows H - \sigma + O - \sigma \quad \text{R. 9}$$

$$H_2O + 2\sigma \rightleftarrows H_2 - \sigma + O - \sigma \quad \text{R. 10}$$

$$H_2O + \sigma \rightleftarrows H_2 + O - \sigma \quad \text{R. 11}$$

$$CO - \sigma + OH - \sigma \rightleftarrows CHO_2 - \sigma + \sigma \quad \text{R. 12}$$

$$H_2O + 2\sigma \rightleftarrows H - \sigma + OH - \sigma \quad \text{R. 13}$$

From the quantum calculations on transition metals [44], it was concluded that the hydroxyl dissociation in which the adsorbed hydrogen and oxygen are formed has an unfavourably high activation barrier under FT synthesis conditions. There is also evidence that the formate species is more favourable than the direct oxidation mechanism, as in situ, the existence of formate species was confirmed by infrared spectroscopy under an FT reaction condition; however, the conclusion was made on the Fe-based catalyst [45]. In addition, in situ formate species over some transition metals was detected by Fourier transform infrared spectroscopy (FTIR) in the diffuse reflectance mode (DRIFTS) [46]. Corresponding to models WGS-VI and WGS-VII, the kinetics analysis also showed that it is not possible to distinguish whether water reacts as an associative state ($-H_2O$, considering reactions R. 14 and R. 15), or a dissociative form (R. 13), in the surface reaction if the RDS is the dissociation of formate intermediate to CO_2 (R. 16); since the outcomes of these two kinetics forms were nearly theoretically identical. This conclusion was also supported by Dry [47].

$$H_2O + \sigma \rightleftarrows H_2O - \sigma \quad \text{R. 14}$$

$$H_2O - \sigma + \sigma \rightleftarrows H - \sigma + OH - \sigma \quad \text{R. 15}$$

$$CHO_2 - \sigma \rightleftarrows H - \sigma + CO_2 \quad \text{R. 16}$$

It was pointed out that different surface chemical reactions and pathways may lead to the same kinetics and rates expression and kinetics studies cannot definitely 'prove' a proposed mechanism. Characterization over the catalyst and also quantum chemical calculation [48] are the ways to discriminate whether water reacts associatively or dissociatively. In addition, microkinetic analysis of every elementary reaction step [49] is necessary. However, these types of works are out of the scope of the present study.

Table 8 Elementary reaction steps for WGS reaction

Model	No.	Elementary reaction steps	Model	No.	Elementary reaction steps
WGS-I	1	$CO + \sigma \rightleftarrows CO - \sigma$	WGS-V	1	$CO + \sigma \rightleftarrows CO - \sigma$
	2	$H_2O + 2\sigma \rightleftarrows H - \sigma + OH - \sigma$		2	$H_2O + \sigma \rightleftarrows H_2 + O - \sigma$
	3	$OH - \sigma + \sigma \rightleftarrows H - \sigma + O - \sigma$		3	$CO - \sigma + O - \sigma \rightleftarrows CO_2 - \sigma + \sigma$
	4	$CO - \sigma + O - \sigma \rightleftarrows CO_2 + 2\sigma$		4	$CO_2 - \sigma \rightleftarrows CO_2 + \sigma$
	5	$2H - \sigma \rightleftarrows H_2 + 2\sigma$			
WGS-II	1	$CO + \sigma \rightleftarrows CO - \sigma$	WGS-VI	1	$CO + \sigma \rightleftarrows CO - \sigma$
	2	$H_2O + 2\sigma \rightleftarrows H - \sigma + OH - \sigma$		2	$H_2O + \sigma \rightleftarrows H_2O - \sigma$
	3	$OH - \sigma + \sigma \rightleftarrows H - \sigma + O - \sigma$		3	$CO - \sigma + H_2O - \sigma \rightleftarrows CHO_2 - \sigma + H - \sigma$

	4	$CO-\sigma+O-\sigma \rightleftarrows CO_2-\sigma+\sigma$		4	$CHO_2-\sigma \rightleftarrows CO_2+H-\sigma$
	5	$CO_2-\sigma \rightleftarrows CO_2+\sigma$		5	$2H-\sigma \rightleftarrows H_2+2\sigma$
	6	$2H-\sigma \rightleftarrows H_2+2\sigma$			
WGS-III	1	$CO+\sigma \rightleftarrows CO-\sigma$	WGS-VII	1	$CO+\sigma \rightleftarrows CO-\sigma$
	2	$H_2O+2\sigma \rightleftarrows H_2-\sigma+O-\sigma$		2	$H_2O+2\sigma \rightleftarrows H-\sigma+OH-\sigma$
	3	$CO-\sigma+O-\sigma \rightleftarrows CO_2-\sigma+\sigma$		3	$CO-\sigma+OH-\sigma \rightleftarrows CHO_2-\sigma+\sigma$
	4	$CO_2-\sigma \rightleftarrows CO_2+\sigma$		4	$CHO_2-\sigma \rightleftarrows H-\sigma+CO_2$
	5	$H_2-\sigma \rightleftarrows H_2+\sigma$		5	$2H-\sigma \rightleftarrows H_2+2\sigma$
WGS-IV	1	$CO+\sigma \rightleftarrows CO-\sigma$			
	2	$H_2O+2\sigma \rightleftarrows H_2-\sigma+O-\sigma$			
	3	$CO-\sigma+O-\sigma \rightleftarrows CO_2+2\sigma$			
	4	$H_2-\sigma \rightleftarrows H_2+\sigma$			

3.3.1. **Derivation of WGS rate equation**

As explained, in order to derive the rate expressions, the FT reactions (hydrocarbon formation) and WGS reaction were assumed to proceed on different active sites. One rate-determining step (RDS) was considered in the sequence of the WGS elementary reaction steps; while the remaining elementary reaction steps were assumed to be at quasi-equilibrium. Corresponding to the reaction mechanisms listed in Table 8 and reaction rate expression in Appendix A. Table A. 9 to Table A. 15, WGS-II RDS-4 means that the reaction mechanism is WGS-II, and the RDS-4 means that step-4 of the elementary reaction steps is the slowest step (RDS) and other reactions are at quasi-equilibrium condition. From the WGS-II RDS-4, the rate of formation of CO_2 (i.e. rate of WGS reaction) was written as:

$$R_{WGS} = k_{WGS_4}\sigma_{CO}\sigma_O - k_{WGS_{-4}}\sigma_{CO_2}\sigma \qquad \text{Equation 68}$$

Considering the elementary reaction steps 1-3 and 5-6 in model WGS-II that proceed at quasi-equilibrium, the net rate of the above-mentioned reactions will be zero. As a result, the intermediate species e.g. σ_{CO}, σ_{OH}, σ_O, σ_{CO_2}, and σ_H were equated from elementary reaction steps 1, 2, 3, 5, and 6, respectively (see Equation 69 to Equation 73). From the Langmuir adsorption theory in a multicomponent system of a single site type, the area coverage fraction of species was written as in the stoichiometric balance of the form of Equation 74:

$$\sigma_{CO} = K_{W_1} P_{CO}\, \sigma \qquad \text{Equation 69}$$

$$\sigma_{OH} = \frac{K_{W_2}P_{H_2O}\sigma^2}{\sigma_H} = \frac{K_{W_2}P_{H_2O}\sigma^2}{\sqrt{\frac{P_{H_2}}{K_{W_6}}}\sigma} = K_{W_2}K_{W_6}^{0.5}\frac{P_{H_2O}}{\sqrt{P_{H_2}}}\sigma \qquad \text{Equation 70}$$

$$\sigma_O = \frac{K_{W_3}\sigma_{OH}\sigma}{\sigma_H} = \frac{K_{W_3}\left(K_{W_2}K_{W_6}^{0.5}\frac{P_{H_2O}}{\sqrt{P_{H_2}}}\sigma\right)\sigma}{\sqrt{\frac{P_{H_2}}{K_{W_6}}}\sigma} = K_{W_2}K_{W_3}K_{W_6}\frac{P_{H_2O}}{P_{H_2}}\sigma \qquad \text{Equation 71}$$

$$\sigma_{CO_2} = \frac{P_{CO_2}}{K_{W_5}}\sigma \qquad \text{Equation 72}$$

$$\sigma_H = \sqrt{\frac{P_{H_2}}{K_{W_6}}}\sigma \quad \text{Equation 73}$$

$$\sigma + \sigma_{CO} + \sigma_O + \sigma_{OH} + \sigma_{CO_2} + \sigma_H = 1 \quad \text{Equation 74}$$

Substitution of Equation 69-Equation 73 into Equation 74 gave the final form of σ (Equation 75) in terms of partial pressure of different species and the equilibrium constant parameters. Substituting the surface intermediates (Equation 69, Equation 71 and Equation 73) into the early WGS rate expression (Equation 68) gave the Equation 76 with respect to the total active site. Therefore the final form of the WGS reaction rate expression (Equation 77) for the model WGS-II with RDS-4 was derived by substituting Equation 75 into Equation 76.

$$\sigma = \frac{1}{\left(1 + K_{W_1}P_{CO} + \sqrt{\frac{P_{H_2}}{K_{W_6}}} + K_{W_2}K_{W_3}K_{W_6}\frac{P_{H_2O}}{P_{H_2}} + K_{W_2}K_{W_6}^{0.5}\frac{P_{H_2O}}{\sqrt{P_{H_2}}} + \frac{P_{CO_2}}{K_{W_5}}\right)} \quad \text{Equation 75}$$

$$R_{WGS} = k_{WGS_4}\left(K_{W_1}P_{CO}\sigma\right)\left(K_{W_2}K_{W_3}K_{W_6}\frac{P_{H_2O}}{P_{H_2}}\sigma\right) - k_{WGS_{-4}}\frac{P_{CO_2}}{K_{W_5}}\sigma\sigma \quad \text{Equation 76}$$

$$R_{WGS} = \frac{\left(k_{WGS_4}K_{W_1}K_{W_2}K_{W_3}K_{W_6}\frac{P_{CO}P_{H_2O}}{P_{H_2}} - k_{WGS_{-4}}\frac{P_{CO_2}}{K_{W_5}}\right)}{\left(1 + K_{W_1}P_{CO} + \sqrt{\frac{P_{H_2}}{K_{W_6}}} + K_{W_2}K_{W_3}K_{W_6}\frac{P_{H_2O}}{P_{H_2}} + K_{W_2}K_{W_6}^{0.5}\frac{P_{H_2O}}{\sqrt{P_{H_2}}} + \frac{P_{CO_2}}{K_{W_5}}\right)^2} \quad \text{Equation 77}$$

All the above-mentioned WGS rate expressions developed from the proposed kinetics models were initially coupled with the FT synthesis rate expressions developed in section 3.2.1 and then they were each evaluated against the experimental data at a variety of operating conditions. The results and discussion obtained from the overall kinetics models are explained in section 4.

3.3.2. **Formulation (equating) of the reverse rate constant**

The rate constant for the reverse reaction ($k_{WGS_{-1}}$) in the above rate equation can be represented by the equilibrium constant, K_p, of the WGS reaction. Generally, K_p in the WGS reaction can be expressed by the equilibrium partial pressure of CO, H_2, CO_2 and H_2O species as Equation 78. The partial pressures of CO, H_2, CO_2 and H_2O were obtained by rearranging Equation 69, Equation 73, Equation 72 and Equation 69 respectively. In Equation 79, the term ($\frac{\sigma_{CO_2}\sigma}{\sigma_{CO}\sigma_O}$) should be also defined with respect to equilibrium constants. Considering elementary step 4 and assuming that step 3 reached the equilibrium state, one can obtain Equation 80. The K_p term was eventually expressed by substituting Equation 80 into Equation 79 in the form OF Equation 81. According to the above-mentioned details of the chemical reaction equilibrium and since the equilibrium constant is the ratio of the rate constant for the forward reaction to the rate constant for the reverse reaction, therefore the term $k_{WG\psi_{-1}}$ was obtained by Equation 82.

$$K_p = \frac{P_{CO_2} P_{H_2}}{P_{CO} P_{H_2O}} \quad \text{Equation 78}$$

$$K_p = \frac{\left(\frac{\sigma_{CO_2} K_{W_5}}{\sigma}\right)\left(\frac{\sigma_{H_2} K_{w_6}}{\sigma}\right)}{\left(\frac{\sigma_{CO}}{K_{W_1}\sigma}\right)\left(\frac{\sigma_O \sigma_{H_2}}{K_{W_2}\sigma^2}\right)} \quad \text{Equation 79}$$

$$\frac{\sigma_{CO_2}\sigma}{\sigma_{CO}\sigma_O} = K_{W_3} K_{W_4} \quad \text{Equation 80}$$

$$K_p = K_{W_1} K_{W_2} K_{W_3} K_{W_4} K_{W_5} K_{w_6} \quad \text{Equation 81}$$

$$k_{WGS_{-1}} = K_{W_2} K_{W_3} K_{W_4} K_{W_5} K_{w_6} k_{WGS_1} / K_p \quad \text{Equation 82}$$

3.3.3. **Development of the WGS Reaction Equilibrium Constant (temperature dependence correlation)**

Generally the value of equilibrium constant K_P depends on the value of the standard free energy change of reaction, which is the free energy of formation difference between the products and the reactants, with both in their standard states (1 atm and the temperature of the system). Thus the equilibrium constant is a function of temperature and its dependency on temperature is given by Equation 83 [42]. The value of ΔG_R° was computed from the available literature standard free energy of formation data at a temperature of 298.15 *K*. These values were substituted into Equation 84 to compute the standard free energy of formation at 298.15 *K*, so that the K_P value at the reference temperature (298.15 *K*) was computed from Equation 83. Here, α_i and α_k stand for a stoichiometric coefficient of 'i' and 'k' species, respectively. In addition, the K_P value at other temperatures can be calculated from the classic van't Hoff equation via Equation 85. By integrating this equation, one can compute for equilibrium constant K_P, at any temperature (Equation 86).

$$lnK_p = -\frac{\Delta G_R^\circ}{R_g T} \quad \text{Equation 83}$$

$$\Delta G_{R,298.15}^\circ = \frac{1}{\alpha_k}\left(\sum_i^{Products} \alpha_i \, \Delta G_{f,298.15}^\circ - \sum_i^{Reactants} \alpha_i \, \Delta G_{f,298.15}^\circ\right) \quad \text{Equation 84}$$

$$\frac{lnK_P}{dT} = -\frac{\Delta H_R^\circ}{R_g T^2} \quad \text{Equation 85}$$

$$ln\left(\frac{K_P}{K}\right) = -\frac{\Delta H_R^\circ}{R_g}\left(\frac{1}{T} - \frac{1}{T_r}\right) \quad \text{Equation 86}$$

The enthalpy changes that accompany the temperature changes were calculated by the heat capacities of the respective mixtures. The heat of reaction at temperature *T* was the sum of enthalpy changes for: i) the temperature of the reactants from *T* to 298.15 *K*. ii) carrying out the reaction at 298.15 *K*. and iii) the temperature of the products to the (same) temperature *T*. The heat of reaction can therefore be computed from Equation 87 and normalized to species *k*, to Equation 88. The difference in heat capacity between products and reactants was determined from Equation 89. The polynomial temperature dependency of the heat capacity and the coefficients' changes (i.e. Δa, Δb, Δc and Δd) are determined by Equation 90 and Equation 91 to Equation 94, respectively. The coefficients were obtained from the literature [42] and they are tabulated in Table 9.

$$\Delta H^{\circ}_{R,T} = \frac{1}{\alpha_k}\left[\sum_{i}^{Reactants}\int_{T}^{298.15}\alpha_i C_P dT\right] + \Delta H^{\circ}_{R,298.15} + \frac{1}{\alpha_k}\left[\sum_{i}^{Products}\int_{298.15}^{T}\alpha_i C_P dT\right] \quad \text{Equation 87}$$

$$\Delta H^{\circ}_{R,T} = \Delta H^{\circ}_{R,298.15} + \frac{1}{\alpha_k}\left[\int_{298.15}^{T}\left(\sum_{i}^{Products}\alpha_i\, C_P - \sum_{i}^{Reactants}\alpha_i\, C_P\right)dT\right] \quad \text{Equation 88}$$

$$\Delta C_P = \left(\sum_{i}^{Products}\alpha_i\, C_P - \sum_{i}^{Reactants}\alpha_i\, C_P\right) \quad \text{Equation 89}$$

$$\Delta C_P = \Delta a + \Delta b + \Delta c + \Delta d \quad \text{Equation 90}$$

$$\Delta a = \left(\sum_{i}^{Products}\alpha_i\, a_i - \sum_{i}^{Reactants}\alpha_i\, a_i\right) \quad \text{Equation 91}$$

$$\Delta b = \left(\sum_{i}^{Products}\alpha_i\, b_i - \sum_{i}^{Reactants}\alpha_i\, b_i\right) \quad \text{Equation 92}$$

$$\Delta c = \left(\sum_{i}^{Products}\alpha_i\, c_i - \sum_{i}^{Reactants}\alpha_i\, c_i\right) \quad \text{Equation 93}$$

$$\Delta d = \left(\sum_{i}^{Products}\alpha_i\, d_i - \sum_{i}^{Reactants}\alpha_i\, d_i\right) \quad \text{Equation 94}$$

Table 9 Enthalpy and free energy of formation at 298.15 *K* and constant coefficients of heat capacity polynomial, Cp in unit J mol^{-1} K^{-1} [42]

Species	Molar mass	ΔH_f°	ΔG_f°	a	b	c	d
CO	28.01	-110.6	-137.4	28.11	$0.1672\cdot10^{-2}$	$0.5363\cdot10^{-5}$	$-2.218\cdot10^{-9}$
H_2O	18.02	-242.0	-228.7	32.19	$0.1920\cdot10^{-2}$	$1.054\cdot10^{-5}$	$-3.589\cdot10^{-9}$
CO_2	44.01	-393.8	-394.6	22.22	$5.9711\cdot10^{-2}$	$-3.495\cdot10^{-5}$	$7.457\cdot10^{-9}$
H_2	2.02	0	0	29.06	$-0.1913\cdot10^{-2}$	$-0.8690\cdot10^{-5}$	$-0.8690\cdot10^{-9}$

From the above computation, an expression was derived for the equilibrium constant as a function of temperature (Equation 95). This equation was used in the present study to calculate the WGS equilibrium constant at different experimental temperature conditions.

$$ln(K_P) = -3.72 + \frac{4861.49}{T} - 6.90\cdot10^{-3}\cdot T + 1.33\cdot10^{-5}\cdot T^2 - 8.38\cdot10^{-9}\cdot T^3 + 1.25\cdot10^{-12}\cdot T^4 \quad \text{Equation 95}$$

4. Results and discussion

4.1. Kinetics results using power-law rate model

Using the empirical power-law rate expression developed in section 3.1, the model aimed at predicting the conversion of syngas species (CO and H_2) as well as selectivity of carbon dioxide and hydrocarbon products by estimating the kinetic parameters which consisted of: order of reaction with respect to CO and H_2 partial pressures; pre-exponential factor; and activation energy for each proposed chemical reaction listed in Table 6. A total of 84 responses were incorporated in estimation of the parameters. These responses encompassed seven species: CO conversion; CO_2; methane (CH_4); light hydrocarbons (i.e. C_2, C_3, and C_4) and total FT liquid hydrocarbons' (C_{5+}) selectivities which were calculated at twelve different experimental conditions (listed in

Table 10); availability for calibration, with respect to reaction temperature, total pressure and gas hourly space velocity (GHSV) in the range of 503-543 *K*, 10-25 *bar* and 1800-3600 $Nm\ell\ (STP)\ g_{cat}^{-1}\ h^{-1}$, respectively. Table 11 shows the kinetic parameters estimated by the empirical power-law rate expression (see Equation 23 and Equation 24 to Equation 34). The predicted results were compared to those of the experiments with respect to the above components. The goodness of fit was examined by employing the *F*-test and the Mean Absolute Percentage Deviation (MAPD) values were computed based on the formula provided previously [50]. From Table 11, since the F_{ratio} with value of 55.34 exceeded the critical value ($F_{critical}$), with a significance level of 0.01 (i.e. the cumulative probability of 0.99), hence one can be confident that the model is significant. In addition, the MAPD value of 13.23% that were obtained indicated that the model can fit the experimental results with reasonable accuracy. In fact, the calculated value of MAPD was in the range of the available literature, and kinetic parameters were all physically meaningful. Nevertheless, part of the scope of the present study was to achieve a model prediction much better than that obtained by the literature and predicted by power-law empirically. It will be shown that the results were not satisfactorily predicted by the power-law model for some species at some specific operating conditions those which significantly affected the model predictions. It will be explained that this model may not be able to predict well at a wide range of process conditions; however, this model is suitable when a narrower range is selected.

Table 10 Values of experimental data employed in the present study considered for the power-law model

	T	P_0	*GHSV*	Conversion	Selectivities					
				CO	CO_2	CH_4	C_2	C_3	C_4	C_{5+}
	(*K*)	(*bar*)	$Nm\ell\ (STP)\ g_{cat}^{-1}\ h^{-1}$	(%)	(%)	(%)	(%)	(%)	(%)	(%)
Test-01	503	10	1800	78.04	4.52	7.06	0.58	1.00	0.90	90.45
Test-02	503	15	2400	79.34	4.46	16.59	1.47	2.79	2.93	76.23
Test-03	503	20	3000	66.55	2.63	11.17	1.52	2.90	2.53	81.88
Test-05	518	10	2400	93.03	14.1	23.27	2.28	3.14	2.74	68.57
Test-06	518	15	1800	99.15	14.68	10.96	1.05	1.48	1.22	85.29
Test-07	518	20	3600	92.52	10.25	24.38	2.38	3.48	3.24	66.52
Test-10	528	15	3600	96.81	17.05	38.25	3.89	4.66	4.27	48.93
Test-11	528	20	1800	99.96	20.7	21.55	2.05	2.53	2.14	71.72
Test-12	528	25	2400	99.74	18.34	28.25	2.78	3.52	3.04	62.41
Test-13	543	10	3600	93.95	21.01	39.66	3.74	4.61	3.62	48.38
Test-14	543	15	3000	99.74	24.75	35.89	3.45	3.64	3.00	54.03
Test-15	543	20	2400	99.59	25.36	55.82	10.69	5.55	4.34	23.61

In addition, the significance of individual kinetic parameters was statistically examined by the *t*-test analysis in order to ensure that the kinetic model and parameters were relevant. The detail of computation of t_{value} was explained in literature [51]. The *t*-test results (e.g. t_{value} and $t_{critical}$) are shown in Table 11. Absolute t_{value} of all parameters fell within the range of 7.14−100.34, which were greater than the $t_{critical}$ with the value of 2.4 at a 0.99% confidence interval, indicating that all parameters in the power-law kinetic model contributed relevantly.

Table 11 Values of kinetic parameters estimated in the present study considering power-law kinetic model presented in section 3.1 as well as F_{ratio} and t_{value} calculated from the statistical analyses

Reaction	n_j*	t_{value}	m_j*	t_{value}	E_j*	t_{value}	A_j*	t_{value}
	$(-)$		$(-)$		$(kJ\ mol^{-1})$		$\left(mol\ g_{cat}^{-1}\ s^{-1}Pa^{(n_j+m_j)}\right)$	
R. 1	-0.39	53.34	1.02	97.25	101.15	69.25	5.45E+01	68.44
R. 2	-0.24	60.14	0.15	7.14	78.79	30.05	1.20E-03	64.59
R. 3	-0.26	15.71	0.18	7.25	59.95	51.82	1.45E-03	52.98
R. 4	-0.55	93.36	0.25	94.23	33.73	64.99	2.32E-06	16.80
R. 5	-0.82	34.23	0.35	55.94	23.04	100.34	2.81E-09	32.70
R. 6	-0.76	17.34	0.32	70.30	17.83	93.86	6.57E-10	15.85
R. 7	-0.15	88.67	1.25	26.19	21.25	63.83	3.24E-08	62.38
R. 8	-1.10	51.44	1.26	100.08	50.24	80.59	5.99E-05	34.95

*Results of statistical analysis:
(i) *F*-test: $F_{\text{ratio}} = 55.34 > F_{critical}\ (n-m, m-1; 1-\alpha) = F_{critical}\ (84-32, 32-1; 1-0.01) = 2.07$
(ii) *t*-test: lowest t-value $= 7.14 > t_{critical}\ (n-m; 1-\alpha) = t_{critical}\ (84-32; 1-0.01) = 2.4$

Furthermore, the parity diagram as well as relative residual percentage plots were illustrated in Figure 2 and Figure 3 (a-g) respectively, representing the overall adequacy of the prediction with respect to the individual variables (i.e. CO, CO_2, CH_4, C_2, C_3, C_4 and C_{5+}) and total response. It was seen that around 60% of the results were predicted with a relative error of less than 15% and all the data points were predicted below 32% error, indicating that the rate model did not effectively predict the rate of reactions at all operating conditions. From the predicted results, it was found that at high temperature conditions, especially when $T \geq 528\ K$, the predicted results were not in good agreement with the measured data in which the predicted values presented a higher relative residual than those obtained at a lower temperature. However, the results presented in the past studies [33-36, 52] revealed that with the narrower temperature range, for instance when *T* changes between 500-528 *K*, the power-law model provided satisfactory prediction with the MAPD less than 7% in which about 89% of the data points were obtained with an error below 10%. Considering a wider range for the process conditions, the selectivities of CO_2 and CH_4 were overestimated, while those of C_2-C_3 and C_4 were underestimated. This implies that the temperature can significantly impact on the estimation of the parameters and the mathematical modelling predictions. Indeed, this was due to the temperature dependency of the activation energies and the Arrhenius equation (Equation 66) in the rate formula: at a high temperature condition; predicting a lower value of activation energy would increment the rate constant as well as rate of products' formation; while at a lower temperature condition this would be vice versa. For instance, Figure 3 (b) shows the relative residual between the calculated and experimental values in terms of CO_2 selectivity, indicating the overestimation of the results at higher temperature conditions since some of data points were predicted below -15%. Referring to Table 11, R. 8 was the reaction responsible for the production of CO_2 and its activation value was 50.24 $kJ\ mol^{-1}$, which was considerably lower than the expectation. It will be discussed in details that the order of reaction (i.e. 'm' and 'n' in Equation 66) of H_2 and CO partial pressures would have significant effects on the products rate of formation concurrently and can significantly control the estimation. Hence, the temperature would not be the only reason for the overestimation and/or underestimation of the modelling results. Figure 3 (d) to (f), represent the relative

error in terms of C_2, C_3, and C_4 selectivities. In contrast to CO_2 and CH_4, these components were underestimated. From Table 11, the order of reaction with respect to H_2 partial pressure ('m') for R. 3.6 to R. 3.10 was lower than 0.35. Since 'm' is a positive value for each of these reactions then it has direct influence on the rate of formation: decreasing 'm' would decrease the value of $P_{H_2}^m$ and as $P_{H_2}^m \propto R_i$, hence the rate of formation would gradually decrease.

From the optimization of the kinetic parameters, the CH_4 activation energy, corresponding to the Co/SiO_2 catalyst, was calculated to be 101.15 $kJ\ mol^{-1}$. This result was consistent with the literature values of 100−145 $kJ\ mol^{-1}$ on Co, Fe, and Ni catalysts [53-57] and also fell within the range estimated by van Santen *et al.* [58] using the DFT technique (100−170 $kJ\ mol^{-1}$). In contrast, this value was significantly higher than the value of 63−65 $kJ\ mol^{-1}$ for a Re−Co/ Al_2O_3 catalyst reported by Todic *et al.* [59] and much lower than the value of 177.4 $kJ\ mol^{-1}$ for a Co/Al_2O_3 catalyst estimated by Visconti *et al.* [60]. Nevertheless, further investigation revealed the fact that the CH_4 formation was overestimated by the model, as can be seen in Figure 3 (c). However, the activation energy value (101 $kJ\ mol^{-1}$) was higher than expected; which can be explained by its relatively higher estimated pre-exponential factor, being at least four orders of magnitude greater than the same parameter for other reactions, and the order of reaction of CO partial pressure, being of a lower negative value than expected.

From Table 6, R. 1 is responsible for predicting the rate of CH_4 formation. The reaction orders obtained for the partial pressures of CO and H_2 were determined to be −0.39 and 1.02, respectively (see Table 11). The negative order of reaction for CO partial pressure suggested a CO inhibition effect, by its adsorption on Co/SiO_2 catalyst, and a significant influence of partial pressure of H_2 on CH_4 formation. This implied that the CH_4 formation rate is controlled by the hydrogenation of either unassisted or H-assisted carbon species dissociation; but the CO adsorption on Co/SiO_2, as indicated by a negative number (−0.39), obstructs the steps of the hydrogenation process. These values were in line with the reported values for Co, Fe, Ru, and Ni catalysts; the reaction order for P_{CO} and P_{H_2} was in the range of −1.3 to −0.2 and 0.8 to 1.6 respectively, from the literature studies [55-57].

As pointed out, the P_{CO} has an inhibiting effect which means that the lower negative value of order of reaction would result in having less inhibition effects and therefore would estimate higher CH_4 formation and selectivity than is expected. From the CH_4 kinetic model and results, this was expected since a smaller negative and positive order for the P_{CO} and P_{H_2}, like −0.04 and 0.02 respectively, results in differential changes in the CH_4 formation rate with respect to partial pressures (see Figure 4 (a)).

It will be shown later that the prediction of CH_4 selectivities were improved considerably by using a mechanistic kinetic model (i.e. FT−III (RDS−2)), indicating that the discrepancy (overestimation) of CH_4 selectivity from the power-law kinetic was due to the estimated low value for the P_{CO} reaction order. Numerical analyses were continued to see the changes of CH_4, C_2, C_3, C_4, and C_{5+} rates of formation with respect to partial pressures of CO or H_2. Assuming the power-law kinetic model, the results were illustrated in Figure 4 (a-e). At a constant CO or H_2 partial pressure, increasing the partial pressure of H_2 or CO significantly raised or reduced the CH_4 rate, respectively (see Figure 4 (a)). Indeed, the changes in CO partial pressure shows a weaker influence on the CH_4 formation rate and its selectivity than that of H_2 partial pressure as it can be seen from the ratios of the CH_4 rate

changes to the variation of CO and H_2 partial pressure: $\Delta R_{CH_4}/\Delta P_{CO} = 2.96$ and $\Delta R_{CH_4}/\Delta P_{H_2} = 6.57$. This was not in agreement with a recent kinetic study of Re-promoted Co/CNT catalysts by Yang *et al.* [61] and Ma *et al.* [62] who reported that CO partial pressure has a greater impact on CH_4 formation rate and selectivity than H_2 partial pressure. This confirmed the above conclusion related to the reaction order of P_{CO} which was expected to be a higher negative value than the estimated value (i.e. -0.39), so that CO partial pressure would have more inhibiting effects on the CH_4 reaction rate.

It can be concluded that the power-law rate models have some limitations in the representation of catalytic reactions; that is to say, they could predict the rates almost well enough but only over a narrow range of experimental conditions; whereas, as it will be shown, Langmuir–Hinshelwood (LH) rate expressions, due to their fundamental origin, predict the rates over wider range of conditions. It was unclear which combination of a number of rate expressions and kinetics models proposed for syngas conversion and product selectivity, as well as the water gas shift reaction on cobalt, can provide the best representation of the available data. Nevertheless, section 3.2 contributed to this uncertainty mentioned above and provided adequate and comprehensive details regarding the kinetics of the FT reaction together with the WGS reaction. The results obtained from the numerical studies will be explained in section 4.2

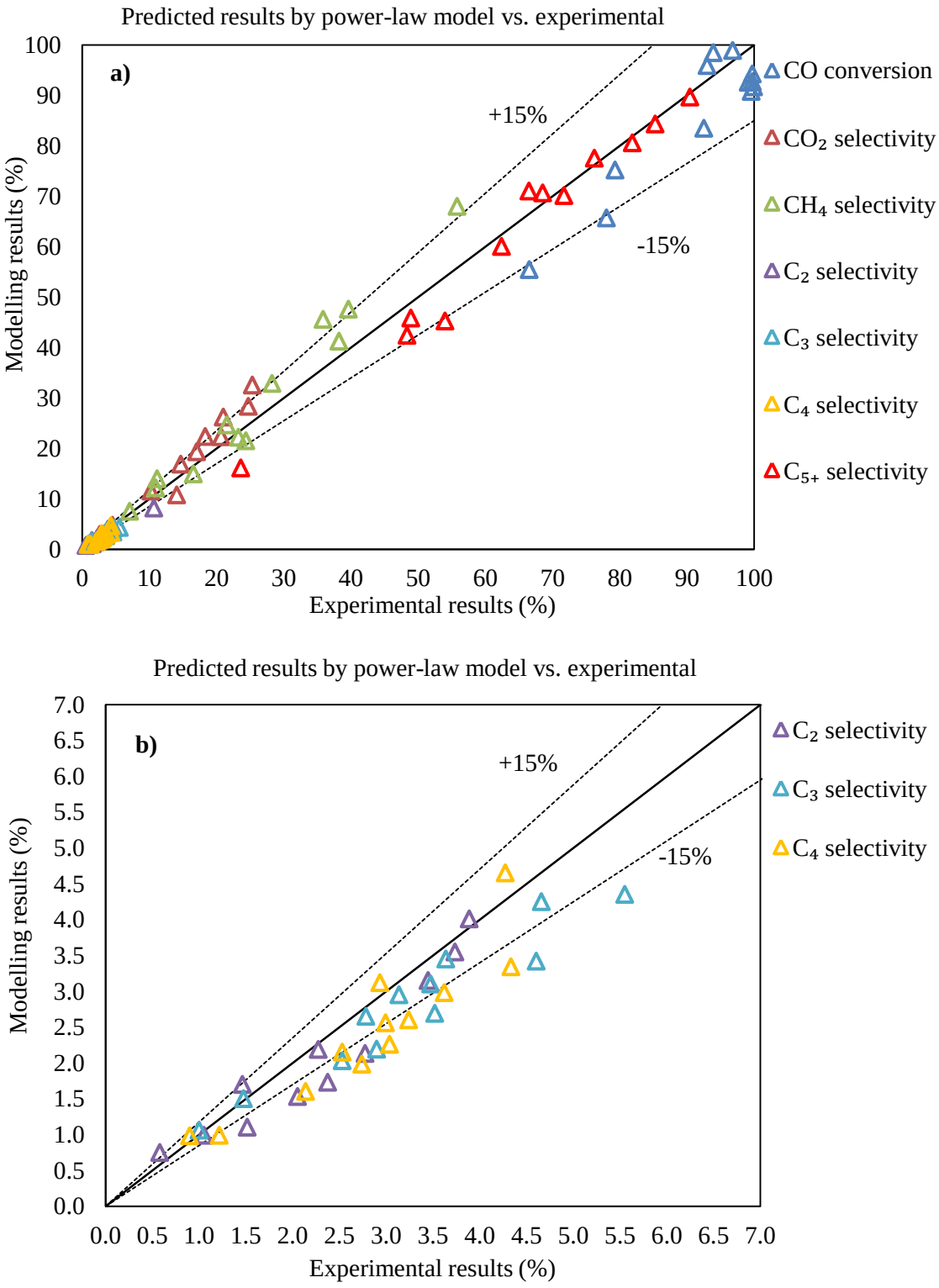

Figure 2 Parity plot and comparison of experimental data and predicted results obtained from power-law rate model, a) all existing components used for prediction such as CO conversion, CO_2, CH_4, C_2, C_3, C_4, and C_{5+} selectivities, b) products with a very low range selectivities e.g. C_2, C_3, and C_4.

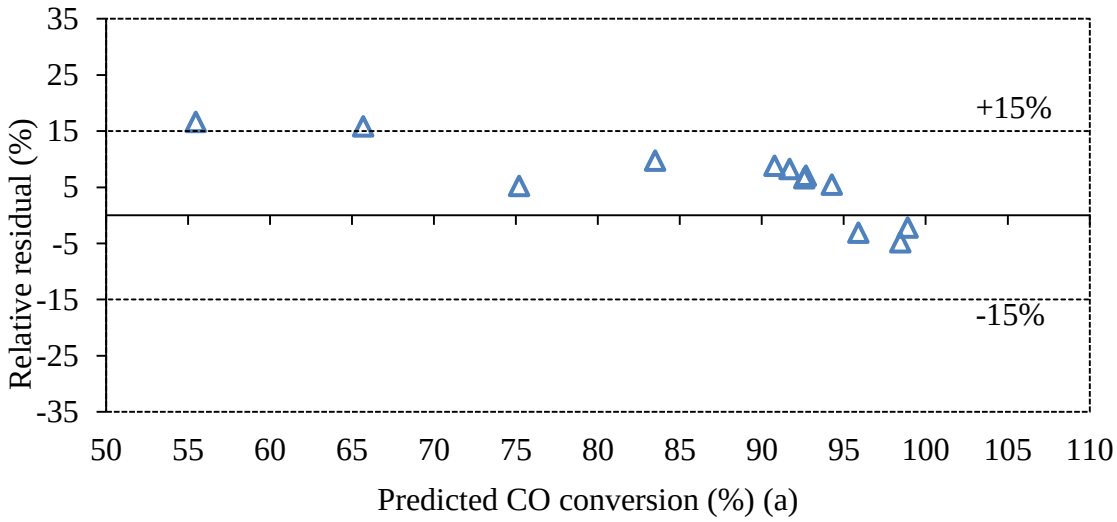
35
25
15
5
-5
-15
-25
-35
Relative residual (%)
+15%
-15%
50
55
60
65
70
75
80
85
90
95
100
105
110
Predicted CO conversion (%) (a)

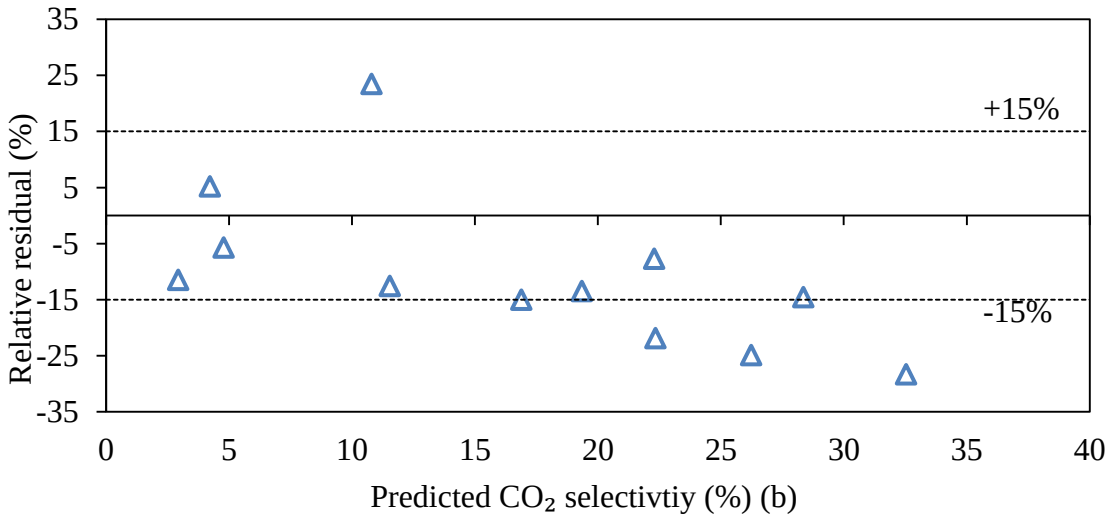
35
25
15
5
-5
-15
-25
-35
Relative residual (%)
+15%
-15%
0
5
10
15
20
25
30
35
40
Predicted CO2 selectivtiy (%) (b)

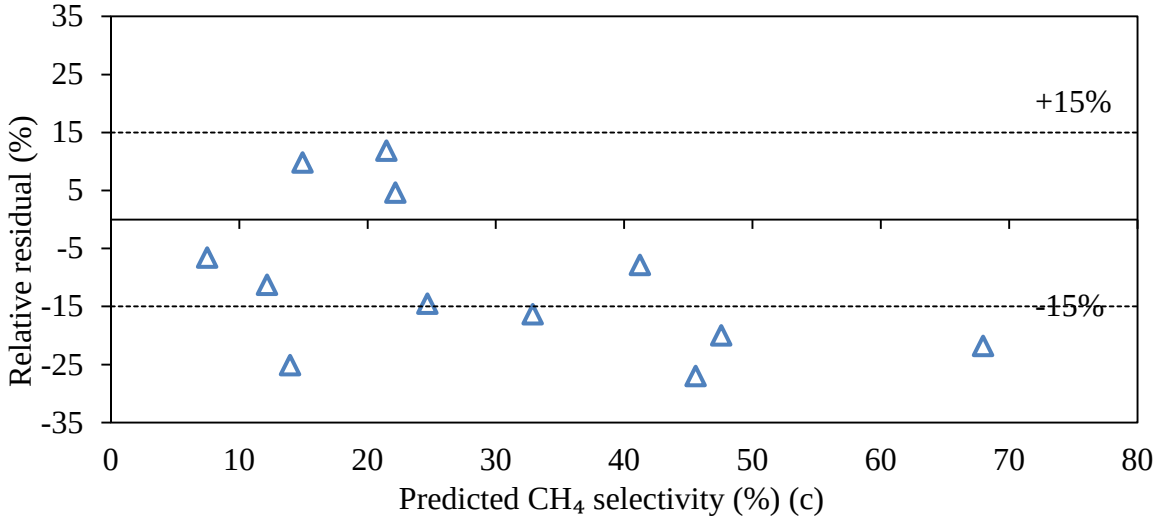
35
25
15
5
-5
-15
-25
-35
Relative residual (%)
+15%
-15%
0
10
20
30
40
50
60
70
80
Predicted CH4 selectivity (%) (c)

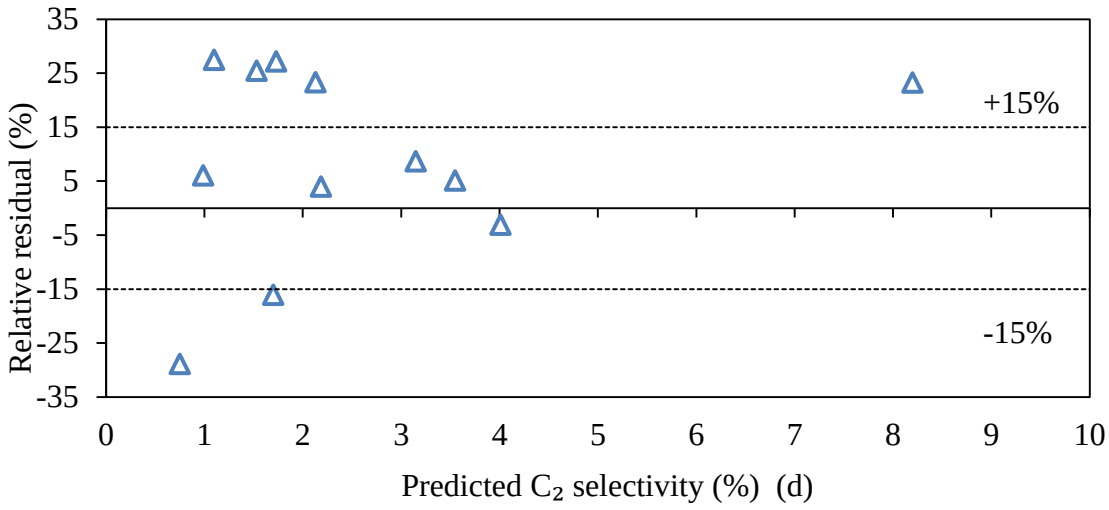
Relative residual (%)
35
25
15
5
-5
-15
-25
-35
+15%
-15%
0
1
2
3
4
5
6
7
8
9
10
Predicted C2 selectivity (%) (d)

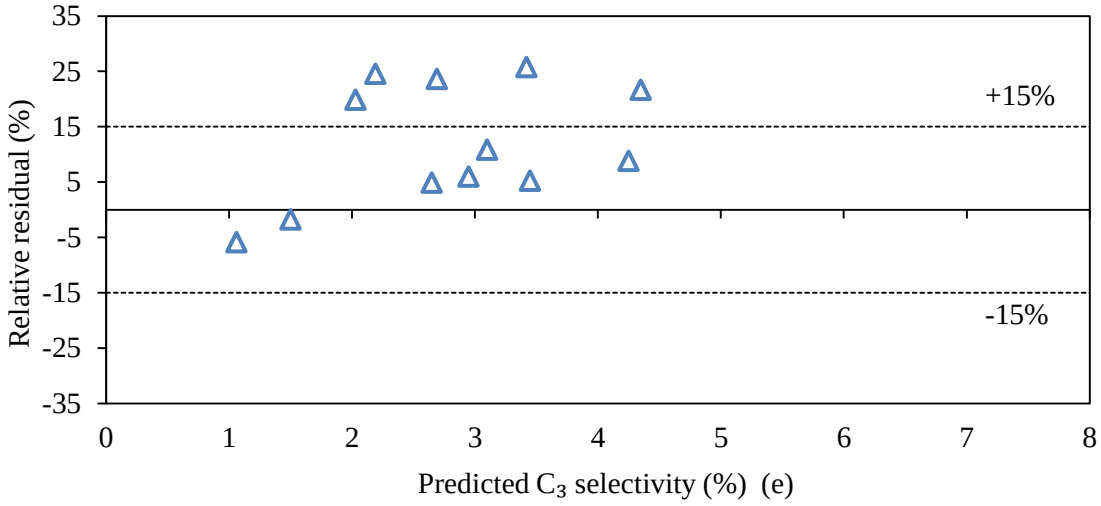
Relative residual (%)
35
25
15
5
-5
-15
-25
-35
+15%
-15%
0
1
2
3
4
5
6
7
8
Predicted C3 selectivity (%) (e)

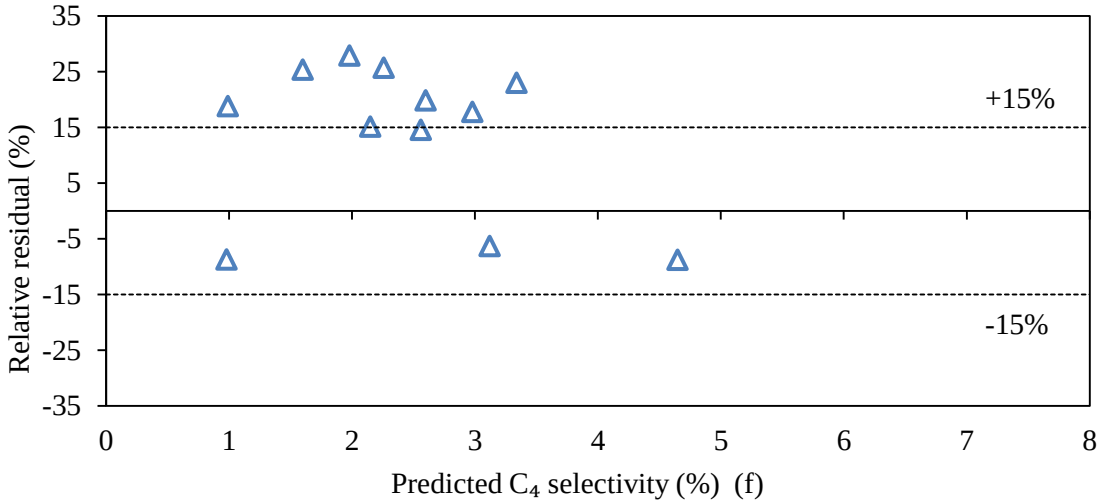
Relative residual (%)
35
25
15
5
-5
-15
-25
-35
+15%
-15%
0
1
2
3
4
5
6
7
8
Predicted C4 selectivity (%) (f)

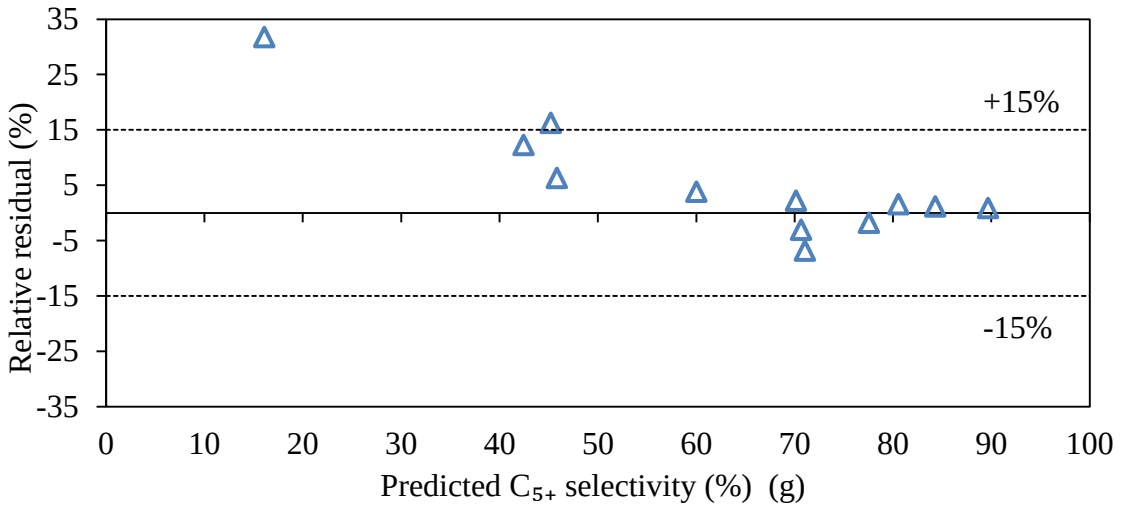

Figure 3 Relative residual percentages of experimental data and modelling values for each component; (a) CO conversion, (b) CO_2 selectivity, (c) CH_4 selectivity, (d) C_2 selectivity, (e) C_3 selectivity, (f) C_4 selectivity, (g) C_{5+} selectivity.

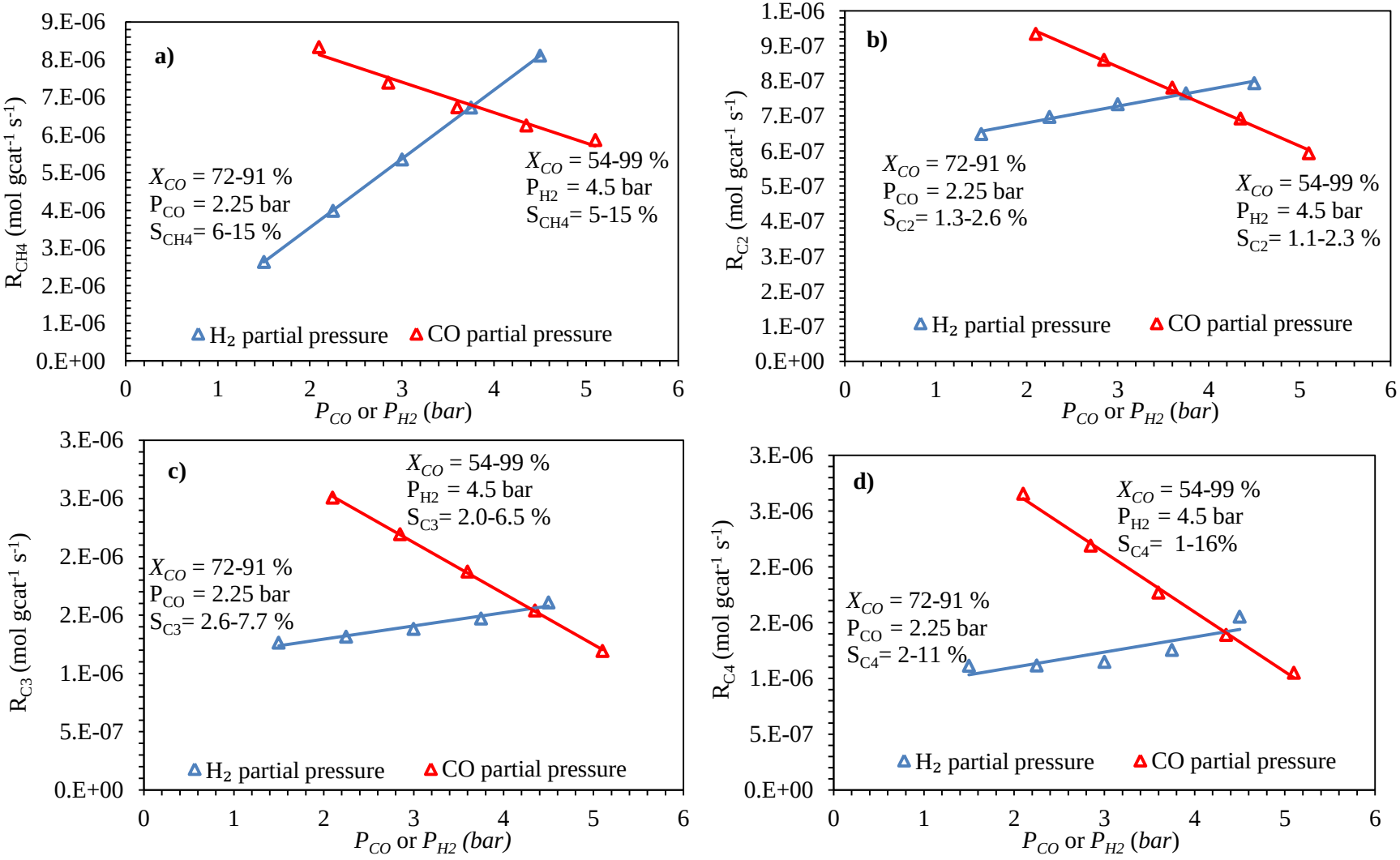

Figure 5-6 (*continued*).

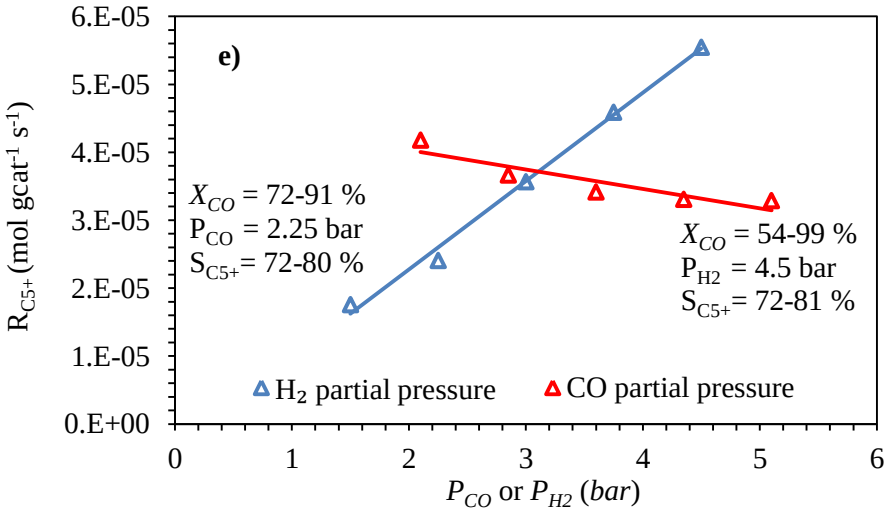

Figure 4 The influence of partial pressure of CO and H_2 on CH_4 formation rate over Co/SiO_2 catalyst. Constant reaction condition: T=503 (K), P=15 (bar) H_2/CO= 0.5-2, and GHSV=2400 ($Nm\ell$ (STP) g_{cat}^{-1} h^{-1}).

4.2. Kinetic results using mechanistic developed rate models

4.2.1. Comparison of results obtained based on different kinetic models

All the rate models developed in the present study, were employed to fit the experimental results collected in a mini-scale fixed bed reactor at a steady-state condition in the wide range of total pressure of 10-25 *bar*, temperature of 503-543 *K* and GHSV of 1800-3600 $Nm\ell$ (STP) g_{cat}^{-1} h^{-1}. The kinetic parameters involved in each model were estimated and the models were examined against the experiments to find the best mechanistic model that predicted the FT synthesis experimental data satisfactorily, as well as satisfying the consistency of the physicochemical properties and statistical analyses. Such information can provide guidelines for the design of more active and selective catalyst materials. The adequacy of the best developed kinetic model to describe the experimental data with respect to CO conversion as well as CO_2, CH_4, C_2H_4, C_2H_6, C_3H_6, C_3H_8, C_4H_{10}, C_5H_{12}, C_6H_{14}, C_7H_{16}, and C_{5+} (total liquid products) selectivities at all investigated operating conditions was demonstrated by the parity plot and relative residuals which will be discussed in the following section.

The results obtained from a total of 336 combined FT/WGS rate models (twenty-four FT rate model along with fourteen WGS rate model) indicated the errors between the experimental data and predicted data for the total of 144 data points ($N_{exp} \times N_{resp}$), consisted of twelve different chemical components mentioned above at twelve experimental conditions, falling in the range of 5.93−53.73%. The rival models were discriminated by determining relative residual (RR), MAPD and statistical analysis performed by an *F*-test. These criteria were essential procedures that should be accomplished to identify a model that has the best fit to the experimental data and has the most significant physically meaningful kinetic parameters [51].

Four out of eight proposed kinetic models, from FT−II to FT−V, were based on an H−assisted CO dissociation mechanism (see Table 7). Considering the model fit obtained from FT−II to FT−V, the results (see values of MAPD listed in Table 12) indicated the important role of H−assisted pathways as the kinetically-relevant CO dissociation steps on a cobalt catalyst at reaction conditions essential for significant chain initiation and

propagation. As can be seen from the elementary reaction steps in Table 7, these pathways (Model FT−II to FT−V) instead of directly dissociating CO−ψ into O-atoms and carbon atoms (as in model FT−I), gave precedence to the rejection of the O-atoms in CO as H_2O either via direct cleavage of species such as HCO−ψ and $CH_2O-\psi$ (see model FT–IV and FT–V respectively), or via the direct formation of OH−ψ precursors through either the COH−ψ species (see model FT–II) formed through interaction between CO−ψ and H−ψ or the HCOH−ψ species (see model FT–III) formed through interactions between chemisorbed H−ψ and HCO−ψ. Based on the adequacy of the results, these assisted pathways signified the exclusive CO activation paths on the surfaces of cobalt catalysts at the reaction conditions. The results obtained from H−assisted pathways indicated more accurate results than those obtained from FT−I reaction paths which requires quasi-equilibrated CO−ψ dissociation via unassisted routes. This may imply that the latter pathways may have higher energy barriers compared to the former. In fact, this was in agreement with a recent study [39] that employed Density Functional Theory (DFT) calculations which indicated high CO dissociation activation barriers with a value of 367 $kJ\ mol^{-1}$ on a CO-saturated cobalt surface, proposing that alternate paths for CO activation must be kinetically-accessible during FT synthesis catalysis i.e. H-assisted routes. In addition, direct CO dissociation was unfavourable compared with H-assisted dissociation, because of the higher MAPD value of the former (i.e. ranging from 12.72% to 39.25%) compared to the latter (i.e. ranging from 5.93% to 53.73%). Also, the best FT kinetic model was found to be model FT−III (i.e. H-assisted CO dissociation through formation of hydroxymethylene) with MAPD in a range of 5.9% to 31.38% for various WGS rate models. Also, there is evidence that an H-assisted pathway, which includes the initial addition of H−ψ to CO−ψ to form formyls (HCO−ψ), has a relatively much lower barrier (E_f = 138 $kJ\ mol^{-1}$) than direct CO−ψ dissociation on Co-saturated catalyst (E_f = 367 $kJ\ mol^{-1}$). Also the addition of another H−ψ to HCO−ψ gives HCOH−ψ with a relatively low activation energy barrier (E_f = 90 $kJ\ mol^{-1}$), followed by dissociation to CH-ψ and OH-ψ (E_f = 106 $kJ\ mol^{-1}$), in which both have relatively lower activation barriers, favourable pathways for monomer formation. Furthermore, the results indicate that the first H-addition to CO−ψ is equilibrated and the second H-addition is the kinetically-relevant step on Co catalysts. Comparing the predicted results by model FT−II to FT−I, the former model was closer to the experimental data that can be described by its lower forward energy barrier of 125 $kJ\ mol^{-1}$; compared to that of FT−I with CO dissociation activation barriers with a value of 367 $kJ\ mol^{-1}$, when COH−ψ intermediate was formed via the addition of another H−ψ to CO−ψ, signifying that the former route was more favourable for FT synthesis at typical process conditions. Nevertheless, this path was followed by dissociation to C−ψ and OH−ψ with a very high activation energy (i.e. E_f = 315 $kJ\ mol^{-1}$), indicating that it was an unfavourable pathway for monomer formation compared to model FT−III with lower energy barriers as explained above. Considering the FT−IV, the addition of H−ψ to CO−ψ produced formyl which dissociated to yield CH−ψ + O−ψ. In this path, CH−ψ species formed $CH_3-\psi$ via the addition of molecular hydrogen without forming the chain growth monomers ($CH_2-\psi$), causing the predicted result to deviate from the experiments and was kinetically unfavourable and unproductive in hydrocarbon synthesis. Considering FT−V, the addition of H−ψ to the C−atom in HCO−ψ formed $CH_2O-\psi$ with a 58 $kJ\ mol^{-1}$ barrier; $CH_2O-\psi$ species can be followed by dissociation to $CH_2-\psi$ and O−ψ in which the oxygen atom was rejected through this step possessing high activation barriers (E_f = 157 $kJ\ mol^{-1}$). A relatively higher error obtained by this model suggested that this route did not satisfactorily contribute as much as model FT−III to the FT growth mechanism. Alternate molecular H_2 assisted CO dissociation via direct reactions of H_2 (g) with

$CO-\psi$, forming either $C-\psi$ + H_2O or $HCOH-\psi$ comprising very high activation barriers, suggested that these steps do not contribute to hydrogenation or CO activation pathways. Hence, the last three kinetic models (i.e. FT−VI, FT−VII and FT−VIII) generally did not contribute to the FT growth mechanism compare to that of FT−III as was shown by their higher MAPD values.

The results listed in Table 12 indicated that the formate mechanism generally provided a better fit to the experimental data than the direct oxidation mechanism (see MAPD of model WGS-VI and WGS-VII). The results showed that the best WGS kinetics model achieved from the formate ($CHO_2-\psi$) mechanism (i.e. WGS-VII (RDS-4)) with MAPD of 5.93% is better in fitting to the experimental data than the best model from the direct oxidation mechanism (WGS-II (RDS-4)) with MAPD of 11.68%. Presumably, this can be explained by the fact that the dissociation of hydroxyl intermediate to adsorbed $O-\psi$ and $H-\psi$ species (which was step 3 in this reaction scheme) is not energetically favourable under FT synthesis reaction conditions. This conclusion was also supported by quantum calculation on transition metals that the hydroxyl dissociation is energetically unfavourable with a relatively high activation barrier [44]. In addition, in situ infrared spectroscopy confirmed the existence of formate ($CHO_2-\psi$) species on different surface catalysts [45, 46, 63]. Furthermore, the formate species was detected in situ by Fourier transform infrared spectroscopy (FTIR) in the diffuse reflectance mode (DRIFTS) over some transition metals. From the tabulated values (in Table 12) obtained for $CHO_2-\psi$ routes (WGS-VII) with different RDSs (RDS-4 and RDS-3), it can be seen that MAPD value was below 10% indicating satisfactory prediction of experimental results. The elementary steps CO adsorption, H_2O dissociation and H_2 formation (for instance steps 1, 2 and 5 in model WGS-I respectively, Table 8) are not the RDSs in the WGS reaction under the FT synthesis reaction conditions because of the large deviations of these models from the experimental data, hence their errors were not listed in Table 12. Considering the redox mechanism, the MAPD obtained for rate models of WGS-I with RDS-4 and RDS-5 were identical to that of WGS-III with RDS-4 and RDS-5, respectively. From the derived rate equations (Table A. 9 and Table A. 11), it was seen that the two kinetics models had the same rate expression formula despite having different reaction kinetic routes. This suggested that the kinetic models cannot discriminate whether surface oxygen intermediate formed directly from the dissociation of water molecule (step 2 in model WGS-III, Table 8) or via dissociation of hydroxyl species decomposed from water (steps 2 and 3 in model WGS-I, Table 8) if the RDS is the formation of CO_2 from either by adsorbed $O-\sigma$ into $CO-\sigma$ or decomposition of $CO_2-\sigma$ from the catalyst surface.

The minimum error (i.e. 5.93%) was achieved when the adsorbed CO molecule on a catalyst surface dissociated via the H-assisted route. In this reaction pathway, the formyl and hydroxymethylene intermediates ($HCO-\psi$ and $HCOH-\psi$) formed via two successive hydrogenation of the chemisorbed CO and the produced $HCO-\psi$ in which the second hydrogenation was assumed to be the slowest step and kinetically considered to be more relevant compare to other elementary steps in this route (RDS-2). Considering the WGS reaction kinetics, the formate mechanism in which the formate species was formed through the reaction between adsorbed CO intermediate and a hydroxyl surface species ($-OH$), was considered as the most kinetically relevant route [64]. The above-mentioned novel reaction mechanisms for the formation of paraffins and olefins' products as well as carbon dioxide are illustrated in Figure 5.

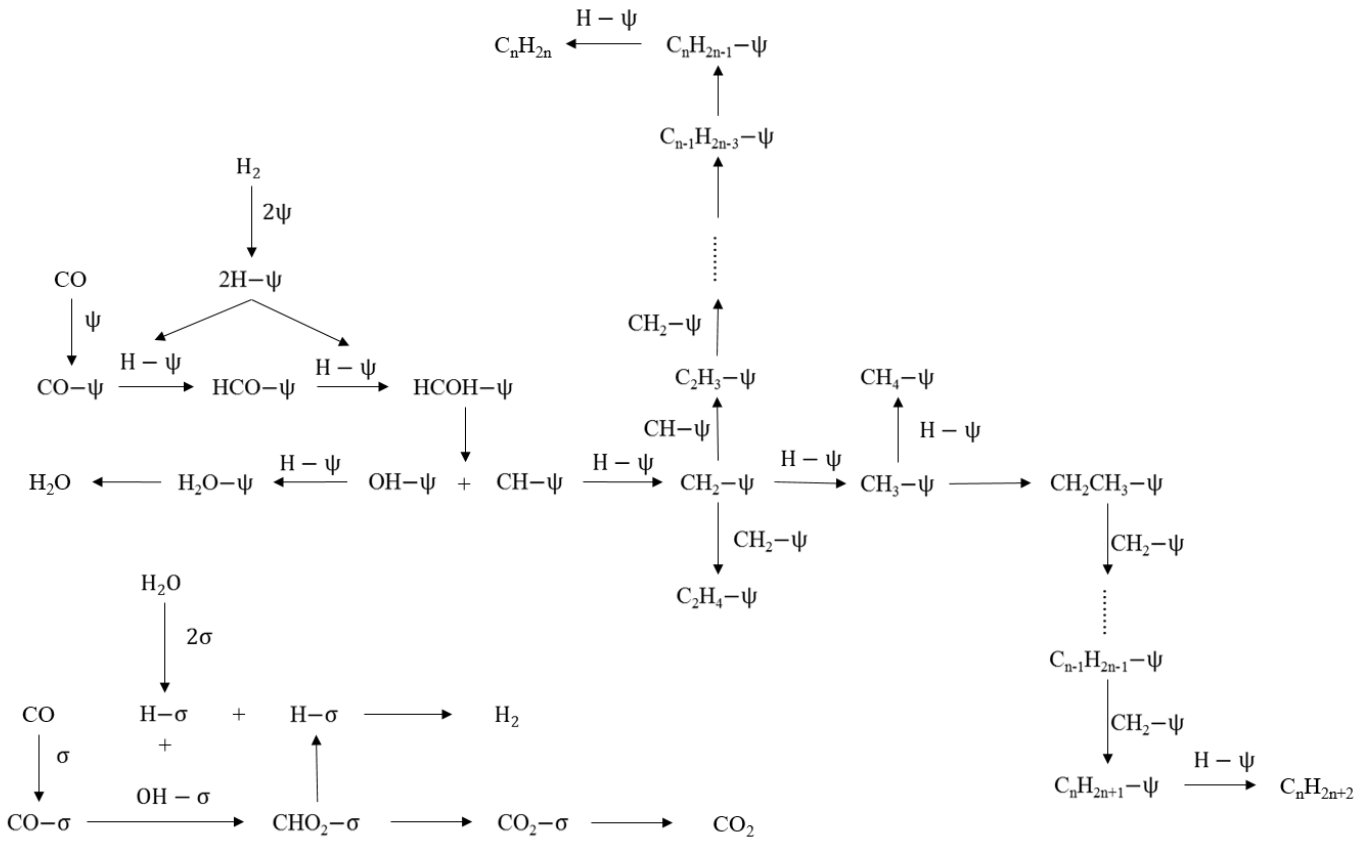

Figure 5 Reaction mechanism for the formation of paraffinic hydrocarbons (C_nH_{2n+2}) via alkyl species, olefins' products (C_nH_{2n}) via vinyl intermediates and WGS reaction via formation of formate intermediates (developed combined FT/WGS mechanism).

Table 12 Values of MAPD obtained from optimization of each proposed FT/WGS combination rate model: twenty-four FT reaction rate models with fourteen WGS reaction rate models in total were considered in the present thesis (to be continued on the next page)

No.	Reaction model	1 FT−I (RDS-1)	2 FT−I (RDS-2)	3 FT−I (RDS-3)	4 FT−II (RDS-1)	5 FT−II (RDS-2)	6 FT−II (RDS-3)	7 FT−III (RDS-1)	8 FT−III (RDS-2)	9 FT−III (RDS-3)	10 FT−IV (RDS-1)
1	WGS-I (RDS-3)	23.85	29.69	23.83	32.44	30.15	28.18	20.30	14.21	22.62	38.30
2	WGS-I (RDS-4)	25.43	31.15	25.15	34.31	31.62	30.06	20.95	14.95	24.42	40.89
3	WGS-II (RDS-3)	22.67	28.42	22.49	30.65	28.71	27.01	18.32	13.95	21.17	36.33
4	WGS-II (RDS-4)	19.15	25.56	19.80	27.12	26.65	23.95	15.32	11.68	18.16	32.86
5	WGS-II (RDS-5)	21.12	27.01	21.05	28.66	27.70	25.03	17.12	12.65	19.82	35.06
6	WGS-III (RDS-3)	27.36	32.77	26.75	35.62	32.98	31.26	21.65	16.95	26.22	43.86
7	WGS-III (RDS-4)	25.43	31.15	25.15	34.31	31.62	30.06	20.95	14.95	24.42	40.89
8	WGS-IV (RDS-3)	30.21	35.72	30.25	38.28	36.25	33.72	22.63	18.35	29.04	46.38
9	WGS-V (RDS-3)	31.36	37.62	31.99	39.86	37.26	35.33	22.93	20.16	30.33	49.29
10	WGS-V (RDS-4)	33.21	39.25	33.02	40.90	38.53	36.56	24.50	21.60	31.38	51.46
11	WGS-VI (RDS-3)	17.33	23.85	17.96	25.84	24.66	22.83	13.95	11.25	16.67	31.19
12	WGS-VI (RDS-4)	15.95	22.15	15.96	24.25	23.57	21.08	13.60	10.12	14.67	28.75
13	WGS-VII (RDS-3)	14.68	20.33	14.29	22.29	21.58	19.64	11.88	8.93	12.98	26.37
14	WGS-VII (RDS-4)	12.72	19.33	13.27	20.63	19.81	18.58	9.50	5.93	11.25	24.36

No.		11	12	13	14	15	16	17	18	19	20	21	22	23	24
	Reaction model	FT−IV (RDS-2)	FT−IV (RDS-3)	FT−V (RDS-1)	FT−V (RDS-2)	FT−V (RDS-3)	FT−VI (RDS-1)	FT−VI (RDS-2)	FT−VI (RDS-3)	FT−VII (RDS-1)	FT−VII (RDS-2)	FT−VII (RDS-3)	FT−VIII (RDS-1)	FT−VIII (RDS-2)	FT−VIII (RDS-3)
1	WGS-I (RDS-3)	36.02	39.87	25.07	21.41	25.57	29.24	26.54	30.74	36.57	32.31	40.75	36.16	32.09	36.02
2	WGS-I (RDS-4)	37.43	42.79	26.76	22.49	27.55	31.48	27.78	31.97	38.89	34.09	42.48	38.12	33.27	37.43
3	WGS-II (RDS-3)	33.11	37.18	23.11	19.96	23.99	28.16	24.59	29.42	34.65	29.52	39.74	34.78	29.55	33.11
4	WGS-II (RDS-4)	29.83	33.68	19.96	16.18	21.37	23.55	21.59	25.96	31.65	26.71	34.92	30.35	24.87	29.83
5	WGS-II (RDS-5)	31.48	35.84	21.42	18.02	22.42	25.89	22.73	28.37	32.87	28.34	37.31	32.68	26.64	31.48
6	WGS-III (RDS-3)	38.93	44.86	28.27	24.18	28.62	32.82	29.41	33.17	40.09	35.61	43.53	40.64	35.45	38.93
7	WGS-III (RDS-4)	40.31	47.83	29.36	26.05	30.41	35.07	30.86	35.16	41.31	37.59	45.67	41.81	36.91	40.31
8	WGS-IV (RDS-3)	42.47	50.54	30.56	27.63	32.26	36.37	32.67	37.92	43.35	40.47	47.55	43.96	38.79	42.47
9	WGS-V (RDS-3)	43.97	52.63	31.89	28.90	33.30	38.28	33.69	40.63	44.43	43.04	49.47	45.46	40.94	43.97
10	WGS-V (RDS-4)	46.37	53.73	33.19	30.53	34.66	40.34	35.09	42.47	45.69	45.12	51.15	46.47	43.43	46.37
11	WGS-VI (RDS-3)	27.09	32.14	18.46	14.97	19.75	22.40	20.22	24.18	30.21	25.51	32.45	27.78	23.29	27.09
12	WGS-VI (RDS-4)	25.29	30.82	17.13	13.46	18.15	20.84	18.93	23.13	28.79	23.70	29.63	26.63	20.73	25.29
13	WGS-VII (RDS-3)	22.67	29.79	15.63	12.12	16.85	19.31	17.32	21.17	25.82	21.44	27.57	24.01	18.96	22.67
14	WGS-VII (RDS-4)	20.65	27.65	13.69	10.50	15.27	16.58	15.58	19.52	23.58	20.14	26.50	21.52	17.65	20.65

4.2.2. **Goodness of model prediction compared to available literature**

The best mechanistically developed model for complete FT synthesis (i.e. model FT−III with RDS-2/WGS-VII with RDS-4) was compared to the experimental values with respect to CO conversion, as well as the selectivity of CO_2, CH_4, C_2H_4, C_2H_6, C_3H_6, C_3H_8, C_4H_{10}, C_5H_{12}, C_6H_{14}, C_7H_{16}, and C_{5+} species. The parity plot that compares experiments against modelling prediction is presented in Figure 6 (a) and (b). These figures show that the relative error percentage between the model and experimental data of almost all data points was within $\pm$10%. The best mechanistically developed model for complete FT synthesis was compared to the most recent findings in detailed kinetics of FT synthesis with respect to CO conversion and CO_2 selectivity, as well as the total experimental responses including both conversion and selectivities. The best complete model estimated the CO conversion at all process conditions with a mean relative error percentage of 3.3%. This value was lower than the lowest error reported by Yang et al (see Figure 7 (b)) and Teng et al (see Figure 7 (a)), Atashi *et al.* [27] with 9.2%, Mirzaei *et al.* [65] with 9.7%, Visconti *et al.* [31, 60] with 14.5% and 7.3% all accounted for CO conversion and were also better than that estimated for the power-law kinetic model developed in section 3.1, with 7.8% error. In addition, the best model predicted an average relative error of 10.3%, in terms of CO_2 selectivity, which was comparable with that obtained by Yang *et al.* [66] with the error of 10.04% and Teng *et al.* [43, 67] with errors of 7.53% and 11.93% respectively. In fact, the study conducted by Teng *et al.* [43] was solely based on the WGS reaction mechanism and as a result twelve WGS rate models were derived with an error in a range of 7.85-23.44%.

In addition, the best model estimated all experimental responses (including the conversion and selectivities) at all process conditions with a MAPD value of 5.93%, whereas Yang *et al.* [66] reported the value of 18.6% and 19.2% for their two best models considering combined FT and WGS mechanisms. Even the values of 33.99% and 35.52% reported by Wang *et al.* [68] and Teng *et al.* [67] respectively, was based on the total syngas consumption rate and product selectivity. The error obtained by the proposed mechanistic model was even better than that obtained by the power-law kinetic model developed in section 3.1, with a value of 13.23%. Another significant point was the ability of the model to predict the CO conversion, lighter product formation and CO_2 selectivity as a function of pressure and temperature. The model indicates a significant improvement compare to the previously developed rate model by the power-law kinetic rate expression (in section 3.1), that underestimated the CO_2, C_3, C_4, selectivity at a high temperature range ($T > 528$) and overestimated CO conversion and CH_4 selectivity at a low temperature range ($T < 528$).

In addition, the details of product selectivities were predicted by the developed model which are illustrated in Figure 9, Figure 10, and Figure 11 for all experimental runs performed at different operating conditions with respect to temperature, pressure and space velocity. These figures show the model's fit in terms of n-paraffins and α-olefins with carbon atom number in the range of available hydrocarbons obtained from quantitative analysis of experimental studies. The model's fit was compared to an ASF product distribution model and the deviations of the experimental results in term of n-paraffin and α-olefins from the ASF model are clearly shown; while a satisfactory agreement with the developed kinetic model FT−III (RDS-2) with WGS-VII (RDS-4) is signified. Indeed, the change of the ASF slope with a growing carbon atoms number, as well as the high selectivity to methane and low ethylene selectivity, were the main causes of the typical deviations of the

experimental distribution from the ASF model (see in Figure 9, Figure 10, and Figure 11). In contrast, the postulated mechanism and rate models could overcome the deviations of the experimental data, by adopting separate reaction sequences for methane and ethylene formation, and by postulating the combined alkyl/alkenyl mechanisms, in which the alkyl represents the paraffinic compounds and the alkenyl expressing the olefin hydrocarbons. As a consequence, separate rate constants (i.e. k_{meth} and k_{eth}) were defined for the reaction sequences that were responsible for the formation of these two components; while only one representative rate constants was introduced for the termination steps of both n-paraffin and α-olefin (i.e. $k_{t,par}$ and $k_{t,olef}$). These values are listed in Table 14 and will be discussed in detail in section 4.2.3.

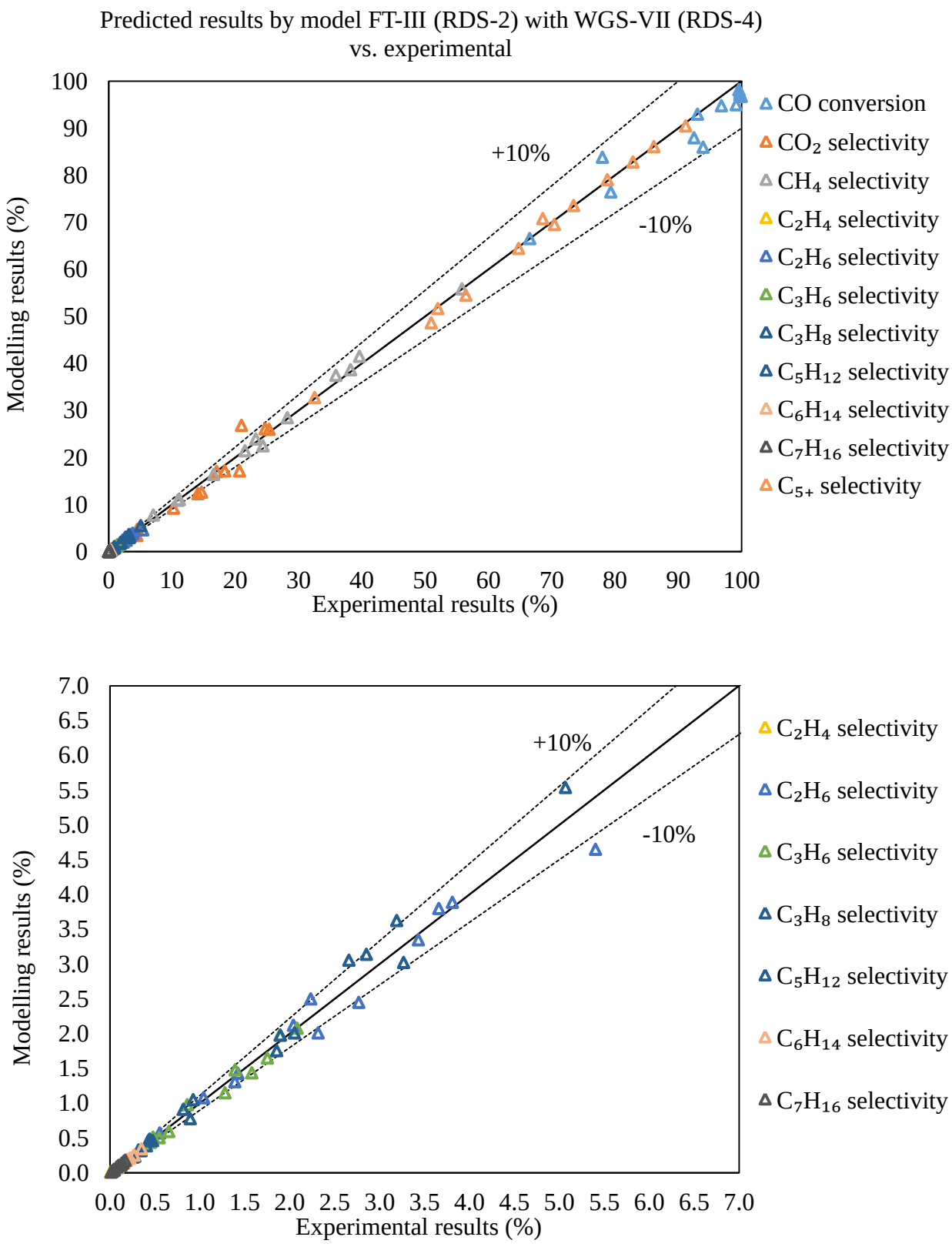

Figure 6 Parity plot: modelling prediction against experiments using best kinetic model (i.e. FT−III (RDS-2) with WGS-VII (RDS-4)).

Table 13 Model calibration against experimental data using kinetic model FT−III (RDS-2) with WGS-VII (RDS-4)

Experimental Run	Experiments vs. predictions	x_{CO}	S_{CO_2}	S_{CH_4}	$S_{C_2H_4}$	$S_{C_2H_6}$	$S_{C_3H_6}$	$S_{C_3H_8}$	$S_{C_4H_{10}}$	$S_{C_5H_{12}}$	$S_{C_6H_{14}}$	$S_{C_7H_{16}}$	$S_{C_{5+}}$
Test-01	Experiment	78.04	4.52	7.063	0.028	0.554	0.655	0.346	0.175	0.100	0.090	0.047	91.18
	Prediction	83.85	4.75	7.76	0.026	0.573	0.596	0.325	0.187	0.105	0.085	0.040	90.533
Test-02	Experiment	79.34	4.46	16.588	0.075	1.390	1.892	0.893	0.342	0.258	0.155	0.132	78.82
	Prediction	76.47	3.45	16.4	0.072	1.310	1.980	0.780	0.371	0.227	0.143	0.134	79.087
Test-03	Experiment	66.55	2.63	11.170	0.095	1.422	2.085	0.817	1.576	0.120	0.085	0.013	82.84
	Prediction	66.55	2.63	11.1	0.102	1.430	2.080	0.914	1.505	0.113	0.089	0.013	82.869
Test-05	Experiment	93.03	14.1	23.271	0.042	2.235	1.282	1.856	0.873	0.443	0.186	0.077	70.44
	Prediction	93.00	12.35	23.99	0.047	2.500	1.150	1.758	0.978	0.486	0.192	0.084	69.577
Test-06	Experiment	99.15	14.68	10.962	0.012	1.041	0.548	0.927	0.334	0.154	0.069	0.022	86.18
	Prediction	95.00	12.63	10.9	0.012	1.080	0.507	1.050	0.348	0.165	0.075	0.021	86.103
Test-07	Experiment	92.52	10.25	24.383	0.060	2.316	1.579	1.898	1.172	0.407	0.269	0.120	68.59
	Prediction	88.00	9.24	22.5	0.058	2.010	1.438	1.978	1.188	0.389	0.255	0.110	70.828
Test-10	Experiment	96.81	17.05	38.249	0.080	3.812	1.393	3.268	1.174	0.475	0.352	0.170	52.02
	Prediction	94.78	17.05	38.68	0.077	3.890	1.480	3.025	1.168	0.465	0.348	0.181	51.6804
Test-11	Experiment	99.96	20.7	21.549	0.010	2.044	0.479	2.054	0.382	0.085	0.066	0.044	73.48
	Prediction	96.80	17.17	21.43	0.011	2.120	0.514	2.010	0.329	0.091	0.062	0.050	73.5857
Test-12	Experiment	99.74	18.34	28.254	0.008	2.770	0.862	2.660	0.647	0.277	0.178	0.100	64.80
	Prediction	97.58	17.15	28.46	0.008	2.450	0.980	3.056	0.599	0.240	0.172	0.105	64.4474
Test-13	Experiment	93.95	21.01	39.656	0.078	3.660	1.753	2.854	1.026	0.346	0.223	0.145	50.97
	Prediction	86.00	26.85	41.53	0.076	3.800	1.650	3.140	1.150	0.319	0.213	0.145	48.654
Test-14	Experiment	99.74	24.75	35.888	0.018	3.433	0.449	3.192	0.549	0.318	0.125	0.027	56.47
	Prediction	97.12	26.12	37.5	0.017	3.350	0.470	3.627	0.526	0.331	0.138	0.029	54.51
Test-15	Experiment	99.59	25.36	55.817	0.021	5.404	0.451	5.068	0.701	0.427	0.073	0.024	32.56
	Prediction	98.23	26.03	55.89	0.023	4.650	0.440	5.540	0.687	0.465	0.077	0.022	32.793

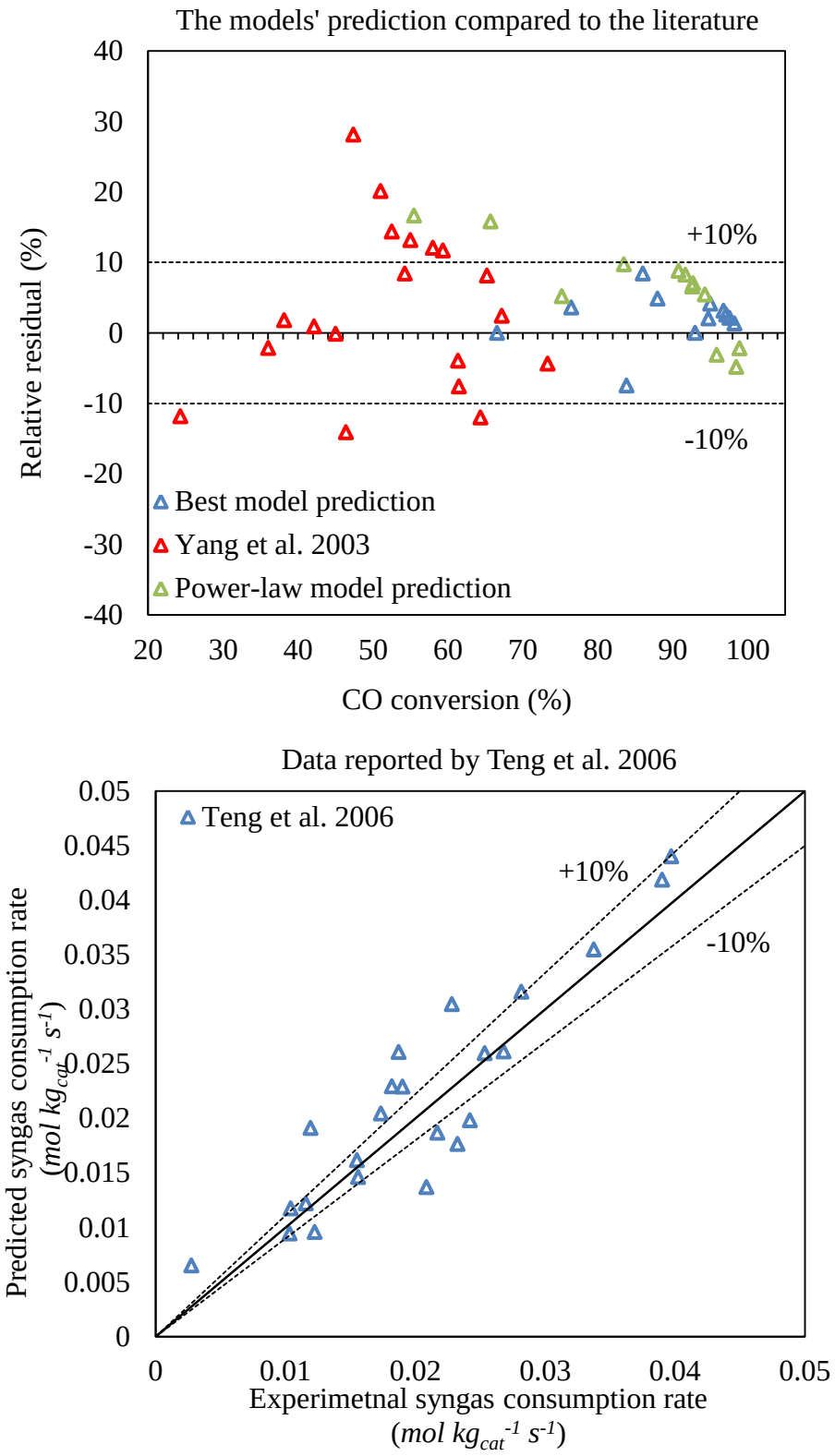

Figure 7 Comparison of calculated and experimental CO conversion obtained by the FT−III (RDS-2)/WGS-VII (RDS-4) mechanistic model, developed empirical power-law model, and those reported by Yang *et al.* [66] and Teng *et al.* [43, 67].

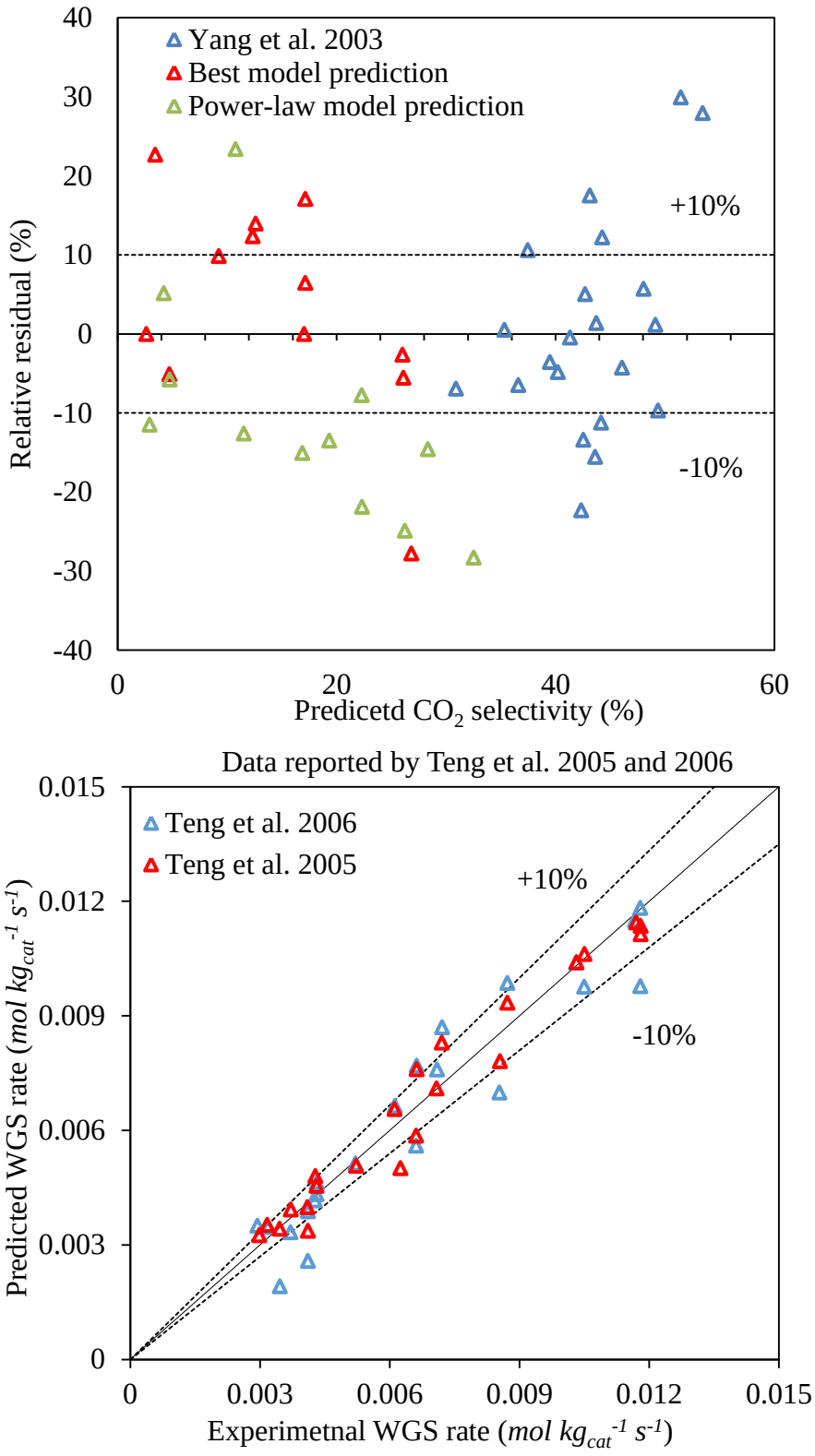

Figure 8 Comparison of calculated and experimental CO_2 selectivity obtained by the FT−III (RDS-2)/WGS-VII (RDS-4) model, power-law model, and those reported by Yang *et al.* [66] and Teng *et al.* [43, 67].

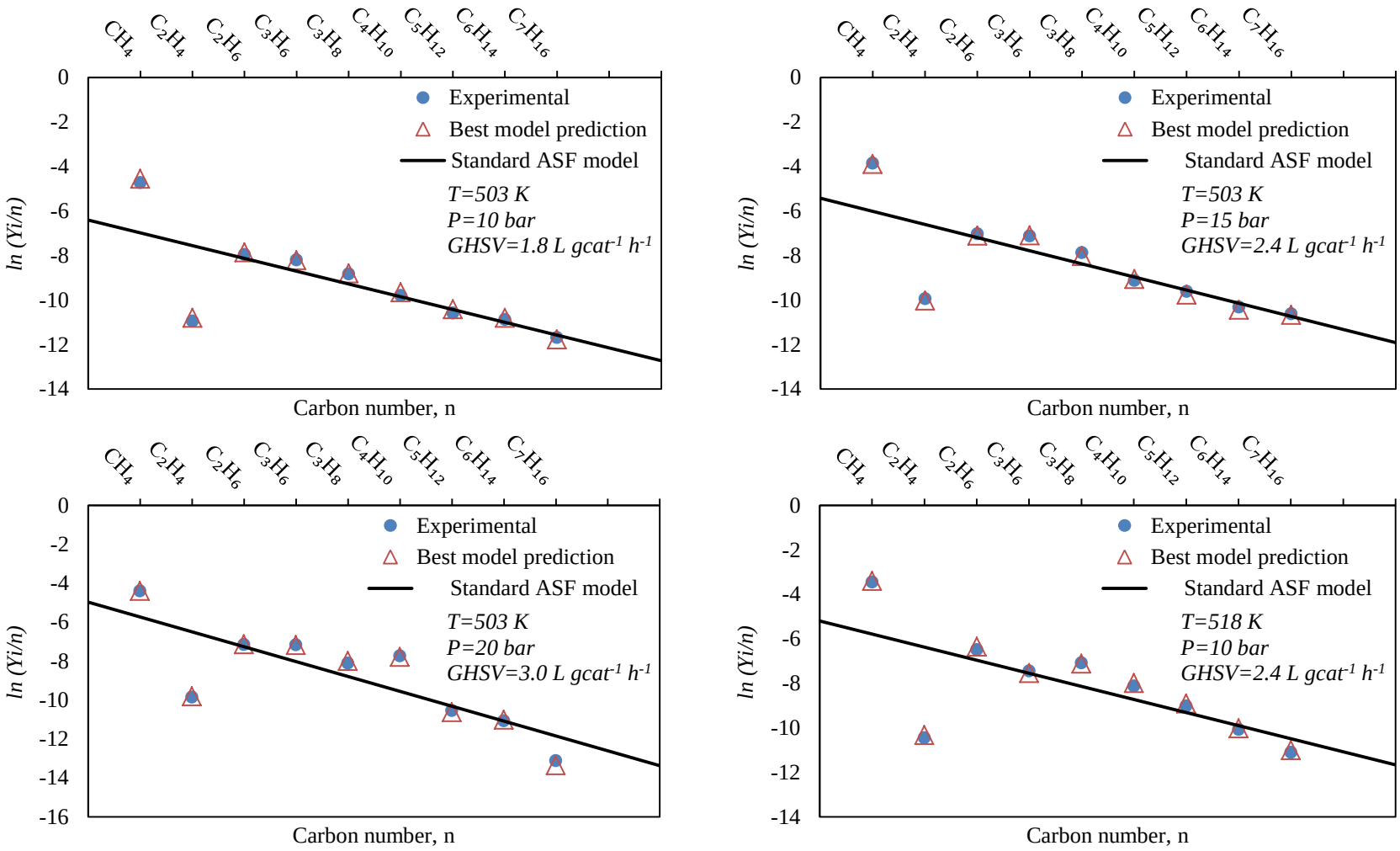

Figure 9 Product distribution comparison between FT−III (RDS-2)/WGS-VII (RDS-4) model prediction, standard ASF model, and the experimental results, logarithmic of mole-fraction (Y_i) to carbon number (n) ratio versus n; a): Test-01, b): Test-02, c): Test-03, d): Test-05.

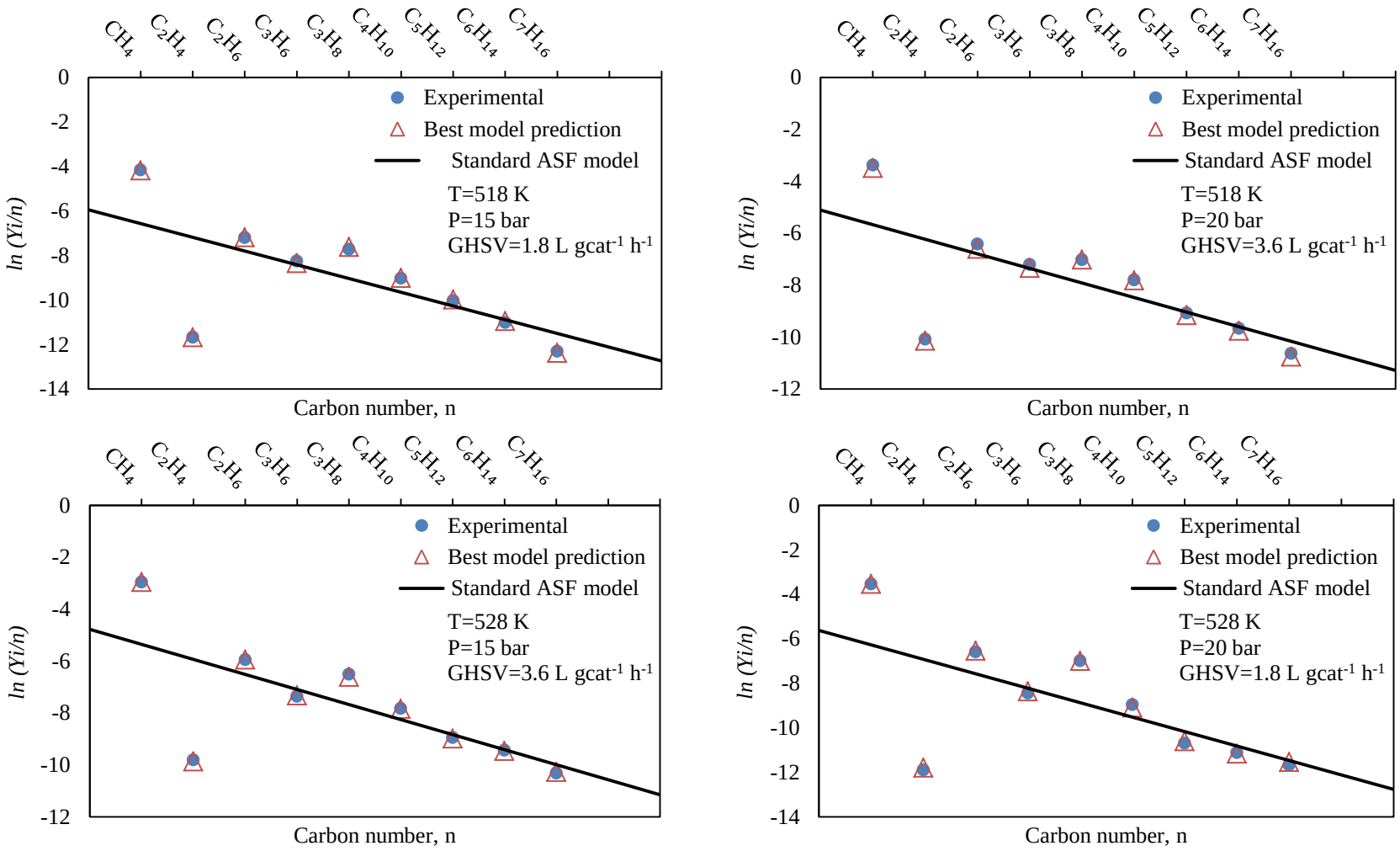

Figure 10 Product distribution comparison between FT−III (RDS-2)/WGS-VII (RDS-4) model prediction, standard ASF model, and the experimental results, logarithmic of mole-fraction (Y_i) to carbon number (n) ratio versus n; a): Test-06, b): Test-07, c): Test-10, d): Test-11.

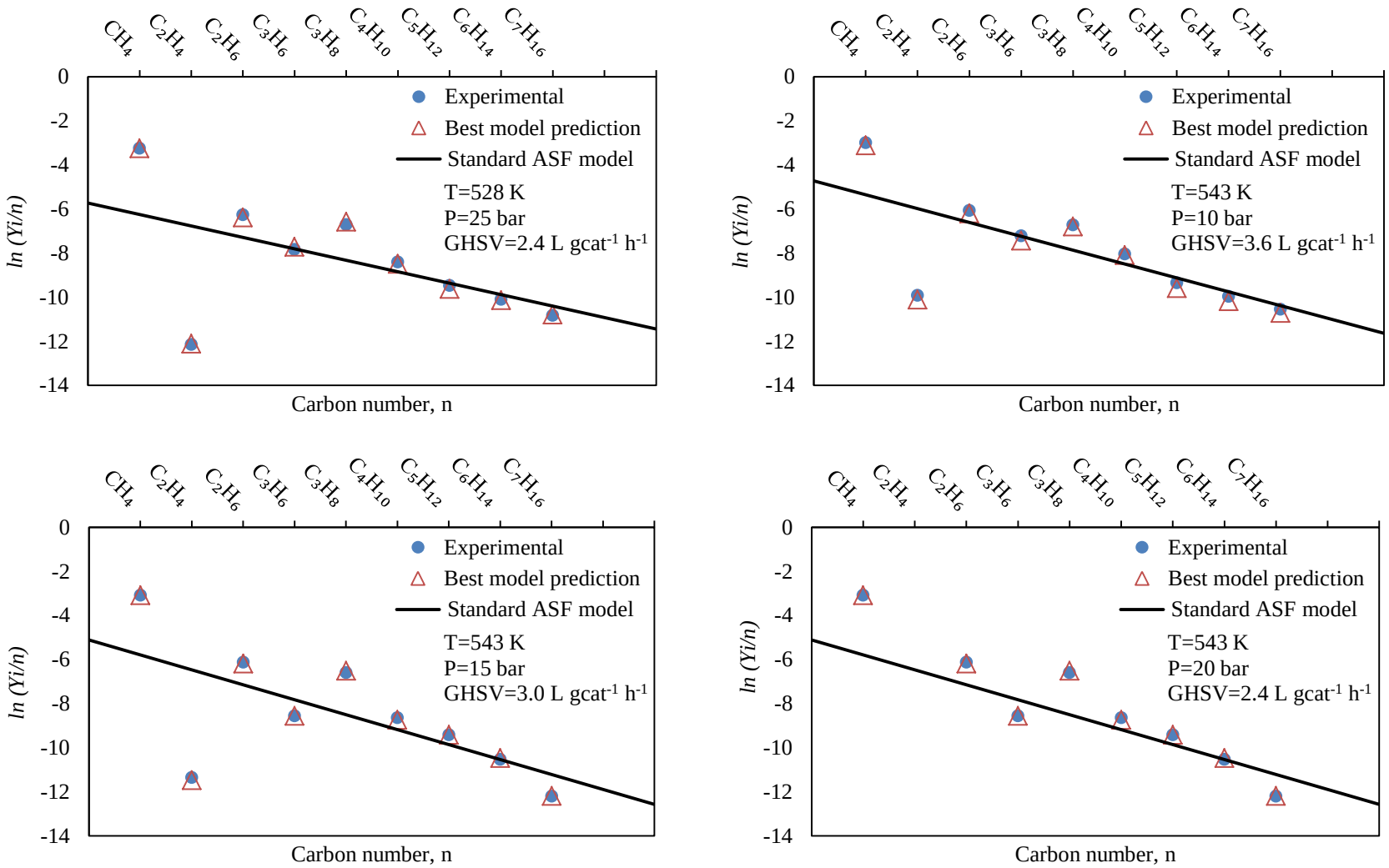

Figure 11 Product distribution comparison between FT−III (RDS-2)/WGS-VII (RDS-4) model prediction, standard ASF model, and the experimental results, logarithmic of mole-fraction (Y_i) to carbon number (n) ratio versus n; a): Test-12, b): Test-13, c): Test-14, d): Test-15.

4.2.3. **Evaluation of kinetic parameters**

The estimated kinetic parameters for the comprehensive (combined) FT−III (RDS-2) with WGS-VII (RDS-4) kinetic model over a Co/SiO_2 catalyst, assuming that the slowest paths (RDSs) in the FT reaction model are steps 4, 8-15 and that of the WGS reaction is step 4, are listed in Table 14. It is worth noting that the numerical value of each parameter in this work, in addition to obtaining a satisfactory fit of the experimental data, was physically relevant and in good agreement with the expectations and literature studies. For instance, the adsorption equilibrium constant of hydrogen (K_{H_2}) was obtained three orders of magnitude lower than that of carbon monoxide (K_{CO}), which is comparable with the data reported by [69] with K_{CO}/K_{H_2} of $1.78/4.81\times10^{-3}$ (K_{CO} was three order of magnitude higher than K_{H_2}). This is related to the strong CO adsorption over a Co catalyst which was also indicated by the negative reaction order for CO partial pressure, as shown in section 4.1 by the empirical power-law rate expressions.

In addition, both the rate of reaction and the rate constant ($R_{i,par}$ and $k_{i,par}$) of step 8 in the FT−III (RDS-2) rate model, representing the formation of surface methyl species (chain initiator) in the chain initiation step, were found to be few orders of magnitude lower than the similar parameters (R_4 and k_4) for the reaction step 4, leading to the formation of $CH_2{-}\psi$ species i.e. the chain growth monomer. This signifies the fact that the latter reaction step is faster than the former reaction; therefore the chain initiation step was a more kinetically-relevant step than the CO activation process for the overall reaction scheme. However, $R_{i,par}$ and $k_{i,par}$ were found to be three orders of magnitude higher than those of ($R_{g,par}$ and $k_{g,par}$) in the propagation step (step 12); which in fact depended on the carbon atom number of the growing intermediate ($C_nH_{2n+1}{-}\psi$). Indeed, the paraffins and olefins' formation rates ($R_{paraffins}$ and $R_{olefins}$) were found to be slower than the rate of formation of chain growth (by one order of magnitude), implying that the products' formation steps (steps 13 and 15) are the RDSs in the overall FT process over a Co/SiO_2 catalyst. To sum up, it can be concluded that:

$$k_4 \gg k_8 = k_{CH_3} = k_{i,par} =\gg k_{12} = k_{g,par} \gg k_{13} = k_{paraffins}\ \&\ k_{15} = k_{olefins}$$

$$R_4 \gg R_8 = R_{CH_3} = R_{i,par} =\gg R_{12} = R_{g,par} \gg R_{13} = R_{paraffins}\ \&\ R_{15} = R_{olefins}$$

The activation energies of the chain initiation, propagation and termination steps for the alkyl route, leading to the formation of paraffins, were significantly lower than those of the alkenyl route, leading to the formation of olefins. This is in line with the expectations as the paraffins formation rates were significantly higher than those of the olefins (considering the same carbon atom number) obtained at all experiment conditions. The activation energy for the chain growth step of the alkyl route ($E_{g,par}$) was predicted to be 82.57 $kJ\ mol^{-1}$. This was lower than the activation energies for that of the alkenyl route ($E_{g,olef} = 88.31$ kJ mol^{-1}) and the activation energies for the chain initiation ($E_{i,par} = 90.22\ kJ\ mol^{-1}$ and $E_{i,olef} = 95.34\ kJ\ mol^{-1}$) and termination ($E_{t,par} = 95.63\ kJ\ mol^{-1}$ and $E_{t,olef} = 100.22\ kJ\ mol^{-1}$) steps. The higher activation energies for the chain termination steps indicate that the assumptions related to RDSs for the product formation are reasonable. The relatively higher activation energy barriers of the olefins' ($E_{t,olef}$) formation compared to those of the paraffins ($E_{t,par}$), signifies the higher paraffins' selectivities over the Co/SiO_2 catalyst. Again, the rate of formation of the

paraffins with ''n'' carbon atoms ($R^n_{paraffins}$) was found to be higher than the rate of formation of the corresponding olefins ($R^n_{olefins}$), suggesting the preferred formation of saturated products (i.e. paraffinic compounds) in the FT synthesis over a Co/SiO_2 catalyst. The activation energy of CH_4 formation (E_{meth}) was found to be significantly lower ($76.5\ kJ\ mol^{-1}$) than that of lower carbon atom number formation, suggesting the considerably higher rate of formation as well as selectivity for CH_4 than those of other paraffins and olefins, in line with that reported by the literature [59, 66, 67, 70] and significantly lower than those obtained in the case of Co, Fe-and Ni catalysts by other investigators [53-57, 62]. In addition, the pre-exponential factor for methane formation ($k_{0,meth}$) was estimated to be one order of magnitude greater than the same coefficient for desorption of heavier paraffins ($k_{0,t,par}$). The above statements, together with the higher surface coverage of $CH_3-\psi$ intermediate relative to the other growing species ($C_nH_{2n+1}-\psi$; $n \geq 2$), signifies the main justifications of a higher selectivity to methane than those of other FT synthesis products. The estimated rate constant for ethylene (k_{eth}) was two orders of magnitude smaller than that of the other olefins ($k_{t,olef}$) in order to guarantee a good fit of the product distribution data, which are characterized by a low selectivity to ethylene, as shown in previous sections. Additionally, the activation energy of the ethylene (E_{eth}) was higher than those of olefins, paraffins, and methane which led to its lower rate of formation and productivity. The activation energy barriers of the WGS reaction were found to be $83.6\ kJ\ mol^{-1}$, in line with the expectations regarding the considerable selectivity to CO_2 co-products and in the range of the reported values by other investigators (28–125 $kJ\ mol^{-1}$) [66, 67, 71-74]. This value was higher than that of CH_4, in line with the activation energies for chain growth steps and considerably lower than that for olefins and paraffins' formation steps, which justifies the relatively higher selectivities to CO_2 formation in the present study at specified operating conditions for FT synthesis over a Co/SiO_2 catalyst.

4.3. Model validation results

Model validation was carried out subsequent to completion of the model calibration and the estimation of proper kinetic parameters. The overall purpose of the validation study was to ensure that the model provides a robust and realistic assessment of all the parameters defined by the mathematical model e.g. kinetic parameters, rate of reactants' consumption and products' formation. In order to ensure the model is relevant to an appropriate level, it was assessed against experimental data at four different operating conditions (tabulated in Table 15), which were available for validation, with respect to: temperature; pressure; and space velocity; as well as at a constant H_2/Co molar ratio of 2. Table 15 shows the values of conversion and selectivities obtained from model validation and then compares them with those of the experiments at four different operating conditions (see Table 15 for process conditions). To verify whether or not a model is valid, the MAPD value between predictions and experiments was determined. The MAPD obtained between the variables was at 14.62% which indicates that the model was satisfactorily validated against the measured data.

Table 14 Optimum values of estimated kinetic parameters of comprehensive combined FT−III (RDS-2) and WGS-VII (RDS-4)

Kinetic parameter	Unit	Value	t_{value}	Kinetic parameter	Unit	Value	t_{value}
$k_{0,meth}$	$mol\ kg^{-1}\ s^{-1}$	5.10×10^{7}	162.84	$k_{0,4}$	$mol\ kg^{-1}\ s^{-1}$	9.25×10^{6}	62.10
E_{meth}	$kJ\ mol^{-1}$	76.54	179.98	E_4	$kJ\ mol^{-1}$	74.98	154.63
$k_{0,eth}$	$mol\ kg^{-1}\ s^{-1}$	2.03×10^{4}	223.40	$k_{0,WGS}$	$mol\ kg^{-1}\ s^{-1}$	6.89×10^{5}	130.64
E_{eth}	$kJ\ mol^{-1}$	125.28	49.48	E_{WGS}	$kJ\ mol^{-1}$	83.59	299.32
$k_{0,i,par}$	$mol\ kg^{-1}\ s^{-1}$	1.14×10^{7}	327.70	$K_1(K_{CO})$	bar^{-1}	1.78	381.40
$E_{i,par}$	$kJ\ mol^{-1}$	90.22	248.64	$K_2(K_{H_2})$	bar^{-1}	4.81×10^{-3}	230.29
$k_{0,g,par}$	$mol\ kg^{-1}\ s^{-1}$	3.04×10^{3}	95.79	$K_3(K_{HCO})$	–	5.53	356.09
$E_{g,par}$	$kJ\ mol^{-1}$	82.57	282.68	$K_6(K_{OH})$	–	5.12×10^{-2}	137.05
$k_{0,t,par}$	$mol\ kg^{-1}\ s^{-1}$	7.85×10^{3}	132.00	$K_5(K_{CH})$	–	2.19	348.80
$E_{t,par}$	$kJ\ mol^{-1}$	95.63	191.64	$K_7(K_{CH_2})$	–	4.36	301.85
$k_{0,i,olef}$	$mol\ kg^{-1}\ s^{-1}$	8.44×10^{6}	134.76	K_{W_1}	bar^{-1}	4.15×10^{-2}	367.16
$E_{i,olef}$	$kJ\ mol^{-1}$	95.34	252.90	K_{W_2}	bar^{-1}	7.84×10^{-2}	300.04
$k_{0,g,olef}$	$mol\ kg^{-1}\ s^{-1}$	7.56×10^{3}	45.04	K_{W_3}	–	2.67	390.72
$E_{g,olef}$	$kJ\ mol^{-1}$	88.31	181.78	K_{W_5}	bar	5.40×10^{1}	38.50
$k_{0,t,olef}$	$mol\ kg^{-1}\ s^{-1}$	1.75×10^{3}	75.39				
$E_{t,olef}$	$kJ\ mol^{-1}$	100.22	87.81	MAPD = 5.93%			

*Results of statistical analysis:
(i) *F*-test: $F_{\text{ratio}} = 921.75 > F_{critical}\ (n-m, m-1; 1-\alpha) = F_{critical}\ (144-30, 30-1; 1-0.01) = 2.14$
(ii) *t*-test: lowest t-value $= 38.5 > t_{critical}\ (n-m; 1-\alpha) = t_{critical}\ (144-30; 1-0.01) = 2.36$

Table 15 Results obtained by model validation against experimental data at four different operating conditions with respect to reaction temperature, total inlet pressure and space velocity, values of conversion and selectivities

	T	P_{tot}	GHSV	P_{H_2}	P_{CO}	X_{CO}	S_{CO_2}	S_{CH_4}	$S_{C_2H_4}$	$S_{C_2H_6}$	$S_{C_3H_6}$	$S_{C_3H_8}$	$S_{C_4H_{10}}$	$S_{C_5H_{12}}$	$S_{C_6H_{14}}$	$S_{C_7H_{16}}$	$S_{C_{5+}}$
	(K)	*(bar)*	*($Nm\ell$ (STP) g_{cat}^{-1} h^{-1})*	*(bar)*	*(bar)*	%	%	%	%	%	%	%	%	%	%	%	%
												Measured					
Test-04	503	25	3600	8.5	4.25	66.55	1.71	12.60	0.08	0.97	1.56	0.56	1.22	0.76	0.48	0.23	83.00
Test-08	518	25	3000	8.5	4.25	98.22	11.45	16.25	0.04	1.54	1.28	1.13	0.78	0.47	0.13	0.06	78.97
Test-09	528	10	3000	3.30	1.70	90.78	16.38	28.72	0.10	3.76	2.52	2.85	1.65	1.03	0.64	0.31	60.41
Test-16	543	25	1800	8.5	4.25	99.88	24.93	49.72	0.01	4.54	0.08	4.24	0.41	0.19	0.07	0.02	41.02
												Predicted					
Test-04						69.50	1.86	13.56	0.07	1.10	1.88	0.66	0.99	0.62	0.29	0.14	81.74
Test-08						91.26	10.94	19.60	0.03	1.68	1.12	1.25	0.65	0.39	0.13	0.07	75.67
Test-09						93.60	15.50	30.21	0.08	3.65	2.00	2.20	2.10	1.31	0.63	0.30	59.76
Test-16						95.50	24.00	48.60	0.02	4.54	1.50	3.99	0.51	0.17	0.06	0.01	40.84

5. Conclusion

An in-depth understanding in terms of FT synthesis kinetics and water gas shift (WGS) reaction mechanisms was effectively accomplished. Two different approaches were used to develop a model for the FT synthesis reaction network (i.e. an empirical approach and the novel mechanistic details of FT kinetics). In the first approach, the rate equations were derived by power-law rate expressions, while in the second apporach the rate equations were derived by the Langmuir–Hinshelwood-Hougen-Watson (LHHW) rate theory. The experimental results at sixteen different process conditions were used for calibration and validation of the developed kinetics model. The kinetic models which were developed by the two approaches were assessed against the experimental data. Twelve out of sixteen of the experimental data were used for the calibration of the model. The goodness of fit was assessed by mean absolute percentage deviation and statistically analysed by employing the F-statistic. In addition, it was shown that the obtained kinetic parameters were statistically significant by using the t-statistic. The F_{ratio} and t_{value} of 55.34 and 7.14 (the lowest t_{value}) were obtained respectively when the power-law model was taken into account and the cumulative probability of the F-distribution was 0.99. Similarly, the F_{ratio} and t_{value} of 921.75 and 38.50 (the lowest t_{value}) were attained when the model FT−III with RDS-2/WGS-VII with RDS-4 was postulated. Based on the results obtained the limitations of power-law rate model were identified for the applications that wider range of operating conditions has to be selected. In contrast the advantages of LHHW for predicting a wider range of operating conditions were underlined. A comprehensive plausible mechanism-derived FT kinetics models with eight novel elementary reaction pathways along with seven novel WGS kinetics models were developed. The novel combined model FT−III with RDS-2/WGS-VII with RDS-4 was in excellent agreement with experimental results. The MAPD (mean absolute percentage deviation) value reported in this study was at 5.93% less than that of in the literature studies and achieved by empirical power-law model (13.23%) which highlights the significance, reliability and accuracy of the present model. Such results highlight the potential of this combined mechanistic FT/WGS mechanism as well as reaction networks that can further improve the performance of FT synthesis. Consequently, such information can provide guidelines for the design of more active and selective catalyst materials.

Among different kinetic mechanism for FT and WGS reaction kinetics developed herein, the minimum error (i.e. 5.93%) was achieved when the adsorbed CO molecule on a catalyst surface dissociated via the H-assisted route (i.e. FT-III). The formyl and hydroxymethylene intermediates ($HCO-\psi$ and $HCOH-\psi$) formed via two successive hydrogenation of the chemisorbed CO and the produced $HCO-\psi$ in which the second hydrogenation was assumed to be the slowest step and kinetically considered to be more relevant compare to other elementary steps in this route. Hydroxymethylene dissociation then led to the formation of methylidyne and hydroxyl intermediates; that in turn reacted with adsorbed hydrogen atoms forming the polymerization monomer CH_2, the initiator required for the chain growth (methyl species, CH_3) and products H_2O. Considering the WGS reaction kinetics, the formate mechanism (Model WGS-VII) in which the formate species was formed through the reaction between adsorbed CO intermediate and a hydroxyl surface species ($-OH$), was considered as the most kinetically relevant route. In this mechanism, adsorbed water dissociates into an adsorbed hydroxyl (OH- σ) group and adsorbed atomic hydrogen (H- σ). The hydroxyl group then combines with adsorbed carbon monoxide to form adsorbed formate which eventually decomposes into carbon dioxide and hydrogen via, yielding the WGS products. The kinetic parameters for the comprehensive (combined) FT−III (RDS-2) with

WGS-VII (RDS-4) kinetic model over a Co/SiO_2 catalyst were estimated by considering the fact that the slowest paths (RDSs) in the FT reaction model are steps 4, 8-15 and that of the WGS reaction is step 4 which the adsorbed formate species decomposes into carbon dioxide and hydrogen. It is worth noting that the numerical value of each parameter in this work, in addition to obtaining a satisfactory fit of the experimental data, was physically relevant and in good agreement with the expectations and literature studies.

The model's fit was compared to an ASF product distribution model. Indeed, the change of the ASF slope with a growing carbon atoms number, as well as the high selectivity to methane and low ethylene selectivity, were the main causes of the typical deviations of the experimental distribution from the ASF model. The postulated mechanism and rate models in the present study could overcome the deviations of the experimental data, by adopting separate reaction sequences for methane and ethylene formation, and by postulating the combined alkyl/alkenyl mechanisms, in which the alkyl represents the paraffinic compounds and the alkenyl expressing the olefin hydrocarbons.

Model validation was carried out subsequent to completion of the model calibration and the estimation of proper kinetic parameters. The overall purpose of the validation study was to ensure that the model provides a robust and realistic assessment of all the parameters defined by the mathematical model e.g. kinetic parameters, rate of reactants' consumption and products formation. In order to ensure that the model is precise to an appropriate level, the model was assessed against experimental data at four different operating conditions, which were available for validation, with respect to temperature, pressure, and space velocity. The MAPD obtained between the variables was 14.62% which indicates that the model is satisfactorily validated against measured data. Considering the results of conversion and selectivity, it can be concluded that the implementation of the reactor model, chemical kinetics, and product distribution have been successfully achieved.

The developed rate models proved to be effective for Co-based catalysts; however, it is recommended to investigate the accuracy and reliability of model for other types of catalysts especially iron-based catalysts. The results of such analysis can be used to compare the accuracy of the model for different types of catalysts. One of the advantages of this model is its capability for predicting the longer chain hydrocarbons products by expanding the chain growth probability defined by the model (both olefins and paraffins). Upon the availably of the experimental data for these hydrocarbons, the accuracy of the developed kinetic models can be assessed for the prediction of higher hydrocarbon number.

6. REFERENCES

[1] H. Mahmoudi, "Performance of cobalt-based eggshell catalyst in lowtemperature Fischer-Tropsch synthesis process to produce long-chain hydrocarbons from synthesis gas utilizing fixed-bed reactor technology," Ph.D. Thesis, School of Mechanical Engineering, University of Birmingham, 2015.

[2] Y.-N. Wang, Y.-W. Li, L. Bai, Y.-L. Zhao, and B.-J. Zhang, "Correlation for gas–liquid equilibrium prediction in Fischer–Tropsch synthesis," *Fuel*, vol. 78, no. 8, pp. 911-917, 1999.

[3] M. S. Hadnađev-Kostić, T. J. Vulić, R. P. Marinković-Nedučin, A. D. Nikolić, and B. Jović, "Mg-Fe-mixed oxides derived from layered double hydroxides: a study of the surface properties," *Journal of the Serbian Chemical Society*, vol. 76, no. 12, pp. 1661-1671, 2011.

[4] E. Lira *et al.*, "HMS mesoporous silica as cobalt support for the Fischer–Tropsch Synthesis: Pretreatment, cobalt loading and particle size effects," *Journal of Molecular Catalysis A: Chemical,* vol. 281, no. 1–2, pp. 146-153, 2/18/ 2008.
[5] S. Gill, A. Tsolakis, K. Dearn, and J. Rodríguez-Fernández, "Combustion characteristics and emissions of Fischer–Tropsch diesel fuels in IC engines," *Progress in Energy and Combustion Science,* vol. 37, no. 4, pp. 503-523, 2011.
[6] T. Fu, Y. Jiang, J. Lv, and Z. Li, "Effect of carbon support on Fischer–Tropsch synthesis activity and product distribution over Co-based catalysts," *Fuel Processing Technology,* vol. 110, pp. 141-149, 2013.
[7] W. Brötz, "Zur Systematik der Fischer-Tropsch-Katalyse," *Zeitschrift für Elektrochemie und angewandte physikalische Chemie,* vol. 53, no. 5, pp. 301-306, 1949.
[8] C. C. Hall, D. Gall, and S. L. Smith, "A comparison on the fixed-bed, liquid-phase ("slurry") and fluidized-bed techniques in the Fischer-Tropsch synthesis," *J. Inst. Pet. Technologists,* vol. 38, pp. 845-875, 1952.
[9] R. Anderson, F. Karn, and J. Schulz, "US Bur. Mines," *Bull,* vol. 614, 1964.
[10] M. E. Dry, T. Shingles, and L. J. Boshoff, "Rate of the Fischer-Tropsch reaction over iron catalysts," *Journal of Catalysis,* vol. 25, no. 1, pp. 99-104, 4// 1972.
[11] C.-H. Yang, F. E. Massoth, and A. G. Oblad, "Kinetics of CO + H_2 Reaction over Co-Cu-Al_2O_3 Catalyst," in *Hydrocarbon Synthesis from Carbon Monoxide and Hydrogen*, vol. 178(Advances in Chemistry, no. 178): American Chemical Society, 1979, pp. 35-46.
[12] G. Bub, M. Baerns, B. Büssemeier, and C. Frohning, "Prediction of the performance of catalytic fixed bed reactors for Fischer-Tropsch synthesis," *Chemical Engineering Science,* vol. 35, no. 1, pp. 348-355, 1980.
[13] R. B. Pannell, C. L. Kibby, and T. P. Kobylinski, "Tokyo," In Proceedings of the 7th International Congress on Catalysis pp. 447-459, 1980.
[14] J. Wang, " Ph.D. Thesis, Bringham Young University, Provo, UT," 1987.
[15] A. Jess, R. Popp, and K. Hedden, "Production of diesel oil and wax by Fischer-Tropsch-synthesis using a nitrogen-rich synthesis gas-Investigations on a semi-technical scale," *OIL GAS-EUROPEAN MAGAZINE,* vol. 24, no. 2, pp. 34-43, 1998.
[16] R. Zennaro, M. Tagliabue, and C. H. Bartholomew, "Kinetics of Fischer–Tropsch synthesis on titania-supported cobalt," *Catalysis Today,* vol. 58, no. 4, pp. 309-319, 2000.
[17] X. Zhan, H. J. Robota, and K. B. Arcuri, "Elucidation of Fischer-Tropsch reaction kinetics," *American Chemical Society, Division of Fuel Chemistry,* vol. 49, no. 2, pp. 200-202, 2004.
[18] M. A. Marvast, M. Sohrabi, S. Zarrinpashne, and G. Baghmisheh, "Fischer-Tropsch Synthesis: Modeling and Performance Study for Fe-HZSM5 Bifunctional Catalyst," *Chemical Engineering & Technology,* vol. 28, no. 1, pp. 78-86, 2005.
[19] T. K. Das, W. A. Conner, J. Li, G. Jacobs, M. E. Dry, and B. H. Davis, "Fischer-Tropsch synthesis: kinetics and effect of water for a Co/SiO_2 catalyst," *Energy & fuels,* vol. 19, no. 4, pp. 1430-1439, 2005.
[20] A. O. I. Rautavuoma and H. S. van der Baan, "Kinetics and mechanism of the Fischer-Tropsch hydrocarbon synthesis on abobalt on alumina catalyst," *Appl. Catal.,* vol. 1, pp. 247-272, 1981.
[21] B. Wojciechowski, "The kinetics of the Fischer-Tropsch synthesis," *Catalysis Reviews Science and Engineering,* vol. 30, no. 4, pp. 629-702, 1988.
[22] B. Sarup and B. W. Wojciechowski, "Studies of the fischer-tropsch synthesis on a cobalt catalyst II. Kinetics of carbon monoxide conversion to methane and to higher hydrocarbons," *The Canadian Journal of Chemical Engineering,* vol. 67, no. 1, pp. 62-74, 1989.
[23] I. C. Yates and C. N. Satterfield, "Intrinsic kinetics of the Fischer-Tropsch synthesis on a cobalt catalyst," *Energy & Fuels,* vol. 5, no. 1, pp. 168-173, 1991.
[24] E. Iglesia, S. L. Soled, J. E. Baumgartner, and S. C. Reyes, "Synthesis and catalytic properties of eggshell cobalt catalysts for the Fischer-Tropsch synthesis," *Journal of catalysis,* vol. 153, no. 1, pp. 108-122, 1995.
[25] N. O. Elbashir, D. B. Borough, R. Gupta, and C. B. Roberts, "Reaction pathway and kinetic modeling of Fischer-Tropsch synthesis over an alumina supported cobalt catalyst in supercritical-hexane media," *C1 Chemistry for the Production of Ultra-Clean Liquid Transportation Fuels and Hydrogen,* p. 14, 2004.
[26] F. G. Botes, B. van Dyk, and C. McGregor, "The Development of a Macro Kinetic Model for a Commercial Co/Pt/Al2O3 Fischer− Tropsch Catalyst," *Industrial & Engineering Chemistry Research,* vol. 48, no. 23, pp. 10439-10447, 2009.
[27] H. Atashi *et al.*, "Intrinsic kinetics of the Fischer-Tropsch synthesis over an impregnated cobalt-potassium catalyst," (in English), *Korean Journal of Chemical Engineering,* vol. 29, no. 3, pp. 304-309, 2012/03/01 2012.
[28] C. M. Van Den Bleek, K. Van Der Wiele, and P. J. Van Den Berg, "The effect of dilution on the degree of conversion in fixed bed catalytic reactors," *Chemical Engineering Science,* vol. 24, no. 4, pp. 681-694, 4// 1969.

[29] C. Perego and P. Villa, "Catalyst preparation methods," *Catalysis Today,* vol. 34, no. 3–4, pp. 281-305, 2/28/ 1997.
[30] A. Y. Khodakov, A. Griboval-Constant, R. Bechara, and V. L. Zholobenko, "Pore Size Effects in Fischer Tropsch Synthesis over Cobalt-Supported Mesoporous Silicas," *Journal of Catalysis,* vol. 206, no. 2, pp. 230-241, 3/10/ 2002.
[31] C. G. Visconti, E. Tronconi, L. Lietti, P. Forzatti, S. Rossini, and R. Zennaro, "Detailed kinetics of the Fischer–Tropsch synthesis on cobalt catalysts based on H-assisted CO activation," *Topics in Catalysis,* vol. 54, no. 13-15, pp. 786-800, 2011.
[32] D. van Herk, P. Castaño, M. Quaglia, M. T. Kreutzer, M. Makkee, and J. A. Moulijn, "Avoiding segregation during the loading of a catalyst–inert powder mixture in a packed micro-bed," *Applied Catalysis A: General,* vol. 365, no. 1, pp. 110-121, 8/15/ 2009.
[33] N. Moazami, H. Mahmoudi, K. Rahbar, P. Panahifar, A. Tsolakis, and M. L. Wyszynski, "Catalytic performance of cobalt–silica catalyst for Fischer–Tropsch synthesis: Effects of reaction rates on efficiency of liquid synthesis," *Chemical Engineering Science,* vol. 134, pp. 374-384, 9/29/ 2015.
[34] N. Moazami *et al.*, "Modelling of a fixed bed reactor for Fischer–Tropsch synthesis of simulated N_2-rich syngas over Co/SiO_2: Hydrocarbon production," *Fuel,* vol. 154, no. 0, pp. 140-151, 8/15/ 2015.
[35] N. Moazami, H. Mahmoudi, P. Panahifar, K. Rahbar, A. Tsolakis, and M. L. Wyszynski, "Mathematical Modeling and Performance Study of Fischer-tropsch Synthesis of Liquid Fuel over Cobalt-silica," *Energy Procedia,* vol. 75, pp. 62-71, 8/2015.
[36] N. Moazami, H. Mahmoudi, P. Panahifar, K. Rahbar, A. Tsolakis, and M. L. Wyszynski, "Mathematical Modeling and Performance Study of Fischer-Tropsch Synthesis of Liquid Fuel over Cobalt-Silica," in *The 7th International Conference on Applied Energy – ICAE2015*, Abu Dhabi, United Arab Emirates, 31/03/2015, vol. 75: Energy Procedia.
[37] V. Ponec and W. A. van Barneveld, "The Role of Chemisorption of Fischer-Tropsch Synthesis," *Industrial & Engineering Chemistry Product Research and Development,* vol. 18, no. 4, pp. 268-271, 1979/12/01 1979.
[38] A. Mosayebi and A. Haghtalab, "The comprehensive kinetic modeling of the Fischer–Tropsch synthesis over $Co@Ru/\gamma\text{-}Al_2O_3$ core–shell structure catalyst," *Chemical Engineering Journal,* vol. 259, no. 0, pp. 191-204, 1/1/ 2015.
[39] M. Ojeda, R. Nabar, A. U. Nilekar, A. Ishikawa, M. Mavrikakis, and E. Iglesia, "CO activation pathways and the mechanism of Fischer–Tropsch synthesis," *Journal of Catalysis,* vol. 272, no. 2, pp. 287-297, 6/15/ 2010.
[40] W. A. A. van Barneveld and V. Ponec, "Reactions of CHxCl4−x with hydrogen: Relation to the Fischer-Tropsch synthesis of hydrocarbons," *Journal of Catalysis,* vol. 88, no. 2, pp. 382-387, 8// 1984.
[41] G. P. Van Der Laan and A. Beenackers, "Kinetics and selectivity of the Fischer–Tropsch synthesis: a literature review," *Catalysis Reviews,* vol. 41, no. 3-4, pp. 255-318, 1999.
[42] R. E. Hayes and S. T. Kolaczkowski, *Introduction to catalytic combustion*. CRC Press, 1998.
[43] B.-T. Teng *et al.*, "Water gas shift reaction kinetics in Fischer–Tropsch synthesis over an industrial Fe–Mn catalyst," *Fuel,* vol. 84, no. 7–8, pp. 917-926, 5// 2005.
[44] A. Michaelides and P. Hu, "Catalytic Water Formation on Platinum: A First-Principles Study," *Journal of the American Chemical Society,* vol. 123, no. 18, pp. 4235-4242, 2001/05/01 2001.
[45] V. Perrichon, M. Pijolat, and M. Primet, "Surface species involved during the hydrogenation of CO or CO2 on iron-alumina catalysts," *Journal of Molecular Catalysis,* vol. 25, no. 1–3, pp. 207-217, 7// 1984.
[46] G. Jacobs *et al.*, "Water-gas shift: comparative screening of metal promoters for metal/ceria systems and role of the metal," *Applied Catalysis A: General,* vol. 258, no. 2, pp. 203-214, 2/20/ 2004.
[47] M. E. Dry, "Practical and theoretical aspects of the catalytic Fischer-Tropsch process," *Applied Catalysis A: General,* vol. 138, no. 2, pp. 319-344, 1996.
[48] L. J. Broadbelt and R. Q. Snurr, "Applications of molecular modeling in heterogeneous catalysis research," *Applied Catalysis A: General,* vol. 200, no. 1–2, pp. 23-46, 8/28/ 2000.
[49] J. A. Dumesic, *The Microkinetics of heterogeneous catalysis*. Washington, DC: American Chemical Society, 1993.
[50] N. Moazami, M. L. Wyszynski, K. Rahbari, and A. Tsolakis, "Parametric Study and Multi-Objective Optimization of Fischer-Tropsch Synthesis: Improving formation of FT products and synthetic conversion," *Submitted to Computers & Chemical Engineering, Elsevier,* 2017.
[51] N. Moazami, M. L. Wyszynski, A. Tsolakis, K. Rahbar, and H. Mahmoudi, "Modelling and optimization of Fischer-Tropsch synthesis performance to improve syngas conversion and products selectivity," *Submitted to Journal of Catalysis,* 2016.
[52] N. Moazami, H. Mahmoudi, K. Rahbar, P. Panahifar, A. Tsolakis, and M. L. Wyszynski, "Study of three different kinetics approaches for Fischer-Tropsch synthesis over Co/SiO_2," in *IMechE, Internal Combustion Engine*, London, United Kingdom, 03/12/2015: IMechE.

[53] W. H. Lee and C. H. Bartholomew, "Multiple reaction states in CO hydrogenation on alumina-supported cobalt catalysts," *Journal of Catalysis*, vol. 120, no. 1, pp. 256-271, 1989.
[54] C. H. Bartholomew and W.-H. Lee, "Effects of support on methane selectivity in cobalt-catalyzed Fischer-Tropsch synthesis: A kinetic model," *Studies in Surface Science and Catalysis*, vol. 130, pp. 1151-1156, 2000.
[55] M. A. Vannice, "The catalytic synthesis of hydrocarbons from H_2-CO mixtures over the group VIII metals: II. The kinetics of the methanation reaction over supported metals," *Journal of Catalysis*, vol. 37, no. 3, pp. 462-473, 6/6 1975.
[56] R. A. Dictor and A. T. Bell, "Fischer-Tropsch synthesis over reduced and unreduced iron oxide catalysts," *Journal of Catalysis*, vol. 97, no. 1, pp. 121-136, 1986.
[57] J. G. Ekerdt and A. T. Bell, "Synthesis of hydrocarbons from CO and H 2 over silica-supported Ru: reaction rate measurements and infrared spectra of adsorbed species," *Journal of Catalysis*, vol. 58, no. 2, pp. 170-187, 1979.
[58] S. Shetty, A. Jansen, and R. A. van Santen, "Methane formation on corrugated Ru surfaces," *The Journal of Physical Chemistry C*, vol. 114, no. 51, pp. 22630-22635, 2010.
[59] B. Todic *et al.*, "Kinetic Model of Fischer–Tropsch Synthesis in a Slurry Reactor on Co–Re/Al_2O_3 Catalyst," *Industrial & Engineering Chemistry Research*, vol. 52, no. 2, pp. 669-679, 2013/01/16 2012.
[60] C. G. Visconti, E. Tronconi, L. Lietti, R. Zennaro, and P. Forzatti, "Development of a complete kinetic model for the Fischer–Tropsch synthesis over Co/Al_2O_3 catalysts," *Chemical Engineering Science*, vol. 62, no. 18, pp. 5338-5343, 2007.
[61] J. Yang, D. Chen, and A. Holmen, "Understanding the kinetics and Re promotion of carbon nanotube supported cobalt catalysts by SSITKA," *Catalysis Today*, vol. 186, no. 1, pp. 99-108, 2012.
[62] W. Ma *et al.*, "Fischer–Tropsch Synthesis: Kinetics and Water Effect on Methane Formation over 25% Co/γ-Al_2O_3 Catalyst," *Industrial & Engineering Chemistry Research*, vol. 53, no. 6, pp. 2157-2166, 2014.
[63] W. H. Hung and S. L. Bernasek, "Adsorption and decomposition of ethylene and acetylene on Fe(100)," *Surface Science*, vol. 339, no. 3, pp. 272-290, 10/1/ 1995.
[64] N. Moazami, H. Mahmoudi, A. Tsolakis, K. Rahbar, P. Panahifar, and M. L. Wyszynski, "Mathematical modelling and chemical kinetics study of Fischer-Tropsch synthesis on a cobalt-silica catalyst," in *DECHEMA, European Symposium on Chemical Reaction Engineering (ESCRE 2015)*, Fürstenfeldbruck, Germany, 28/10/2015: DECHEMA.
[65] A. A. Mirzaei, B. Shirzadi, H. Atashi, and M. Mansouri, "Modeling and operating conditions optimization of Fischer–Tropsch synthesis in a fixed-bed reactor," *Journal of Industrial and Engineering Chemistry*, vol. 18, no. 4, pp. 1515-1521, 2012.
[66] J. Yang *et al.*, "Detailed kinetics of Fischer-Tropsch synthesis on an industrial Fe-Mn catalyst," *Industrial & engineering chemistry research*, vol. 42, no. 21, pp. 5066-5090, 2003.
[67] B.-T. Teng *et al.*, "A comprehensive kinetics model of Fischer–Tropsch synthesis over an industrial Fe–Mn catalyst," *Applied Catalysis A: General*, vol. 301, no. 1, pp. 39-50, 2/10/ 2006.
[68] Y.-N. Wang *et al.*, "Kinetics modelling of Fischer–Tropsch synthesis over an industrial Fe–Cu–K catalyst," *Fuel*, vol. 82, no. 2, pp. 195-213, 2003.
[69] W. Qian, H. Zhang, W. Ying, and D. Fang, "The comprehensive kinetics of Fischer–Tropsch synthesis over a Co/AC catalyst on the basis of CO insertion mechanism," *Chemical Engineering Journal*, vol. 228, no. 0, pp. 526-534, 7/15/ 2013.
[70] S. Storsæter, D. Chen, and A. Holmen, "Microkinetic modelling of the formation of C_1 and C_2 products in the Fischer–Tropsch synthesis over cobalt catalysts," *Surface science*, vol. 600, no. 10, pp. 2051-2063, 2006.
[71] N. Park, J.-R. Kim, Y. Yoo, J. Lee, and M.-J. Park, "Modeling of a pilot-scale fixed-bed reactor for iron-based Fischer–Tropsch synthesis: Two-dimensional approach for optimal tube diameter," *Fuel*, vol. 122, no. 0, pp. 229-235, 4/15/ 2014.
[72] E. S. Lox and G. F. Froment, "Kinetics of the Fischer-Tropsch reaction on a precipitated promoted iron catalyst. 2. Kinetic modeling," *Industrial & Engineering Chemistry Research*, vol. 32, no. 1, pp. 71-82, 1993/01/01 1993.
[73] G. P. Van der Laan and A. A. Beenackers, "Intrinsic kinetics of the gas–solid Fischer–Tropsch and water gas shift reactions over a precipitated iron catalyst," *Applied Catalysis A: General*, vol. 193, no. 1, pp. 39-53, 2000.
[74] W. H. Zimmerman and D. B. Bukur, "Reaction kinetics over iron catalysts used for the fischer-tropsch synthesis," *The Canadian Journal of Chemical Engineering*, vol. 68, no. 2, pp. 292-301, 1990.

Appendix A

Table A. 1 Reaction rate expressions derived on the basis of kinetics model FT–I

RDS/No.	Rate equation
5,8-15 Equation 96	$R_{FT}=\dfrac{\left(k_{i,par}k_5K_1K_2^{2.5}K_3K_4K_6K_7\right)^{0.5}P_{H_2}^{1.25}P_{CO}^{0.5}}{\left(\begin{array}{c}1+K_1P_{CO}+\sqrt{K_2}P_{H2}^{0.5}+\dfrac{(k_5K_4K_3K_1)^{0.5}}{K_2^{0.25}\left(k_{i,par}K_6K_7\right)^{0.5}}P_{H_2}^{-0.25}P_{CO}^{0.5}+\cdots\\ \dfrac{K_2^{0.25}\left(k_{i,par}K_1K_3K_6K_7\right)^{0.5}}{(k_5K_4)^{0.5}}P_{H_2}^{0.25}P_{CO}^{0.5}+.\dfrac{K_2^{0.75}\left(k_{i,par}K_1K_3K_4K_6K_7\right)^{0.5}}{k_5^{0.5}}P_{H_2}^{0.75}P_{CO}^{0.5}+\cdots\\ \dfrac{K_2^{0.25}(k_5K_1K_3K_4K_6)^{0.5}}{\left(k_{i,par}K_7\right)^{0.5}}P_{H_2}^{0.25}P_{CO}^{0.5}+\dfrac{K_2^{0.75}(k_5K_7K_6K_4K_3K_1)^{0.5}}{k_{i,par}^{0.5}}P_{H_2}^{0.75}P_{CO}^{0.5}\end{array}\right)^2}$
3, 8-15 Equation 97	$R_{FT}=\dfrac{k_3K_1P_{CO}}{\left(\begin{array}{c}1+K_1P_{CO}+\sqrt{K_2P_{H_2}}+\dfrac{1}{K_5K_4K_2}\dfrac{P_{H_2O}}{P_{H_2}}+\cdots\\ \dfrac{1}{K_5\sqrt{K_2}}\dfrac{P_{H_2O}}{P_{H2}^{0.5}}+\dfrac{k_3K_1}{k_{i,par}K_7K_6K_2^{1.5}}\dfrac{P_{CO}}{P_{H_2}^{1.5}}+\dfrac{k_3K_1}{k_{i,par}K_7K_2}\dfrac{P_{CO}}{P_{H_2}}+\dfrac{k_3K_1}{k_{i,par}\sqrt{K_2}}\dfrac{P_{CO}}{P_{H2}^{0.5}}\end{array}\right)^2}$
8-15 Equation 98	$R_{FT}=\dfrac{k_{i,par}K_7K_6K_5K_4K_3K_2^{2.5}K_1\dfrac{P_{CO}}{P_{H_2O}}P_{H2}^{2.5}}{\left(\begin{array}{c}1+K_1P_{CO}+\sqrt{K_2P_{H_2}}+\dfrac{P_{H_2O}}{K_5K_4K_2P_{H_2}}+\dfrac{P_{H_2O}}{K_5\sqrt{K_2}P_{H2}^{0.5}}+\cdots\\ \dfrac{K_5K_4K_3K_2K_1P_{CO}P_{H_2}}{P_{H_2O}}+K_6K_5K_4K_3K_2^{1.5}K_1\dfrac{P_{CO}}{P_{H_2O}}P_{H_2}^{1.5}+K_7K_6K_5K_4K_3K_2^2K_1\dfrac{P_{CO}}{P_{H_2O}}P_{H_2}^2\end{array}\right)^2}$

Table A. 2 Reaction rate expressions derived on the basis of kinetics model FT–II

RDS/No.	Rate equation
4,7-14 Equation 99	$R_{FT}=\dfrac{\sqrt{k_{i,par}k_5K_1K_2^{2.5}K_3K_4K_6K_7}P_{CO}^{0.5}P_{H_2}^{1.25}}{\left(\begin{array}{c}1+K_1P_{CO}+\sqrt{K_2P_{H_2}}+K_3K_1\sqrt{K_2}P_{CO}P_{H2}^{0.5}\psi+\cdots\\ \sqrt{K_2}K_3K_4K_6k_5\dfrac{\psi_{CO}\psi_H^2}{R_{FT}}\sqrt{P_{H_2}}+K_1K_2^2K_3K_4K_6K_7k_5\dfrac{P_{CO}P_{H_2}^2}{R_{FT}}+\cdots\\ \sqrt{k_{i,par}K_1K_2^2K_3K_4K_6K_7}\dfrac{P_{CO}^{0.5}P_{H_2}^{0.75}}{k_5^{0.5}}+\dfrac{k_5^{0.5}K_4K_3K_1P_{CO}^{0.5}}{\sqrt{k_{i,par}K_1K_2^{1.5}K_3K_4K_6K_7}P_{H_2}^{0.25}}\end{array}\right)^2}$
3, 7-14 Equation 100	$R_{FT}=\dfrac{k_4K_3K_1\sqrt{K_2}P_{CO}P_{H2}^{0.5}}{\left(\begin{array}{c}1+K_1P_{CO}+\sqrt{K_2P_{H_2}}+K_3K_1\sqrt{K_2}P_{CO}P_{H2}^{0.5}+\dfrac{P_{H_2O}}{K_5\sqrt{K_2P_{H_2}}}+\cdots\\ \dfrac{P_{H_2O}}{K_6\sqrt{K_2P_{H_2}}}+\dfrac{k_4K_1K_3}{K_2^{0.5}k_{i,par}K_7}\dfrac{P_{CO}}{P_{H2}^{0.5}}+\dfrac{k_4K_1K_3}{k_{i,par}}P_{CO}\end{array}\right)^2}$

7-14 Equation 101	$$R_{FT}=\frac{k_{i,par}\frac{K_1K_2^{2.5}K_3K_4K_5K_7}{K_6}\frac{P_{CO}P_{H_2}^{2.5}}{P_{H_2O}}}{\left(\begin{array}{c}1+K_1P_{CO}+\sqrt{K_2P_{H_2}}+\frac{P_{H_2O}}{K_6\sqrt{K_2P_{H_2}}}+K_3K_1\sqrt{K_2}P_{CO}P_{H2}^{0.5}+\cdots\\ K_4\left(K_5K_3K_1K_2\frac{P_{CO}P_{H_2}}{P_{H_2O}}\right)+\frac{P_{H_2O}}{K_5\sqrt{K_2P_{H_2}}}+\cdots\\ \frac{K_1K_2^{1.5}K_3K_4K_5}{K_6}\frac{P_{CO}P_{H_2}^{1.5}}{P_{H_2O}}+\frac{K_1K_2^2K_3K_4K_5K_7}{K_6}\frac{P_{CO}P_{H_2}^2}{P_{H_2O}}\end{array}\right)^2}$$

Table A. 3 Reaction rate expressions derived on the basis of kinetics model FT–III

RDS/No.	Rate equation
6,8-15 Equation 102	$$R_{FT}=\frac{\sqrt{k_{i,par}K_7k_6K_5K_1K_2^{2.5}K_3K_4P_{CO}^{0.5}P_{H2}^{1.25}}}{\left(\begin{array}{c}1+K_1P_{CO}+\sqrt{K_2P_{H_2}}+K_2^{0.75}\sqrt{\frac{k_{i,par}K_7K_5K_1K_3K_4}{k_6}}P_{CO}^{0.5}P_{H2}^{0.75}+\\ K_3K_1\sqrt{K_2}P_{CO}P_{H2}^{0.5}+K_1K_2K_3K_4P_{CO}P_{H2}+\\ K_2^{0.25}\sqrt{\frac{k_6K_1K_3K_4K_5}{k_{i,par}K_7}}P_{CO}^{0.5}P_{H2}^{0.25}+\sqrt{\frac{K_7k_6K_5K_1K_2^{1.5}K_3K_4}{k_{i,par}}}P_{CO}^{0.5}P_{H2}^{0.75}\end{array}\right)^2}$$
4, 8-15 Equation 103	$$R_{FT}=\frac{k_4K_1K_2K_3P_{CO}P_{H_2}}{\left(\begin{array}{c}1+K_1P_{CO}+\sqrt{K_2P_{H_2}}+\frac{P_{H_2O}}{K_6\sqrt{K_2P_{H_2}}}+K_3K_1\sqrt{K_2}P_{CO}P_{H2}^{0.5}+\\ \frac{k_4K_1K_3}{k_{i,par}K_5K_6K_7}P_{H_2O}P_{CO}+\frac{k_4K_1K_2^{0.5}K_3}{k_{i,par}K_7}P_{CO}P_{H_2}^{0.5}+\frac{k_4K_1K_2^{0.5}K_3}{k_{i,par}}P_{CO}P_{H_2}^{0.5}\end{array}\right)^2}$$
8-15 Equation 104	$$R_{FT}=\frac{k_{i,par}K_7K_5K_1K_2^{2.5}K_3K_4K_6\frac{P_{CO}P_{H_2}^{2.5}}{P_{H_2O}}}{\left(\begin{array}{c}1+K_1P_{CO}+\sqrt{K_2P_{H_2}}+\frac{P_{H_2O}}{K_6\sqrt{K_2P_{H_2}}}+K_3K_1\sqrt{K_2}P_{CO}P_{H2}^{0.5}+\\ K_1K_2K_3K_4P_{CO}P_{H_2}+K_5K_1K_2^{1.5}K_3K_4K_6\frac{P_{CO}P_{H_2}^{1.5}}{P_{H_2O}}+\\ K_7K_5K_1K_2^2K_3K_4K_6\frac{P_{CO}P_{H_2}^2}{P_{H_2O}}\end{array}\right)^2}$$

Table A. 4 Reaction rate expressions derived on the basis of kinetics model FT–IV

RDS/No.	Rate equation
4,6-13 Equation 105	$$R_{FT}=\frac{\sqrt{k_{i,par}k_6^2K_4K_3K_1K_2^2K_5P_{CO}^{0.5}}P_{H2}^{1.25}}{\left(1+K_1P_{CO}+\sqrt{K_2P_{H_2}}+K_3K_1\sqrt{K_2}P_{CO}P_{H2}^{0.5}+K_1K_2K_3K_4P_{CO}P_{H_2}\right)^{0.5}}$$
3, 6-13 Equation 106	$$R_{FT}=\frac{k_4K_3K_1\sqrt{K_2}P_{CO}P_{H2}^{0.5}}{\left(1+K_1P_{CO}+\sqrt{K_2P_{H_2}}+K_3K_1\sqrt{K_2}P_{CO}P_{H2}^{0.5}+\frac{P_{H_2O}}{K_7K_2K_5P_{H_2}}+\frac{P_{H_2O}}{K_6\sqrt{K_2P_{H_2}}}\right)^2}$$

6-13 Equation 107	$$R_{FT}=\frac{k_{i,par}K_6K_2^{1.5}K_5K_4K_3K_1\frac{P_{CO}P_{H2}^{2.5}}{P_{H_2O}}}{\left(1+K_1P_{CO}+\sqrt{K_2P_{H_2}}+K_3K_1\sqrt{K_2}P_{CO}P_{H2}^{0.5}+K_6K_2^{1.5}K_5K_4K_3K_1\frac{P_{CO}P_{H2}^{1.5}}{P_{H_2O}}\right.}$$ $$\left.\frac{P_{H_2O}}{K_6K_2K_5P_{H_2}}+\frac{P_{H_2O}}{K_6\sqrt{K_2P_{H_2}}}\right)^2$$

Table A. 5 Reaction rate expressions derived on the basis of kinetics model FT–V

RDS/No.	Rate equation
4,5-12 Equation 108	$$R_{FT}=\frac{\sqrt{k_{i,par}\frac{(k_7K_6K_1K_2^{2.5}K_3K_4)}{K_5}}P_{CO}P_{H_2}^{1.25}}{\left(1+K_1P_{CO}+\sqrt{K_2P_{H_2}}+K_3K_1\sqrt{K_2}P_{CO}P_{H2}^{0.5}+K_1K_2K_3K_4P_{CO}P_{H_2}\right.}$$ $$\left.\frac{\left(\sqrt{k_7K_6K_1K_3K_4}K_2^{0.75}\right)}{\sqrt{K_5}}\frac{P_{CO}P_{H_2}^{0.75}}{\sqrt{k_{i,par}}}+\cdots\right.$$ $$\left.\frac{\sqrt{k_{i,par}(K_1K_2^{0.25}K_3K_4)}P_{CO}P_{H_2}^{0.25}}{K_5\sqrt{k_7K_6}}+\sqrt{k_{i,par}\frac{(K_6K_1K_2^2K_3K_4)}{K_5}}\frac{P_{CO}P_{H_2}^{0.5}}{k_7^{0.5}}\right)^2$$
3, 5-12 Equation 109	$$R_{FT}=\frac{k_4K_3K_1K_2P_{CO}P_{H_2}}{\left(1+K_1P_{CO}+\sqrt{K_2P_{H_2}}+K_3K_1\sqrt{K_2}P_{CO}P_{H2}^{0.5}+K_1K_2K_3K_4P_{CO}P_{H_2}\right.}$$ $$\left.\frac{k_4K_3K_1K_2^{0.5}}{k_{i,par}K_7K_2K_5K_5}P_{CO}\frac{P_{H_2O}}{P_{H_2}^{0.5}}+\frac{P_{H_2O}}{K_7K_2K_5P_{H_2}}+\frac{P_{H_2O}}{K_7\sqrt{K_2P_{H_2}}}+\frac{k_4K_3K_1K_2^{0.5}P_{CO}P_{H_2}^{0.5}}{k_{i,par}}\right)^2$$
5-12 Equation 110	$$R_{FT}=\frac{k_{i,par}K_1K_2^{2.5}K_3K_4K_7K_5\frac{P_{CO}P_{H_2}^{2.5}}{P_{H_2O}}}{\left(1+K_1P_{CO}+\sqrt{K_2P_{H_2}}+K_3K_1\sqrt{K_2}P_{CO}P_{H2}^{0.5}+K_1K_2K_3K_4P_{CO}P_{H_2}\right.}$$ $$\left.\frac{k_4K_3K_1K_2^{0.5}}{k_{i,par}K_7K_2K_5K_5}P_{CO}\frac{P_{H_2O}}{P_{H_2}^{0.5}}+\frac{P_{H_2O}}{K_7K_2K_5P_{H_2}}+\frac{P_{H_2O}}{K_7\sqrt{K_2P_{H_2}}}+\frac{k_4K_3K_1K_2^{0.5}P_{CO}P_{H_2}^{0.5}}{k_{i,par}}\right)^2$$

Table A. 6 Reaction rate expressions derived on the basis of kinetics model FT–VI

RDS/No.	Rate equation
3,6-13 Equation 111	$$R_{FT}=\frac{k_3K_1P_{CO}P_{H_2}}{\left(1+K_1P_{CO}+\sqrt{K_2P_{H_2}}\right)}$$
4, 6-13 Equation 112	$$R_{FT}=\frac{k_4K_3K_1\sqrt{K_2}\frac{P_{CO}P_{H_2}^{1.5}}{P_{H_2O}}}{\left(1+K_1P_{CO}+\sqrt{K_2P_{H_2}}+K_3K_1\frac{P_{CO}P_{H_2}}{P_{H_2O}}+\frac{k_4K_3K_1}{k_{i,par}K_5\sqrt{K_2}}\frac{P_{CO}P_{H_2}^{0.5}}{P_{H_2O}}+\frac{k_4K_3K_1}{k_{i,par}}\frac{P_{CO}P_{H_2}}{P_{H_2O}}\right)^2}$$

6-13 Equation 113	$R_{FT} = \frac{k_{i,par} K_1 K_2^{1.5} K_3 K_4 K_5 \frac{P_{CO} P_{H_2}^{2.5}}{P_{H_2O}}}{\left(+ K_1 P_{CO} + \sqrt{K_2 P_{H_2}} + K_3 K_1 \frac{P_{CO} P_{H_2}}{P_{H_2O}} + K_1 \sqrt{K_2} K_3 K_4 \frac{P_{CO} P_{H_2}^{1.5}}{P_{H_2O}} + K_1 K_2 K_3 K_4 K_5 \frac{P_{CO} P_{H_2}^2}{P_{H_2O}} \right)^2}$	

Table A. 7 Reaction rate expressions derived on the basis of kinetics model FT–VII

RDS/No.	Rate equation
5,7-14 Equation 114	$R_{FT} = \frac{\frac{\sqrt{k_5 K_1 K_2^{0.5} K_3 K_4 K_6}}{k_{i,par}^{0.5}} \sqrt{P_{CO}} P_{H_2}^{0.75}}{\left(\begin{array}{c} 1 + K_1 P_{CO} + \sqrt{K_2 P_{H_2}} + K_1 K_3 P_{CO} P_{H_2} + \frac{\sqrt{\frac{k_5 K_1 K_2^{1.5} K_3 K_4}{k_{i,par} K_6}}}{K_2^{0.25}} P_{CO}^{0.5} P_{H_2}^{0.25} + \\ \sqrt{\frac{k_{i,par} K_1 K_2^{1.5} K_3 K_4 K_6}{k_5}} P_{CO}^{0.5} P_{H_2}^{1.25} + \frac{\sqrt{k_5 K_1 K_2^{0.5} K_3 K_4 K_6}}{k_{i,par}^{0.5}} \sqrt{P_{CO}} P_{H_2}^{0.75} \end{array} \right)^2}$
3, 7-14 Equation 115	$R_{FT} = \frac{k_3 K_1 P_{CO} P_{H_2}}{\left(1 + K_1 P_{CO} + \sqrt{K_2 P_{H_2}} + \frac{P_{H_2O}}{K_5} \right)}$
7-14 Equation 116	$R_{FT} = \frac{k_{i,par} K_7 K_5 K_1 K_2^{2.5} K_3 K_4 K_6 \frac{P_{CO} P_{H_2}^{2.5}}{P_{H_2O}}}{\left(\begin{array}{c} 1 + K_1 P_{CO} + \sqrt{K_2 P_{H_2}} + \frac{P_{H_2O}}{K_6 \sqrt{K_2 P_{H_2}}} + K_3 K_1 \sqrt{K_2} P_{CO} P_{H2}^{0.5} + \\ K_1 K_2 K_3 K_4 P_{CO} P_{H_2} + K_5 K_1 K_2^{1.5} K_3 K_4 K_6 \frac{P_{CO} P_{H_2}^{1.5}}{P_{H_2O}} + \\ K_7 K_5 K_1 K_2^2 K_3 K_4 K_6 \frac{P_{CO} P_{H_2}^2}{P_{H_2O}} \end{array} \right)^2}$

Table A. 8 Reaction rate expressions derived on the basis of kinetics model FT–VIII

RDS	Rate equation	No.
4,5-12	$R_{FT} = \frac{K_1 K_3 k_4 P_{CO} P_{H_2}^2}{\left(1 + K_1 P_{CO} + \sqrt{K_2 P_{H_2}} + K_1 K_3 P_{CO} P_{H_2} \right)}$	Equation 117
3, 5-12	$R_{FT} = \frac{K_1 k_3 P_{CO} P_{H_2}}{\left(1 + K_1 P_{CO} + \sqrt{K_2 P_{H_2}} \right)}$	Equation 118
5-12	$R_{FT} = \frac{k_{i,par} K_1 K_3 K_4 \sqrt{K_2} \frac{P_{CO} P_{H_2}^{2.5}}{P_{H_2O}}}{\left(1 + K_1 P_{CO} + \sqrt{K_2 P_{H_2}} + K_1 K_3 P_{CO} P_{H_2} + \frac{K_1 K_3 K_4 P_{CO} P_{H_2}^2}{P_{H_2O}} \right)^2}$	Equation 119

Table A. 9 Reaction rate expressions derived on the basis of kinetics model WGS-I

RDS	Rate equation	No.
1	$R_{WGS}=\dfrac{\left(k_{WGS_1}P_{CO}-k_{WGS_{-1}}\dfrac{1}{K_{W_2}K_{W_3}K_{W_4}K_{W_5}}\dfrac{P_{CO_2}P_{H_2}}{P_{H_2O}}\right)}{\left(1+\dfrac{1}{K_{W_2}K_{W_3}K_{W_4}K_{W_5}}\dfrac{P_{H_2}P_{CO_2}}{P_{H_2O}}+K_{W_2}K_{W_3}K_{W_5}\dfrac{P_{H_2O}}{P_{H_2}}+K_{W_2}K_{W_5}^{0.5}\dfrac{P_{H_2O}}{P_{H2}^{0.5}}+\sqrt{\dfrac{P_{H_2}}{K_{W_5}}}\right)}$	Equation 120
2	$R_{WGS}=\dfrac{\left(k_{WGS_2}P_{H_2O}-k_{WGS_{-2}}\dfrac{1}{K_{W_1}^2K_{W_3}K_{W_4}^2K_{W_5}^{0.5}}\dfrac{P_{H_2}^{0.5}P_{CO_2}^2}{P_{CO}^2}\right)}{\left(1+K_{W_1}P_{CO}+\sqrt{\dfrac{P_{H_2}}{K_{W_5}}}+\dfrac{P_{CO_2}}{K_{W_4}K_{W_1}P_{CO}}+\dfrac{1}{K_{W_1}K_{W_3}K_{W_4}K_{W_5}^{0.5}}\dfrac{P_{CO_2}P_{H_2}^{0.5}}{P_{CO}}\right)^2}$	Equation 121
3	$R_{WGS}=\dfrac{\left(k_{WGS_3}K_{W_5}K_{W_2}\dfrac{P_{H_2O}}{P_{H_2}}-k_{WGS_{-3}}\dfrac{P_{CO_2}P_{H_2}^{0.5}}{K_{W_4}K_{W_1}K_{W_5}^{0.5}P_{CO}}\right)}{\left(1+K_{W_1}P_{CO}+\sqrt{\dfrac{P_{H_2}}{K_{W_5}}}+\dfrac{P_{CO_2}}{K_{W_4}K_{W_1}P_{CO}}+K_{W_5}^{0.5}K_{W_2}\dfrac{P_{H_2O}}{P_{H_2}^{0.5}}\right)^2}$	Equation 122
4	$R_{WGS}=\dfrac{\left(k_{WGS_4}K_{W_1}K_{W_2}K_{W_3}K_{W_5}\dfrac{P_{CO}P_{H_2O}}{P_{H_2}}-k_{WGS_{-4}}P_{CO_2}\right)}{\left(1+K_{W_1}P_{CO}+K_{W_5}K_{W_2}\dfrac{P_{H_2O}}{P_{H_2}}+K_{W_1}K_{W_2}K_{W_3}K_{W_5}\dfrac{P_{CO}P_{H_2O}}{P_{H_2}}+\dfrac{P_{H_2}}{K_{W_5}}\right)}$	Equation 123
5	$R_{WGS}=\dfrac{\left(k_{WGS_5}K_{W_1}K_{W_2}K_{W_3}K_{W_4}\dfrac{P_{CO}P_{H_2O}}{P_{CO_2}}-k_{WGS_{-5}}P_{H_2}\right)}{\left(1+K_{W_1}P_{CO}+\dfrac{1}{K_{W_1}K_{W_3}K_{W_4}}\dfrac{P_{CO_2}}{P_{CO}}+K_{W_1}K_{W_2}K_{W_3}K_{W_4}\dfrac{P_{CO}P_{H_2O}}{P_{CO_2}}+\dfrac{P_{CO_2}}{K_{W_4}}\right)}$	Equation 124

Table A. 10 Reaction rate expressions derived on the basis of kinetics model WGS-II

RDS	Rate equation	No.
1	$R_{WGS}=\dfrac{\left(k_{WGS_1}P_{CO}-k_{WGS_{-1}}\dfrac{1}{K_{W_2}K_{W_3}K_{W_4}K_{W_5}K_{W_6}}\dfrac{P_{H_2}P_{CO_2}}{P_{H_2O}}\right)}{\left(1+\dfrac{1}{K_{W_2}K_{W_3}K_{W_4}K_{W_5}K_{W_6}}\dfrac{P_{H_2}P_{CO_2}}{P_{H_2O}}+\sqrt{\dfrac{P_{H_2}}{K_{W_6}}}+\cdots\right.$ $\left.K_{W_3}K_{W_2}K_{W_6}\dfrac{P_{H_2O}}{P_{H_2}}+K_{W_2}K_{W_6}^{0.5}\dfrac{P_{H_2O}}{P_{H_2}^{0.5}}+\dfrac{P_{CO_2}}{K_{W_5}}\right)}$	Equation 125
2	$R_{WGS}=\dfrac{\left(k_{WGS_2}P_{H_2O}-k_{WGS_{-2}}\dfrac{1}{K_{W_1}K_{W_3}K_{W_5}K_{W_6}}\dfrac{P_{CO_2}P_{H_2}}{P_{CO}}\right)}{\left(1+K_{W_1}P_{CO}+\sqrt{\dfrac{P_{H_2}}{K_{W_6}}}+\dfrac{1}{K_{W_1}K_{W_5}}\dfrac{P_{CO_2}}{P_{CO}}+\dfrac{1}{K_{W_1}K_{W_3}K_{W_5}K_{W_6}^{0.5}}\dfrac{P_{CO_2}P_{H_2}^{0.5}}{P_{CO}}+\dfrac{P_{CO_2}}{K_{W_5}}\right)^2}$	Equation 126
3	$R_{WGS}=\dfrac{\left(k_{WGS_3}K_{W_2}K_{W_6}^{0.5}\dfrac{P_{H_2O}}{\sqrt{P_{H_2}}}-k_{WGS_{-3}}\dfrac{1}{K_{W_1}K_{W_5}K_{W_6}^{0.5}}\dfrac{P_{CO_2}P_{H_2}^{0.5}}{P_{CO}}\right)}{\left(1+K_{W_1}P_{CO}+\sqrt{\dfrac{P_{H_2}}{K_{W_6}}}+\dfrac{1}{K_{W_1}K_{W_5}}\dfrac{P_{CO_2}}{P_{CO}}+K_{W_2}K_{W_6}^{0.5}\dfrac{P_{H_2O}}{\sqrt{P_{H_2}}}+\dfrac{P_{CO_2}}{K_{W_5}}\right)^2}$	Equation 127

4	$R_{WGS}=\frac{\left(k_{WGS_4}K_{W_1}K_{W_2}K_{W_3}K_{W_6}\frac{P_{CO}P_{H_2O}}{P_{H_2}}-k_{WGS_{-4}}\frac{P_{CO_2}}{K_{W_5}}\right)}{\left(1+K_{W_1}P_{CO}+\sqrt{\frac{P_{H_2}}{K_{W_6}}}+K_{W_2}K_{W_3}K_{W_6}\frac{P_{H_2O}}{P_{H_2}}+K_{W_2}K_{W_6}^{0.5}\frac{P_{H_2O}}{\sqrt{P_{H_2}}}+\frac{P_{CO_2}}{K_{W_5}}\right)^2}$	Equation 128
5	$R_{WGS}=\frac{\left(k_{WGS_5}K_{W_1}K_{W_2}K_{W_3}K_{W_4}K_{W_6}\frac{P_{CO}P_{H_2O}}{P_{H_2}}-k_{WGS_{-5}}P_{CO_2}\right)}{\left(1+K_{W_1}P_{CO}+\sqrt{\frac{P_{H_2}}{K_{W_6}}}+K_{W_2}K_{W_3}K_{W_6}\frac{P_{H_2O}}{P_{H_2}}+\cdots\right)}$	Equation 129
6	$R_{WGS}=\frac{\left(k_{WGS_6}K_{W_2}K_{W_1}K_{W_3}K_{W_5}\frac{P_{CO}P_{H_2O}}{P_{CO_2}}-k_{WGS_{-6}}P_{H_2}\right)}{\left(1+K_{W_1}P_{CO}+\sqrt{K_{W_2}K_{W_1}K_{W_3}K_{W_5}}\sqrt{\frac{P_{CO}P_{H_2O}}{P_{CO_2}}}+\cdots\right)^2}$	Equation 130

Table A. 11 Reaction rate expressions derived on the basis of kinetics model WGS-III

RDS	Rate equation	No.
1	$R_{WGS}=\frac{\left(k_{WGS_1}P_{CO}-k_{WGS_{-1}}\frac{1}{K_{W_2}K_{W_3}K_{W_4}K_{W_5}}\frac{P_{H2}P_{CO2}}{P_{H2O}}\right)}{\left(1+\frac{1}{K_{W_2}K_{W_3}K_{W_4}K_{W_5}}\frac{P_{H2}P_{CO2}}{P_{H2O}}+K_{W_5}K_{W_2}\frac{P_{H2O}}{P_{H2}}+\frac{P_{CO2}}{K_{W_4}}+\frac{P_{H2}}{K_{W_5}}\right)}$	Equation 131
2	$R_{WGS}=\frac{\left(k_{WGS_2}P_{H2O}-k_{WGS_{-2}}\frac{1}{K_{W_1}K_{W_3}K_{W_4}K_{W_5}}\frac{P_{H2}P_{CO2}}{P_{CO}}\right)}{\left(1+K_{W_1}P_{CO}+\frac{1}{K_{W_1}K_{W_3}K_{W_4}}\frac{P_{CO2}}{P_{CO}}+\frac{P_{CO2}}{K_{W_4}}+\frac{P_{H2}}{K_{W_5}}\right)^2}$	Equation 132
3	$R_{WGS}=\frac{\left(k_{WGS_3}K_{W_1}K_{W_5}K_{W_2}\frac{P_{CO}P_{H2O}}{P_{H2}}-k_{WGS_{-3}}\frac{P_{CO2}}{K_{W_4}}\right)}{\left(1+K_{W_1}P_{CO}+K_{W_5}K_{W_2}\frac{P_{H2O}}{P_{H2}}+\frac{P_{CO2}}{K_{W_4}}+\frac{P_{H2}}{K_{W_5}}\right)^2}$	Equation 133
4	$R_{WGS}=\frac{\left(k_{WGS_4}K_{W_1}K_{W_2}K_{W_3}K_{W_5}\frac{P_{CO}P_{H2O}}{P_{H2}}-k_{WGS_{-4}}P_{CO2}\right)}{\left(1+K_{W_1}P_{CO}+K_{W_5}K_{W_2}\frac{P_{H2O}}{P_{H2}}+K_{W_1}K_{W_2}K_{W_3}K_{W_5}\frac{P_{CO}P_{H2O}}{P_{H2}}+\frac{P_{H2}}{K_{W_5}}\right)}$	Equation 134
5	$R_{WGS}=\frac{\left(k_{WGS_5}K_{W_1}K_{W_3}K_{W_4}K_{W_2}\frac{P_{CO}P_{H2O}}{P_{CO2}}-k_{WGS_{-5}}P_{H2}\right)}{\left(1+K_{W_1}P_{CO}+\frac{1}{K_{W_1}K_{W_3}K_{W4}}\frac{P_{CO2}}{P_{CO}}+K_{W_1}K_{W_3}K_{W_4}K_{W_2}\frac{P_{CO}P_{H2O}}{P_{CO2}}+\frac{P_{CO2}}{K_{W_4}}\right)}$	Equation 135

Table A. 12 Reaction rate expressions derived on the basis of kinetics model WGS-IV

RDS	Rate equation	No.

1	$R_{WGS}=\frac{\left(k_{WGS_1}P_{CO}-k_{WGS_{-1}}\frac{1}{K_{W_2}K_{W_3}K_{W_4}}\frac{P_{H2}P_{CO2}}{P_{H2O}}\right)}{\left(1+\frac{1}{K_{W_2}K_{W_3}K_{W_4}}\frac{P_{H2}P_{CO2}}{P_{H2O}}+K_{W_2}K_{W_4}\frac{P_{H2O}}{P_{H2}}+\frac{P_{H2}}{K_{W_4}}\right)}$	Equation 136
2	$R_{WGS}=\frac{\left(k_{WGS_2}P_{H2O}-k_{WGS_{-2}}\frac{1}{K_{W_3}K_{W_1}K_{W_4}}\frac{P_{CO2}P_{H2}}{P_{CO}}\right)}{\left(1+K_{W_1}P_{CO}+\frac{1}{K_{W_3}K_{W_1}}\frac{P_{CO2}}{P_{CO}}+\frac{P_{H2}}{K_{W_4}}\right)^2}$	Equation 137
3	$R_{WGS}=\frac{\left(k_{WGS_3}K_{W_1}K_{W_4}K_{W_2}\frac{P_{CO}P_{H2O}}{P_{H2}}-k_{WGS_{-3}}P_{CO2}\right)}{\left(1+K_{W_1}P_{CO}+\frac{K_{W_4}K_{W_2}P_{H2O}}{P_{H2}}+\frac{P_{H2}}{K_{W_4}}\right)^2}$	Equation 138
4	$R_{WGS}=\frac{\left(k_{WGS_4}K_{W_1}K_{W_3}K_{W_4}K_{W_2}\frac{P_{CO}P_{H_2O}}{P_{CO_2}}-k_{WGS_{-4}}P_{H_2}\right)}{\left(1+K_{W_1}P_{CO}+\frac{1}{K_{W_3}K_{W_1}}\frac{P_{CO_2}}{P_{CO}}+\frac{K_{W_1}K_{W_2}K_{W_3}P_{H_2O}P_{CO}}{P_{CO_2}}\right)}$	Equation 139

Table A. 13 Reaction rate expressions derived on the basis of kinetics model WGS-V

RDS	Rate equation	No.
1	$R_{WGS}=\frac{\left(k_{WGS_1}P_{CO}-k_{WGS_{-1}}\frac{1}{K_{W_2}K_{W_3}K_{W_4}}\frac{P_{H_2}P_{CO_2}}{P_{H_2O}}\right)}{\left(1+\frac{1}{K_{W_2}K_{W_3}K_{W_4}}\frac{P_{H2}P_{CO2}}{P_{H2O}}+\frac{K_{W_2}P_{H2O}}{P_{H2}}+\frac{P_{CO_2}}{K_{W_4}}\right)}$	Equation 140
2	$R_{WGS}=\frac{\left(k_{WGS_2}P_{H2O}-k_{WGS_{-2}}\frac{1}{K_{W_1}K_{W3}K_{W4}}\frac{P_{H2}P_{CO2}}{P_{CO}}\right)}{\left(1+K_{W_1}P_{CO}+\frac{1}{K_{W_1}K_{W3}K_{W4}}\frac{P_{CO2}}{P_{CO}}+\frac{P_{CO2}}{K_{W_4}}\right)}$	Equation 141
3	$R_{WGS}=\frac{\left(k_{WGS_3}K_{W_1}K_{W_2}\frac{P_{CO}P_{H2O}}{P_{H2}}-k_{WGS_{-3}}\frac{P_{CO2}}{K_{W_4}}\right)}{\left(1+K_{W_1}P_{CO}+\frac{K_{W_2}P_{H2O}}{P_{H2}}+\frac{P_{CO2}}{K_{W_4}}\right)^2}$	Equation 142
4	$R_{WGS}=\frac{\left(k_{WGS_4}K_{W_3}K_{W_1}K_{W_2}\frac{P_{CO}P_{H2O}}{P_{H2}}-k_{WGS_{-4}}P_{CO2}\right)}{\left(1+K_{W_1}P_{CO}+\frac{K_{W_2}P_{H2O}}{P_{H2}}+K_{W_3}K_{W_1}K_{W_2}\frac{P_{CO}P_{H2O}}{P_{H2}}\right)}$	Equation 143

Table A. 14 Reaction rate expressions derived on the basis of kinetics model WGS-VI

RDS	Rate equation	No.
1	$R_{WGS}=\frac{\left(k_{WGS_1}P_{CO}-k_{WGS_{-1}}\frac{1}{K_{W_4}K_{W_5}K_{W_3}K_{W_2}}\frac{P_{CO2}\,P_{H2}}{P_{H2O}}\right)}{\left(1+\frac{1}{K_{W_4}K_{W_5}K_{W_3}K_{W_2}}\frac{P_{CO2}\,P_{H2}}{P_{H2O}}+\sqrt{\frac{P_{H2}}{K_{W_5}}}+\frac{P_{CO2}\sqrt{P_{H2}}}{K_{W_4}K_{W_5}^{0.5}}+K_{W_2}\,P_{H2O}\right)}$	Equation 144

2	$$R_{WGS}=\frac{\left(k_{WGS_2}\,P_{H2O}-k_{WGS_{-2}}\frac{1}{K_{W_4}K_{W_5}K_{W_3}K_{W_1}}\frac{P_{CO2}\,P_{H2}}{P_{CO}}\right)}{\left(1+K_{W_1}\,P_{CO}+\sqrt{\frac{P_{H2}}{K_{W_5}}}+\frac{P_{CO2}\sqrt{P_{H2}}}{K_{W_4}K_{W_5}^{0.5}}+\frac{1}{K_{W_4}K_{W_5}K_{W_3}K_{W_1}}\frac{P_{CO2}\,P_{H2}}{P_{CO}}\right)}$$	Equation 145
3	$$R_{WGS}=\frac{\left(k_{WGS_3}K_{W_1}K_{W_2}P_{CO}P_{H2O}\;-k_{WGS_{-3}}\frac{P_{CO2}\,P_{H2}}{K_{W_4}\,K_{W_5}}\right)}{\left(1+K_{W_1}\,P_{CO}+\sqrt{\frac{P_{H2}}{K_{W_5}}}+K_{W_2}\,P_{H2O}+\frac{P_{CO2}\sqrt{P_{H2}}}{K_{W_4}\,K_{W_5}^{0.5}}\right)^2}$$	Equation 146
4	$$R_{WGS}=\frac{\left(k_{WGS_4}K_{W_3}K_{W_1}K_{W_2}K_{W_5}^{0.5}\frac{P_{CO}P_{H2O}}{\sqrt{P_{H2}}}-k_{WGS_{-4}}\frac{P_{CO2}\sqrt{P_{H2}}}{\sqrt{K_{W_5}}}\right)}{\left(1+K_{W_1}\,P_{CO}+\sqrt{\frac{P_{H2}}{K_{W_5}}}+K_{W_2}\,P_{H2O}+K_{W_3}K_{W_1}K_{W_2}K_{W_5}^{0.5}\frac{P_{CO}P_{H2O}}{\sqrt{P_{H2}}}\right)}$$	Equation 147
5	$$R_{WGS}=\frac{\left(k_{WGS_5}K_{W_4}K_{W_3}K_{W_1}K_{W_2}\frac{P_{CO}P_{H2O}}{P_{CO_2}}-k_{WGS_{-5}}P_{H_2}\right)}{\left(1+K_{W_1}\,P_{CO}+\sqrt{K_{W_4}K_{W_3}K_{W_1}K_{W_2}}\sqrt{\frac{P_{CO}P_{H2O}}{P_{CO_2}}}+\cdots\right.\\\left.\sqrt{\frac{K_{W_3}K_{W_1}K_{W_2}P_{CO}P_{H2O}P_{CO_2}}{K_{W_4}}}+K_{W_2}\,P_{H2O}\right)^2}$$	Equation 148

Table A. 15 Reaction rate expressions derived on the basis of kinetics model WGS-VII

RDS	Rate equation	No.
1	$$R_{WGS}=\frac{\left(k_{WGS_1}P_{CO}-\frac{k_{WGS_{-1}}}{K_{W_2}K_{W_3}K_{W_4}K_{W_5}}\frac{P_{CO_2}P_{H_2}}{P_{H_2O}}\right)}{\left(1+\frac{1}{K_{W_2}K_{W_3}K_{W_4}K_{W_5}}\frac{P_{CO_2}P_{H_2}}{P_{H_2O}}+\sqrt{\frac{P_{H_2}}{K_{W_5}}}+\frac{P_{CO_2}\sqrt{P_{H_2}}}{K_{W_4}K_{W_5}^{0.5}}+K_{W_2}P_{H_2O}\sqrt{\frac{P_{H_2}}{K_{W_5}}}\right)}$$	Equation 149
2	$$R_{WGS}=\frac{\left(k_{WGS_2}P_{H_2O}-\frac{k_{WGS_{-2}}}{K_{W_1}K_{W_3}K_{W_4}K_{W_5}}\frac{P_{CO_2}P_{H_2}}{P_{CO}}\right)}{\left(1+K_{W_1}\,P_{CO}+\sqrt{\frac{P_{H_2}}{K_{W_5}}}+\frac{P_{CO_2}\sqrt{P_{H_2}}}{K_{W_4}K_{W_5}^{0.5}}+\frac{P_{CO_2}\sqrt{P_{H_2}}}{K_{W_1}K_{W_3}K_{W_4}K_{W_5}^{0.5}P_{CO}}\right)^2}$$	Equation 150
3	$$R_{WGS}=\frac{\left(k_{WGS_3}K_{W_1}K_{W_2}K_{W_5}^{0.5}\frac{P_{CO}P_{H2O}}{P_{H2}^{0.5}}-k_{WGS_{-3}}\frac{P_{CO2}\sqrt{P_{H2}}}{K_{W_4}\,K_{W_5}^{0.5}}\right)}{\left(1+K_{W_1}\,P_{CO}+\sqrt{\frac{P_{H2}}{K_{W_5}}}+\frac{P_{CO2}\sqrt{P_{H2}}}{K_{W_4}\,K_{W_5}^{0.5}}+K_{W_2}K_{W_5}^{0.5}\frac{P_{H2O}}{P_{H2}^{0.5}}\right)^2}$$	Equation 151

4

$$R_{WGS} = \frac{\left(k_{WGS_4} K_{W_3} K_{W_1} K_{W_2} K_{W_5}^{0.5} \frac{P_{H_2O}\, P_{CO}}{P_{H_2}^{0.5}} - k_{WGS_{-4}} P_{CO_2} \sqrt{\frac{P_{H_2}}{K_{W_5}}}\right)}{\left(1 + K_{W_1}\, P_{CO} + \sqrt{\frac{P_{H_2}}{K_{W_5}}} + K_{W_3} K_{W_1} K_{W_2} K_{W_5}^{0.5} \frac{P_{H_2O}\, P_{CO}}{P_{H_2}^{0.5}} + K_{W_2} K_{W_5}^{0.5} \frac{P_{H_2O}}{P_{H_2}^{0.5}}\right)}$$

Equation 152

5

$$R_{WGS} = \frac{\left(k_{WGS_5} K_{W_1} K_{W_2} K_{W_3} K_{W_4} \frac{P_{CO} P_{H_2O}}{P_{CO_2}} - k_{WGS_{-5}} P_{H_2}\right)}{\left(1 + K_{W_1}\, P_{CO} + \sqrt{K_{W_1} K_{W_2} K_{W_3} K_{W_4} \frac{P_{CO} P_{H_2O}}{P_{CO_2}}} + \sqrt{\frac{K_{W_2} P_{H_2O} P_{CO_2}}{K_{W_1} K_{W_3} K_{W_4} P_{CO}}} + \sqrt{\frac{K_{W_1} K_{W_2} K_{W_3}}{K_{W_4}} P_{CO_2} P_{CO} P_{H_2O}}\right)^2}$$

Equation 153